Chapter 3

RESULTS

3.1 Preparation of ligands

2-(Phenylazo)pyridine (azpy) was prepared by modified literature method (Krause and Krause, 1980). The azpy was synthesized by condensing nitrosobenzene with 2-aminopyridine in the presence of sodium hydroxide and benzene. In the preparation of 2-(phenylazo)pyrimidine (azpym), 2-aminopyrimidine was used instead of 2-aminopyridine. Purification was carried out by column chromatography and the reactions were shown in equation (1) and (2).

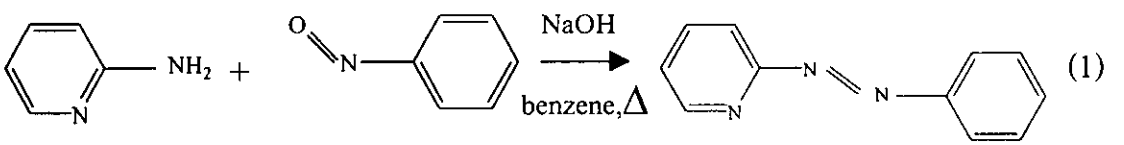

(1)

2-aminopyridine nitrosobenzene 2-(phenylazo)pyridine (azpy)

35% yield

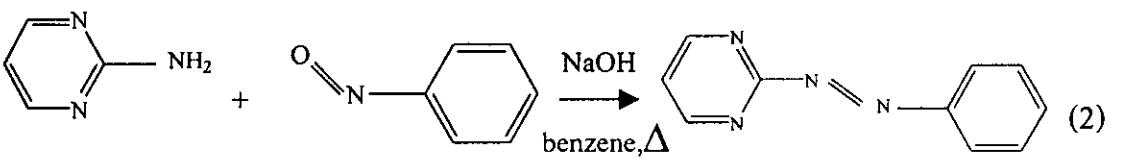

(2)

2-aminopyrimidine nitrosobenzene 2-(phenylazo)pyrimidine (azpym)

24% yield

Ligands were obtained in small yield because of many side reactions. The yield of azpy and azpym ligands were 35% and 24%, respectively. The physical

Table 1 The physical properties of ligands

Ligand	Physical properties		
	Appearance	Color	Melting point (°C)
azpy	Liquid	Orange	32-34[a]
azpym	Liquid	Orange	Liquid at room temperature

[a]Results from Krause and Krause (1980)

Those ligands were well dissolved in almost solvents. The solubility was tested by using 0.0014 g of each ligand in 10 mL of various solvent. Both ligands were well soluble in acetone, chloroform, dichloromethane, ethanol, hexane, and methanol.

3.2 Characterization of ligands

The chemistry of azpy and azpym ligands were confirmed by Infrared spectroscopy, UV-Visible absorption spectroscopy, Nuclear Magnetic Resonance spectroscopy and Cyclic voltammetry.

3.2.1 Infrared spectroscopy

Infrared spectroscopy is a technique to study the functional group of the ligands. Infrared spectroscopy of the azpy and azpym ligands were recorded in a KBr disc in the 4000-370 cm^{-1} region which was helpful in characterization of the ligands. The infrared spectra of both ligands in the range 1800-370 cm^{-1} are show in Figure 2

and Figure 3, respectively. The important vibrational frequencies of both ligands are C=C, C=N, N=N(azo) stretching modes. The summaries of infrared spectroscopic data are listed in Table 2.

Table 2 Infrared spectroscopic data of ligands

Vibration modes	Frequencies (cm^{-1})	
	azpy	azpym
N=N (azo) stretching	1421 (s)	1393 (s)
C=C stretching and C=N stretching	1580 (s) 1491 (m) 1476 (m) 1464 (m)	1565 (s) 1497 (m) 1452 (w)
C-H out of plane bending	790 (s) 738 (s) 688 (s)	816 (s) 766 (s) 690 (s)

s = strong, m = medium, w = weak

Infrared spectra of their ligands exhibited many intense vibrations of different intensities in the range of 1,600-370 cm^{-1}. There are four vibrations bands of ν(C=C), ν(C=N) were observed between 1430 and 1610 cm^{-1} and the ν(N=N) band near 1420 cm^{-1}. In this work, the C=C and C=N stretching modes of azpy appeared at 1580, 1491, 1476 and 1464 cm^{-1} and azpym occurred at 1565, 1497 and 1452 cm^{-1}. The N=N stretching modes of the azpy and azpym ligands occurred at 1421 cm^{-1} and 1393 cm^{-1}, respectively. These data could be confirmed with the literature data.

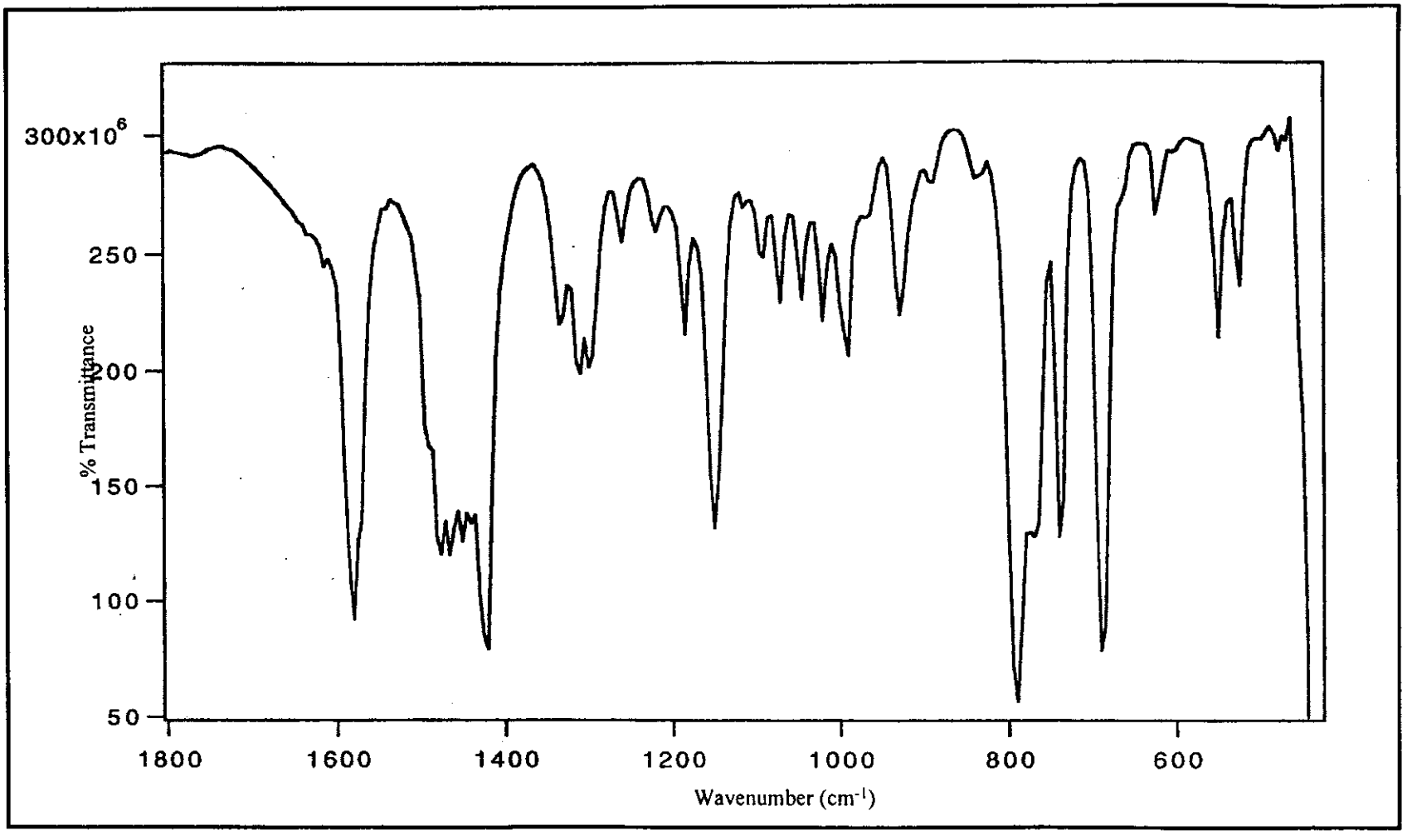

Figure 2 IR spectrum of azpy.

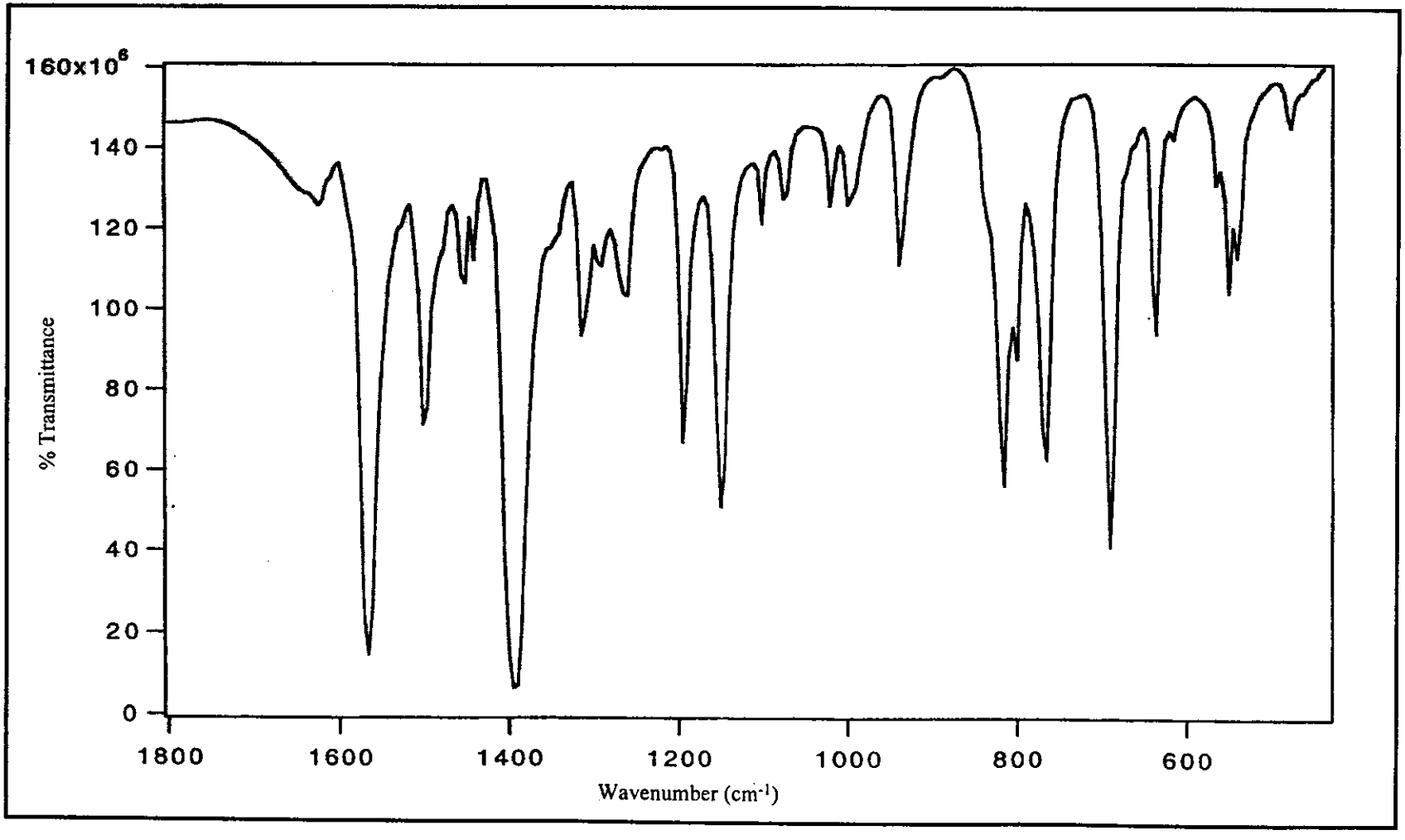

Figure 3 IR spectrum of azpym.

3.2.2 UV-Visible absorption spectroscopy

UV-Visible absorption spectroscopy is a technique to study the electronic transitions of the ligands. The UV-Visible absorption spectra of azpy, azpym, bpy and phen ligands were taken in acetonitrile as shown in Figure 4 to 7, respectively. In addition, their absorption spectra were studied in acetone, dimethyl sulfoxide (DMSO), dichloromethane, ethanol, and methanol. The data are summarized in the Table 3.

Table 3 The UV-Visible absorption spectroscopic data of the azpy and the azpym ligands

Solvent	λ_{max} nm, (ε^a x 10^{-4} $M^{-1}cm^{-1}$)			
	azpy	azpym	bpy	phen
CH_3COCH_3	446(0.4)	439 (0.4)	n	n
CH_3CN	314(1.5) 442 (0.06)	299 (1.6) 446 (0.06)	236(1.2) 280(1.5)	229 (8.1) 263 (6.7)
DMSO	319 (1.7) 449 (0.05)	303 (1.3) 438 (0.05)	n	n
CH_2Cl_2	317 (1.7) 446 (0.05)	304 (1.7) 447 (0.04)	237 (1.3) 280(1.9)	264 (3.1)
EtOH	315 (1.7) 445 (0.04)	304 (1.6) 440 (0.04)	236 (1.2) 280 (1.9)	229 (4.6) 264 (3.8)
MeOH	318 (1.9) 441 (0.04)	304 (1.9) 447 (0.04)	235 (2.1) 280 (3.0)	228 (4.9) 263 (6.7)

[a]Molar Extinction coefficient, n = cannot be observed

The absorption spectra of the azpy and the azpym ligands displayed intense bands in the region 200-400 nm. The absorption occuring in UV region ($\varepsilon \sim 6000$-19000 $M^{-1}cm^{-1}$) attributed to $\pi \rightarrow \pi^*$ transitions. In addition, both ligands showed absorption bands ($\varepsilon \sim 400$-600 $M^{-1}cm^{-1}$) in the visible region which referred to $n \rightarrow \pi^*$ transitions. However, the absorption spectra of the bpy and phen ligands showed only two $\pi \rightarrow \pi^*$ transition in the UV region.

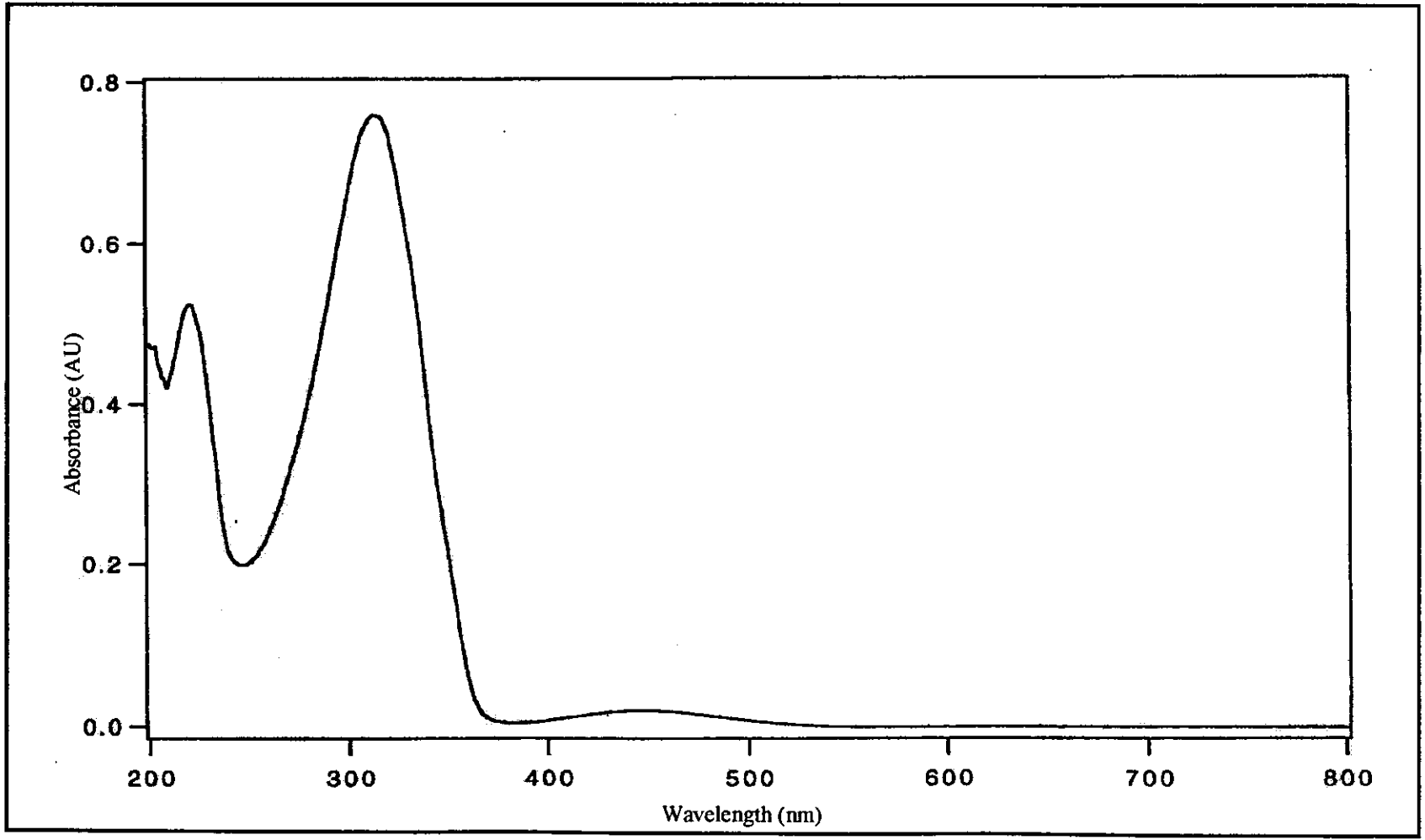

Figure 4 UV-Visible absorption spectrum of azpy in CH_3CN.

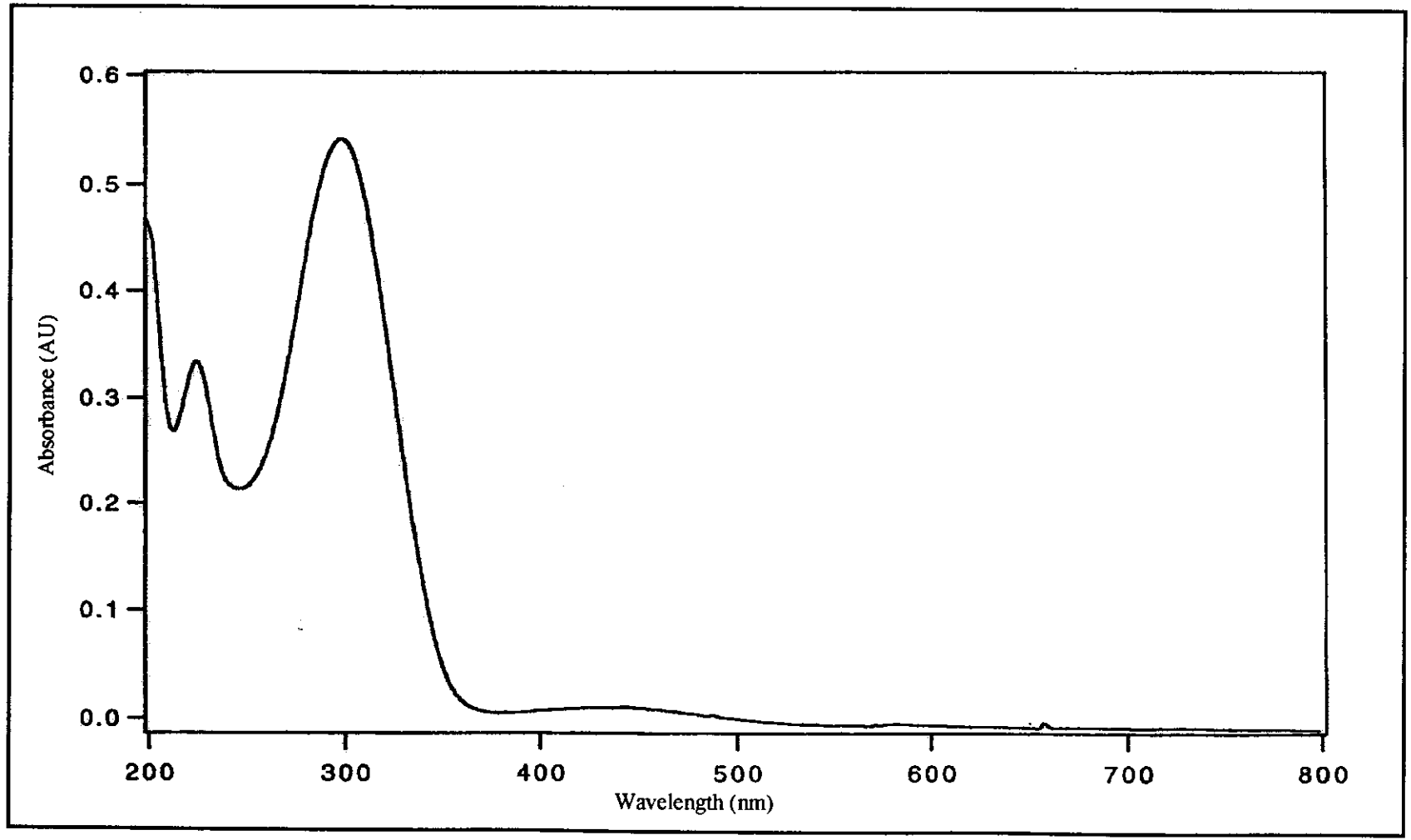

Figure 5 UV-Visible absorption spectrum of azpym in CH_3CN.

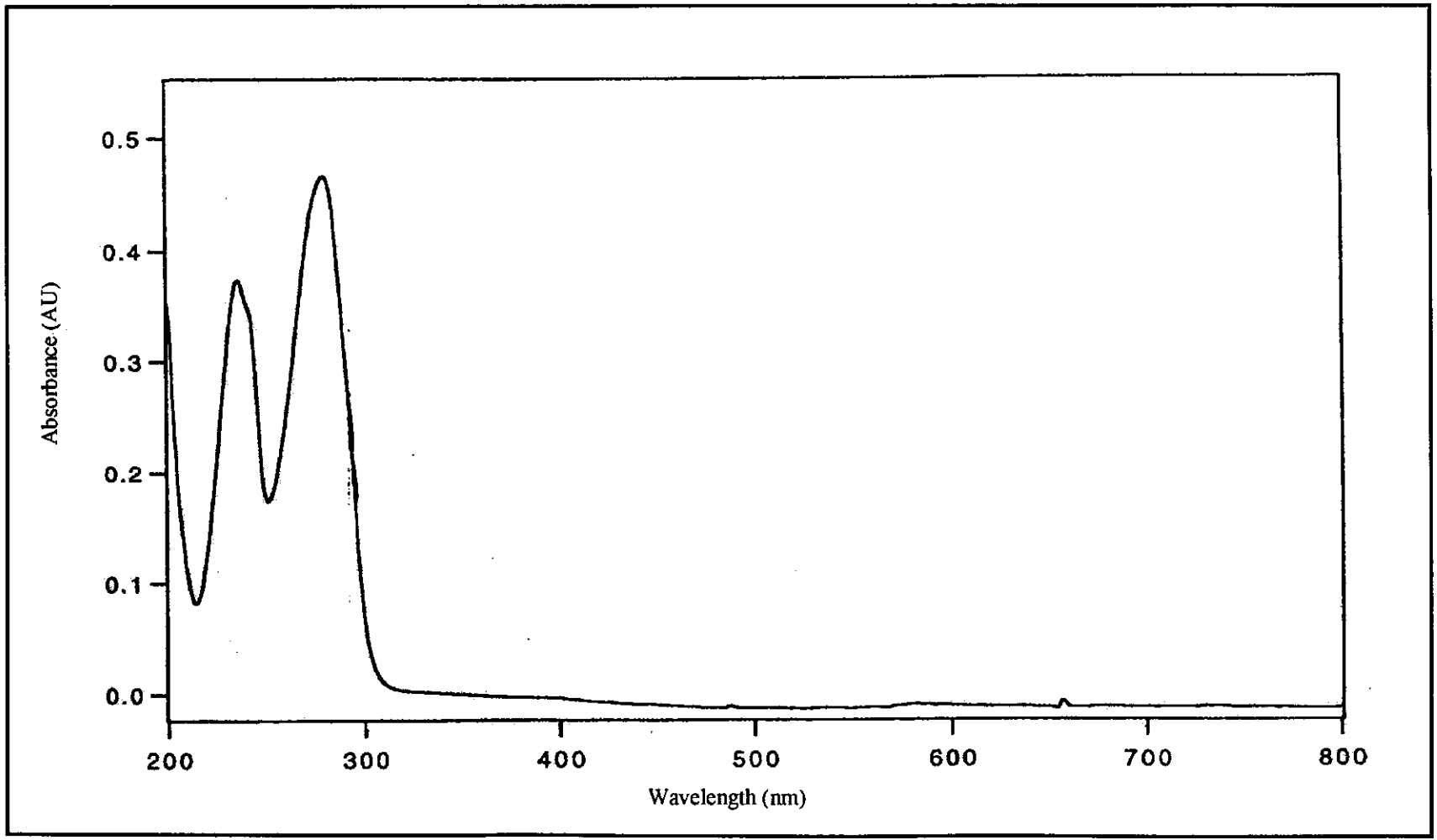

Figure 6 UV-Visible absorption spectrum of bpy in CH_3CN.

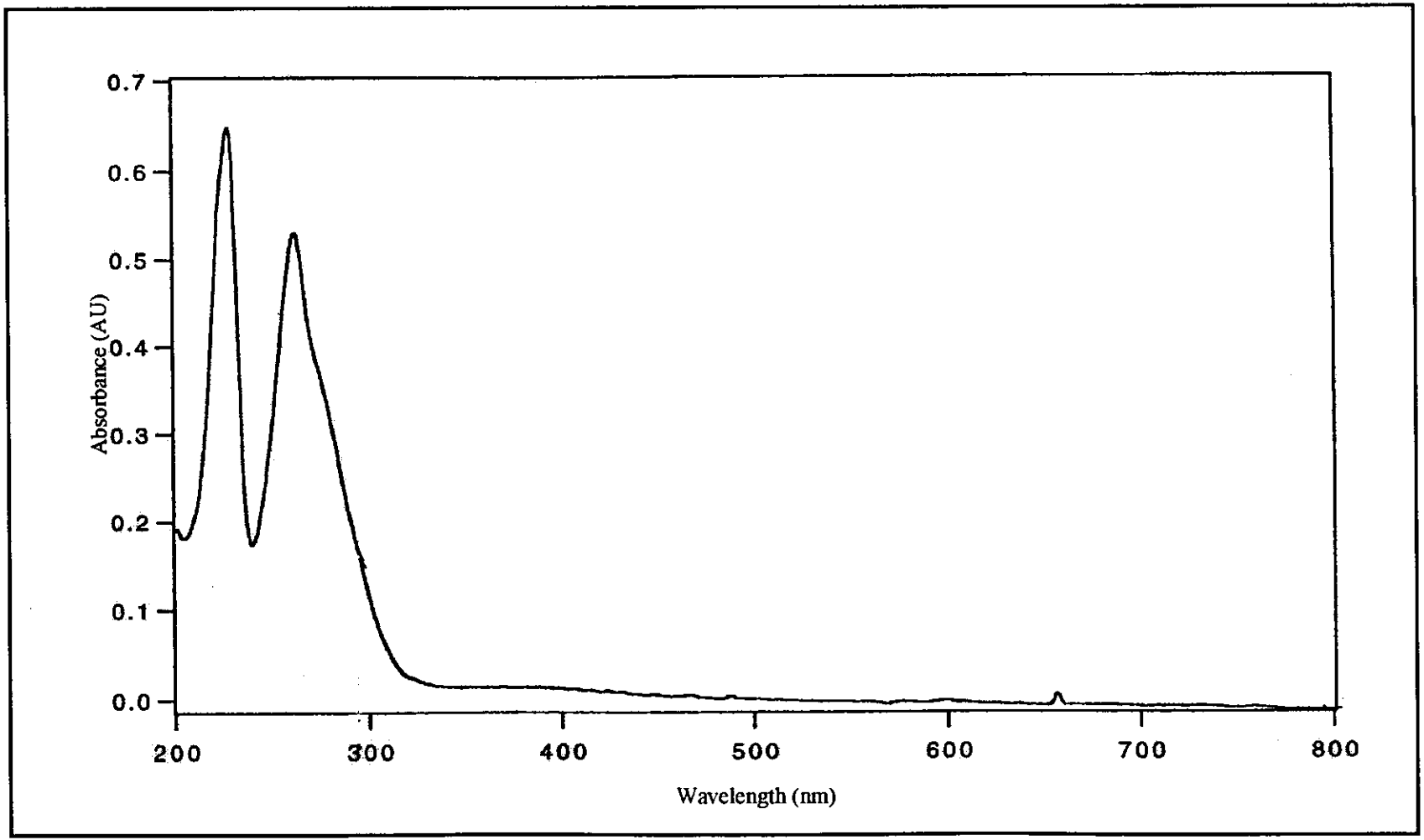

Figure 7 UV-Visible absorption spectrum of phen in CH_3CN.

3.2.3 Nuclear Magnetic Resonance Spectroscopy

Nuclear Magnetic Resonance Spectroscopy is a technique to study the molecular structure of compound. The NMR spectra of azpy, azpym, bpy and phen in acetone-d_6 were recorded and tetramethylsilane (TMS, $(CH_3)_4Si$) was used as an internal reference. The chemical shifts (δ, ppm) and *J*-coupling (Hz) of their ligands were reported in part per million (ppm) downfield from tetramethylsilane. The proton and carbon assignments of each ligands was made on the basis of peak integration, coupling constants and ^{1}H-^{1}H COSY NMR and ^{1}H-^{13}C HMQC NMR experiments. The chemical shift and proton, carbon assignments of these ligands are summarized in Table 4 to 7.

Table 4 The NMR spectroscopic data of the azpy ligand in acetone-d_6

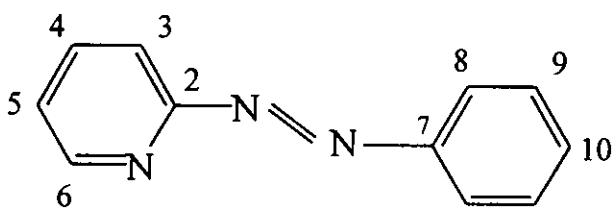

H- Position	^{1}H NMR			^{13}C NMR
	δ (ppm)	*J* (Hz)	Number of H	δ (ppm)
6	8.76 (dd)	5.0, 1.5	1	150.13
4	8.06 (ddd)	7.5, 7.5, 1.5	1	139.32
8	8.04 (dd)	7.5, 2.0	2	123.88
3	7.80 (d)	8.0	1	114.04
9, 10	7.64 (m)		3	132.97 130.10

Table 4 (continued)

H- Position	^{1}H NMR			^{13}C NMR
	δ (ppm)	*J* (Hz)	Number of H	δ (ppm)
5	7.57 (ddd)	7.5, 5.0, 1.0	1	126.25
Quaternary carbon				164.05, 153.09

m = multiplet, d = doublet, dd = doublet of doublet and

ddd = doublet of doublet of doublet

The results of NMR spectrum were used to support the structures of all ligands. The ^{1}H NMR spectrum (Figure 8) of the azpy ligand in acetone-d_6 showed 6 resonances for 9 protons. The spectrum of the azpy ligand belonged to the pyridine ring and the phenyl ring. Figure 9 showed ^{1}H-^{1}H COSY spectrum of the azpy ligand in the same solvent.

The proton H3 on the pyridine ring located near proton H4 and effected by nitrogen of azo function therefore, the signal shifted to lower field more than proton H5 but higher field than proton H4 and H6. This proton signal was splitted by the proton 4 (J = 8.0 Hz), resulting in doublet signal.

The proton H4 was coupled with proton H3 (J = 7.5 Hz), H5 (J = 7.5 Hz) and H6 (J = 1.5), giving doublet of doublet of doublet (ddd) signal at 8.04 ppm.

The proton H5 appeared at highest field (7.57 ppm) and was splitted by proton H6 (J = 5.0 Hz), H4 (J = 7.5 Hz) and H3 (J = 1.0 Hz).

The signal of proton H6 was observed at 8.76 ppm. The signal appeared as doublet of doublet (dd), due to the coupling with proton H5 (J = 5.0 Hz) and H4 (J = 1.5 Hz).

The signal of proton H8 closed to the azo function appeared at lower field

than proton H9 and H10. The proton H8 and H9 were equivalent protons on phenyl ring. Therefore, the signals of proton H8 appeared as doublet of doublet (dd) with the *J*-coupling 7.5 (H9) and 2.0 (H10) Hz at 8.04 ppm.

The proton H9 and H10 showed similar chemical shifts. The splitting of proton H9 and H10 in the azpy ligand appeared as multiplet peak at 7.64 ppm.

The ^{13}C NMR signal assignments (Figure 10) were based on the ^{1}H-^{13}C HMQC spectrum (Figure 11). The ^{13}C NMR spectrum of the azpy ligand showed 9 resonance signals in the aromatic region.There were two quaternary carbons, showed downfield resonance at 164.05 ppm which was assigned to quaternary carbon (C2). The more intense peak at 153.09 ppm belonged to the quaternary carbon (C7). The C3 signal occurred at 114.04 ppm which higher field than C8 (123.88 ppm). The C6 and C4 signal were observed at 150.13 and 139.32 ppm, respectively. The peak at 132.97 and 130.10 ppm represented C9 and C10, respectively.

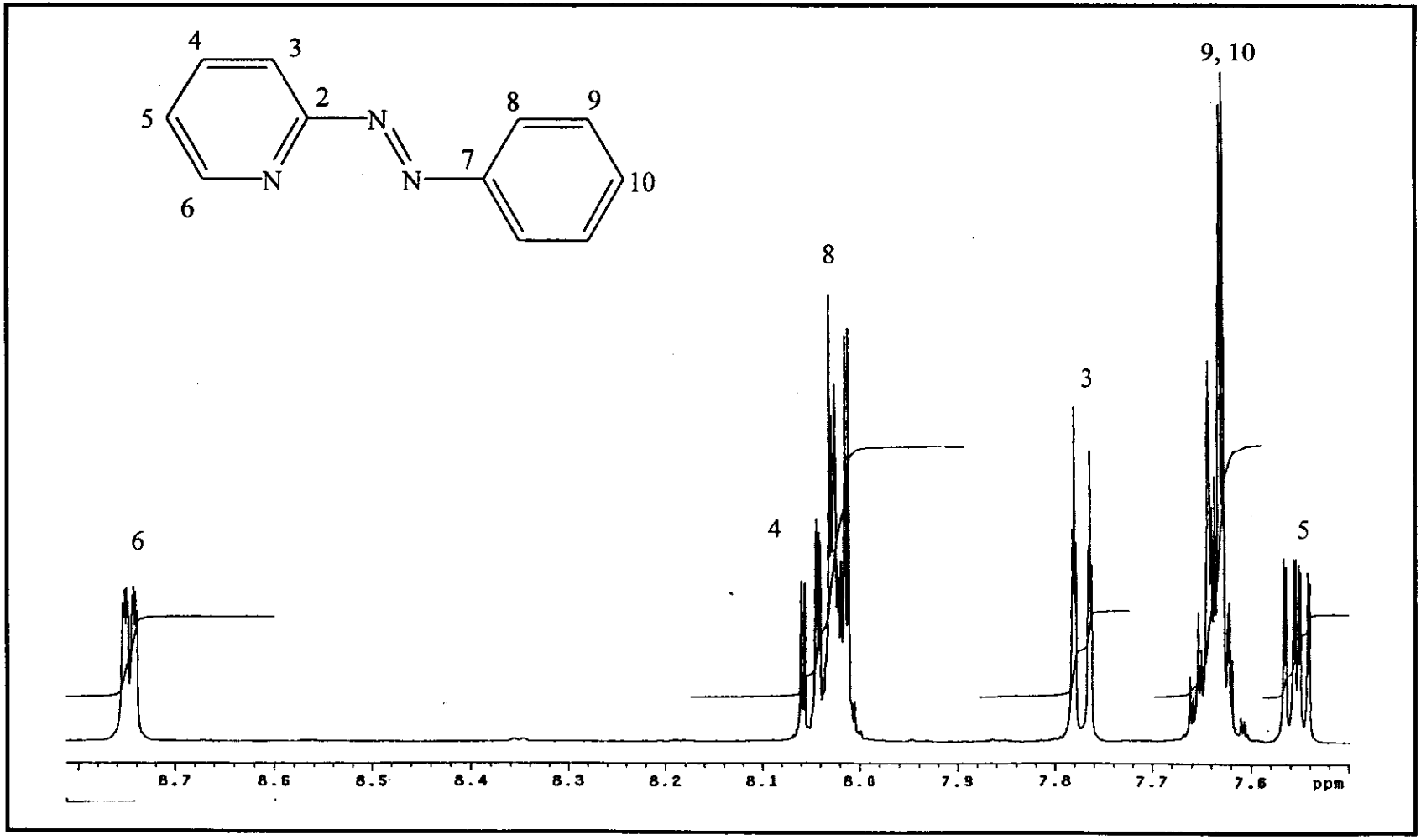

Figure 8 ^{1}H NMR spectrum of azpy in acetone-d_6.

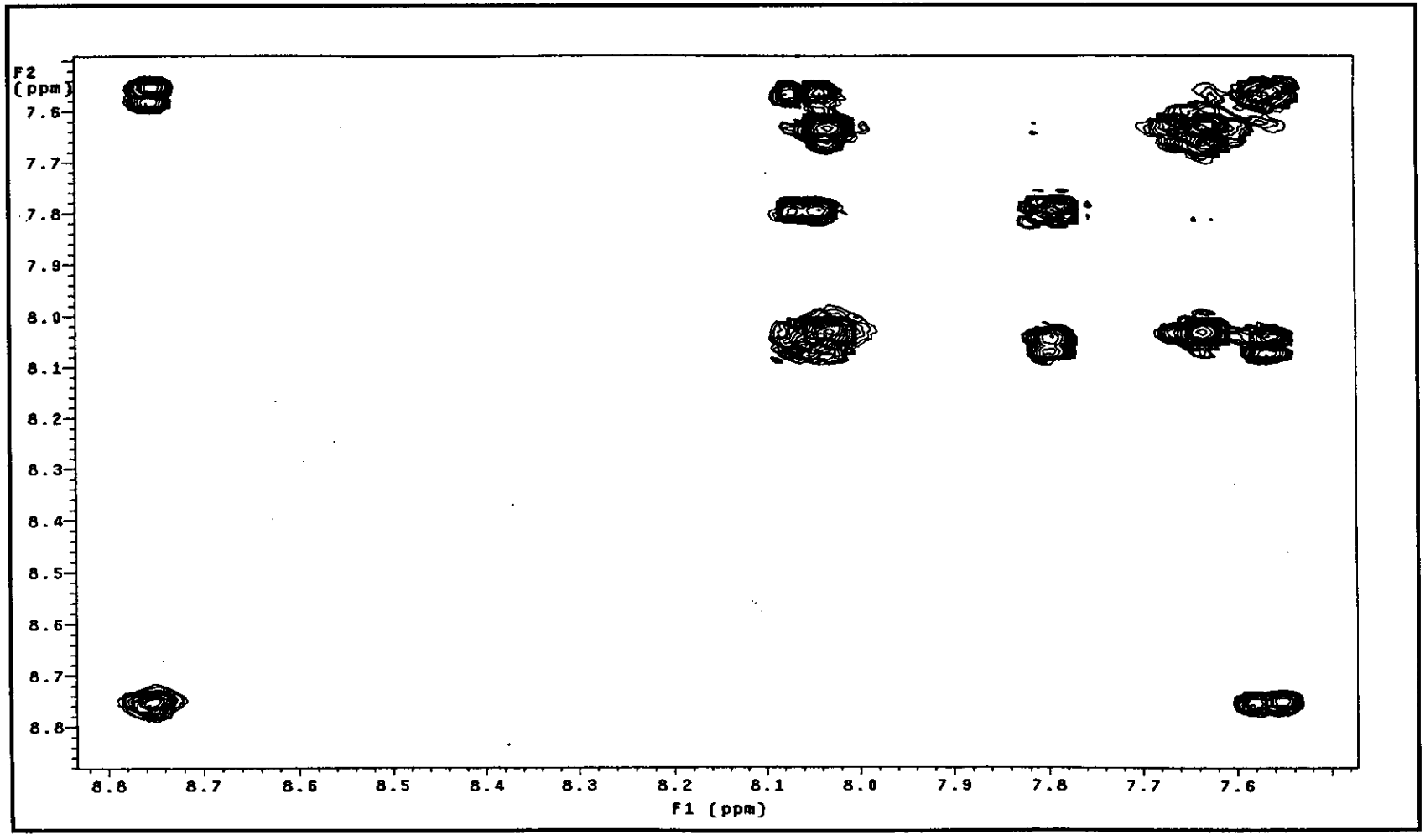

Figure 9 ^{1}H-^{1}H COSY NMR spectrum of azpy in acetone-d_6.

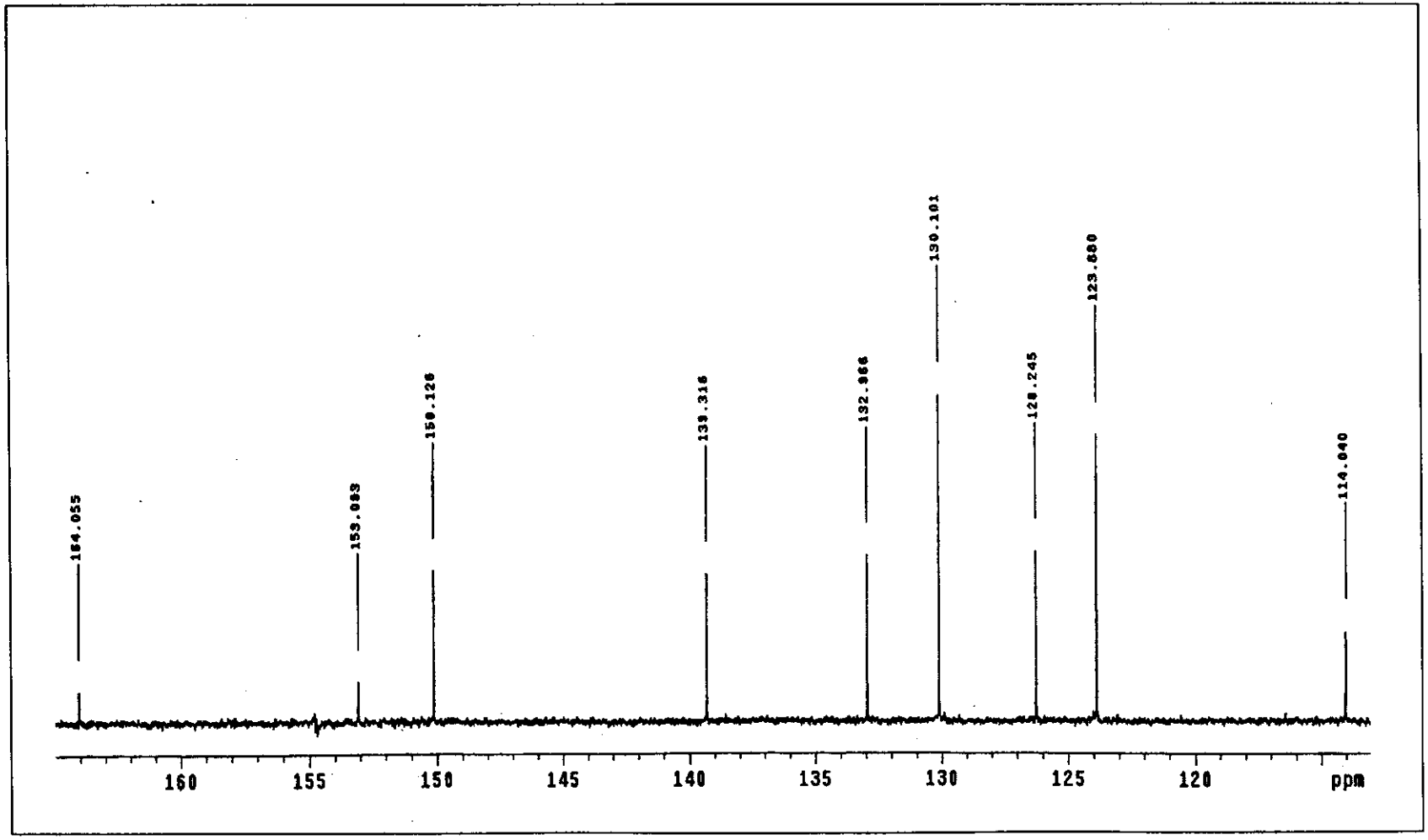

Figure 10 ^{13}C NMR spectrum of azpy in acetone-d_6

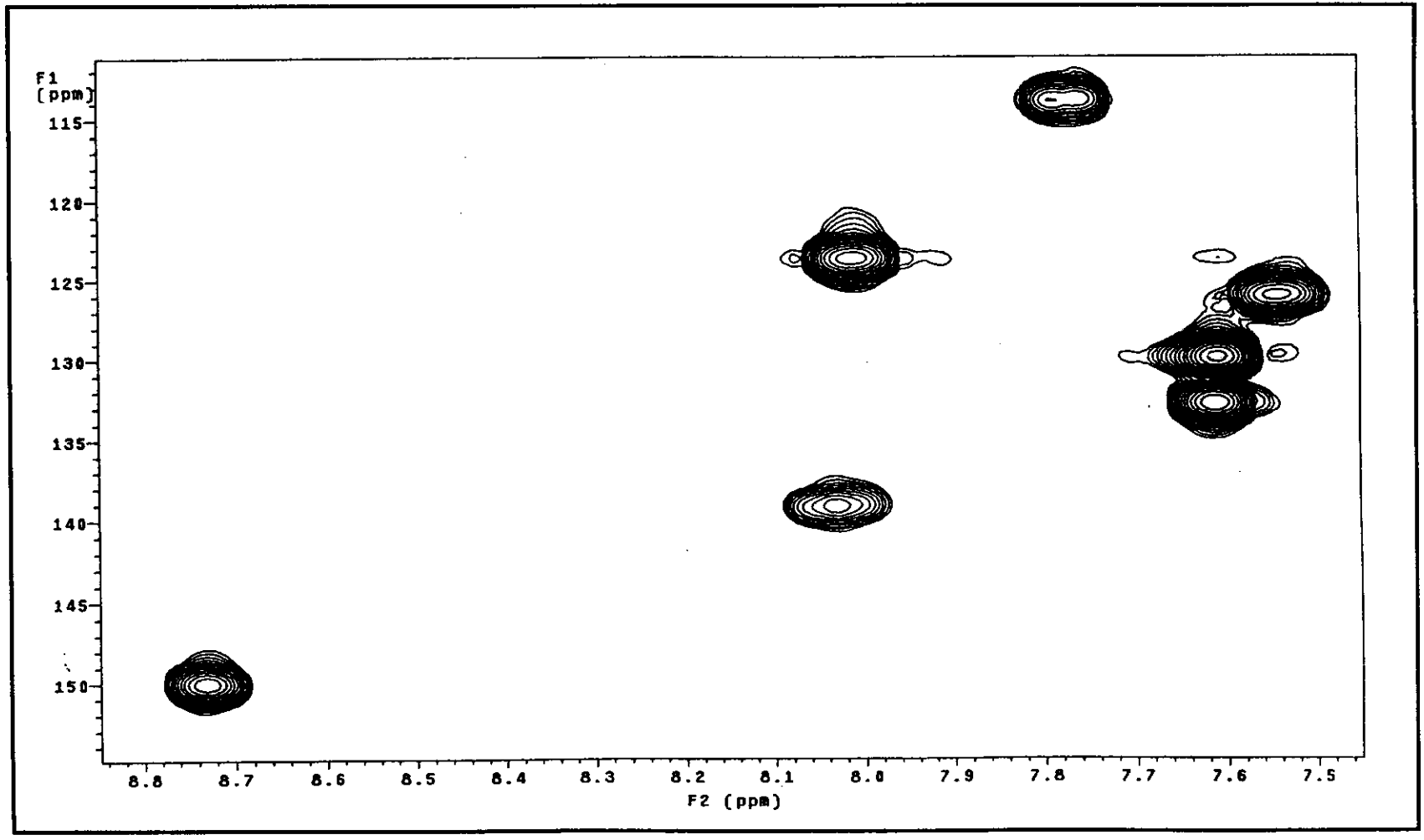

Figure 11 ^{1}H-^{13}C HMQC NMR spectrum of azpy in acetone-d_6.

Table 5 The NMR spectroscopic data of the azpym ligand in acetone-d_6

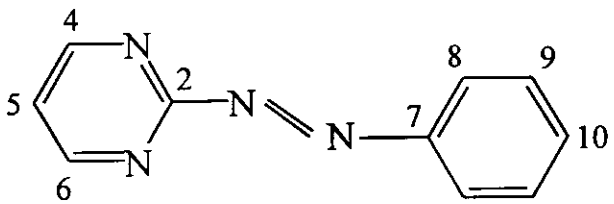

H-Position	^{1}H NMR			^{13}C NMR
	δ (ppm)	*J* (Hz)	Number of H	δ (ppm)
4,6	9.03 (d)	5.0	2	159.84
8	8.05 (dd)	8.0, 1.5	2	124.09
10, 9	7.68 (m)		3	133.72 130.27
5	7.61 (t)	5.0	1	122.16
Quaternary carbon				168.32, 153.29

m = multiplet, d = doublet, dd = doublet of doublet,

ddd = doublet of doublet of doublet and t = triplet

Figure 12 showed the ^{1}H NMR spectrum of azpym ligand. This spectrum displayed 5 signals for 8 protons. The assignment of signals were based on the ^{1}H-^{1}H COSY NMR spectroscopy (Figure 13). The proton H4 and H6 were equivalent and showed at 9.03 ppm. These protons were located near the pyrimidine nitrogen atoms therefore they resonated at the most downfield. These signal was splitted by the proton H5 (J = 5.0 Hz) as doublet (d).

The signal of proton H5 occurred at the highest field (7.61 ppm) than other protons. The signal of proton H5 coupled with proton H4 and H6 (J = 5.0 Hz) was observed.

The proton H8 was two equivalent protons which located near azo nitrogen. It coupled with proton H9 (J = 8.0 Hz) and H10 (J = 1.5 Hz) and gave signal doublet of doublet (dd). The proton H9 and H10 showed multiplet peak at 7.68 ppm.

The ^{13}C NMR signal assignments (Figure 14) were based on the ^{1}H-^{13}C HMQC spectrum (Figure 15). The ^{13}C NMR spectrum of the azpym ligand showed 7 resonance signals in the aromatic region. There were two quaternary carbon. The downfield resonance at 168.32 ppm was assigned to quaternary carbon (C2). The peak at 153.29 ppm belonged to quaternary carbon (C7). The C4 and C6 were appeared at 159.84 ppm which had an identical chemical shift. The peak at 124.09 ppm was due to C8 which higher field than C9 (133.72 ppm) and C10 (130.27 ppm). The signal of C5 appeared at 122.16 ppm. It was due to the highest fields of all carbons.

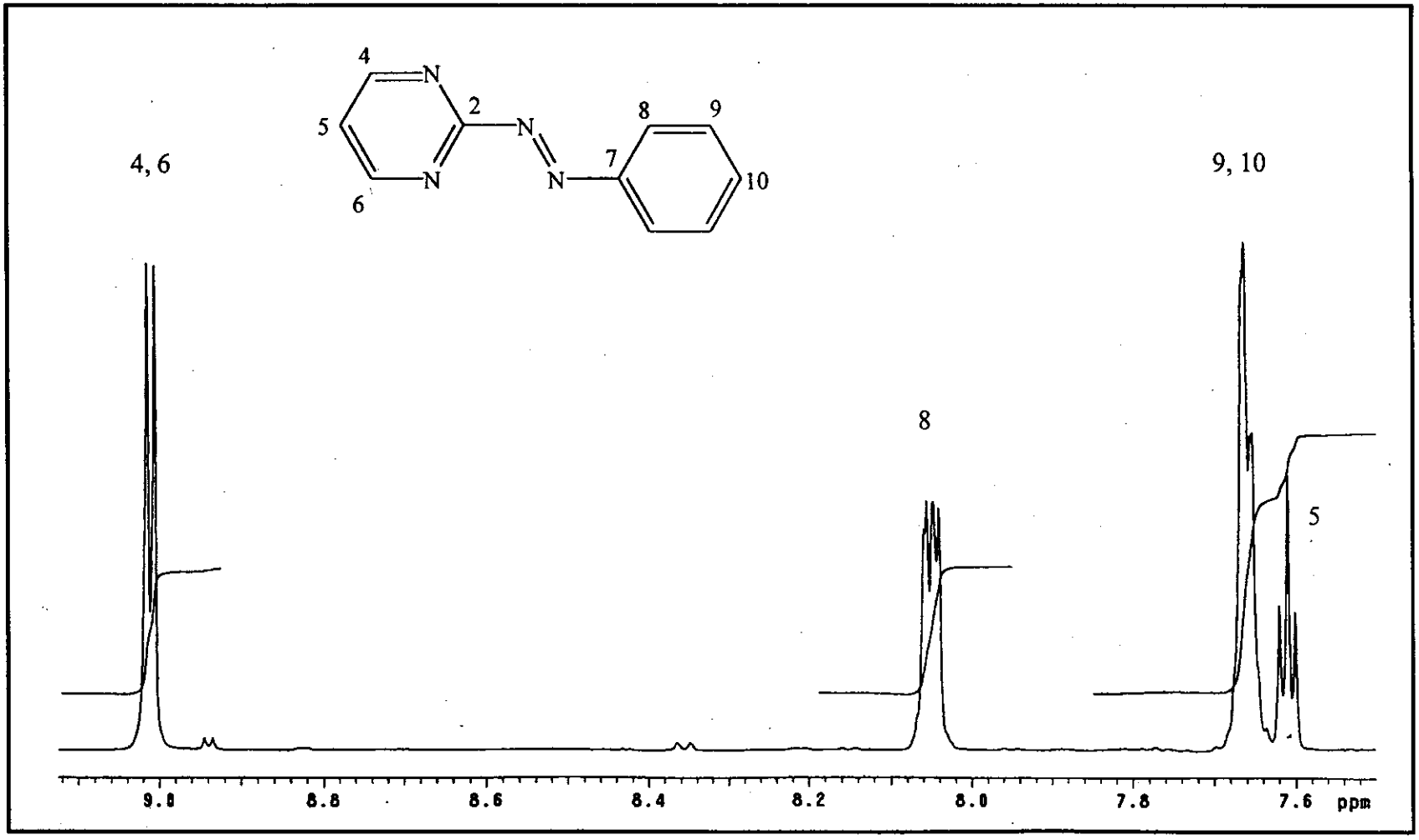

Figure 12 ^{1}H NMR spectrum of azpym in acetone-d_6.

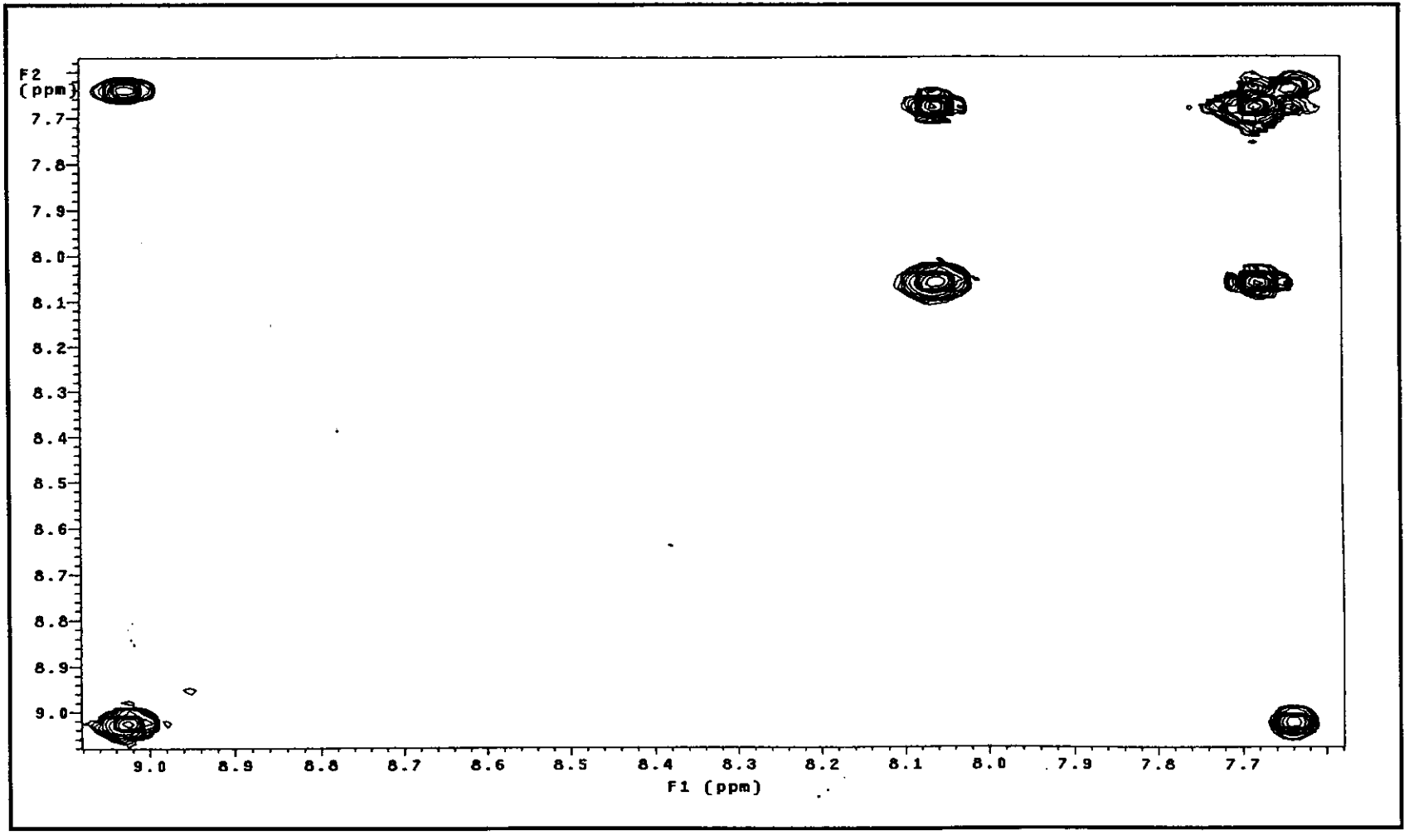

Figure 13 ^{1}H-^{1}H COSY NMR spectrum of azpym in acetone-d_6.

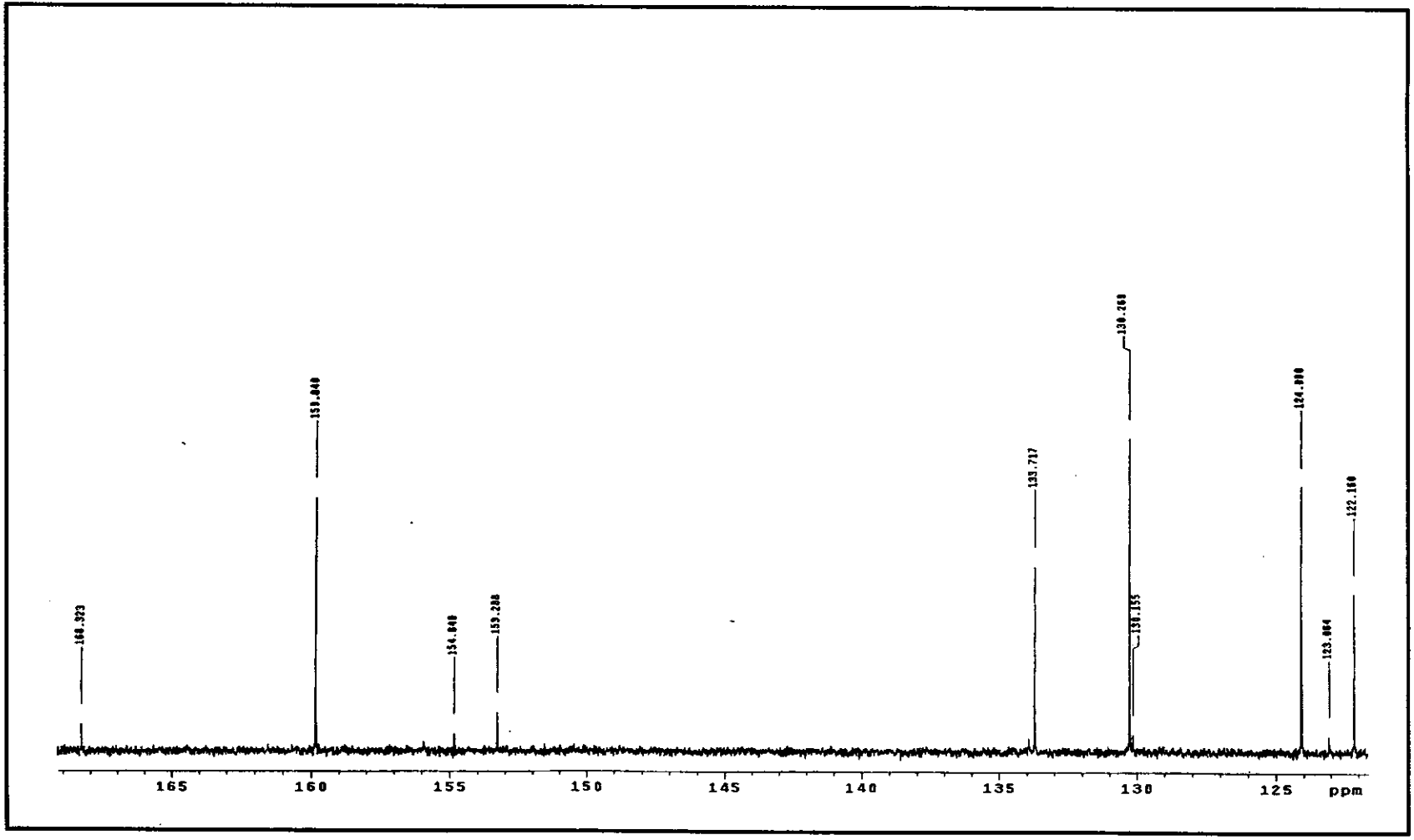

Figure 14 ^{13}C NMR spectrum of azpym in acetone-d_6.

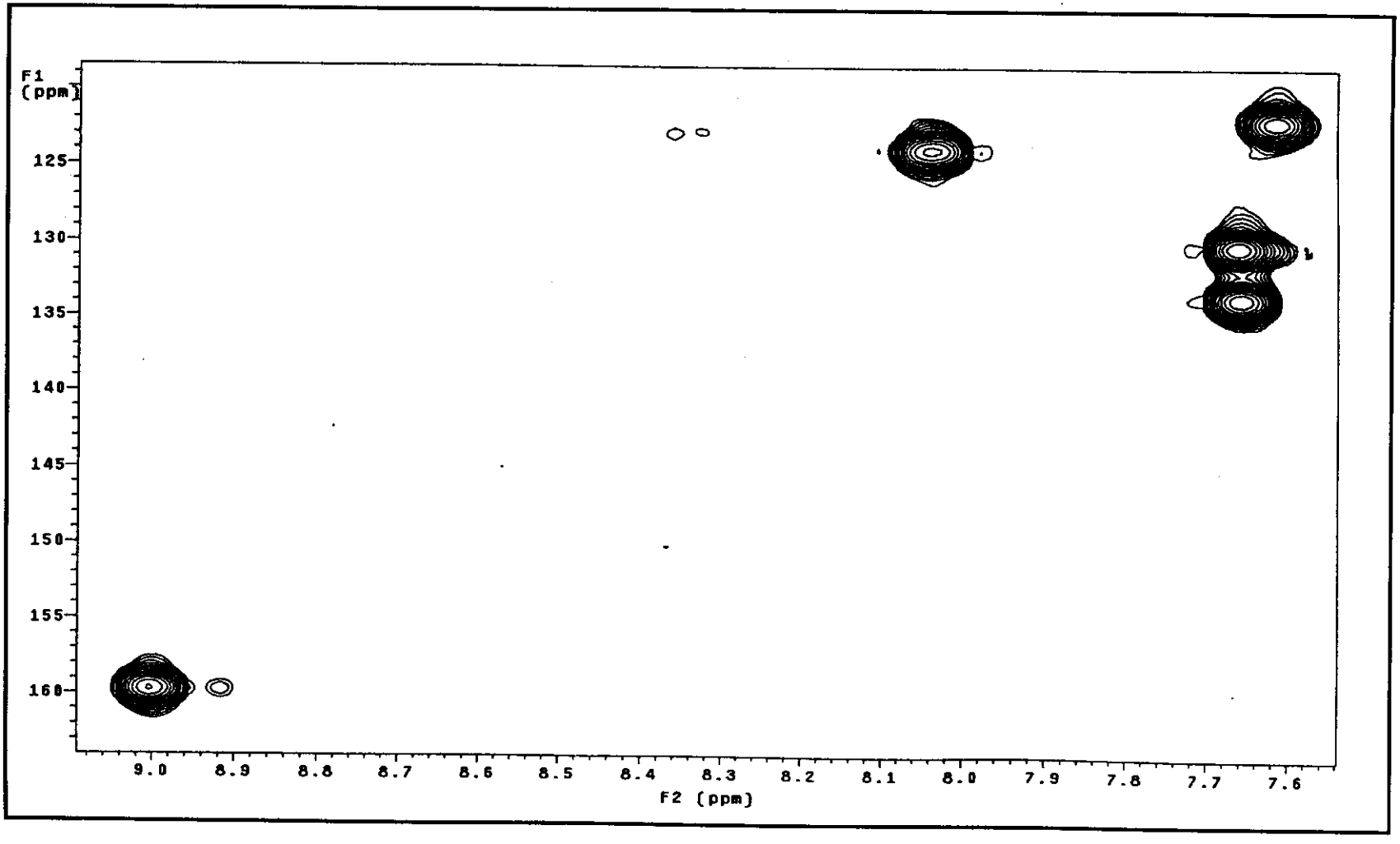

Figure 15 ^{1}H-^{13}C HMQC NMR spectrum of azpym in acetone-d_6.

Table 6 The NMR spectroscopic data of the bpy ligand in acetone-d_6

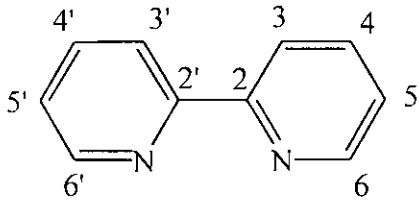

H-Position	^{1}H NMR			^{13}C NMR
	δ (ppm)	*J* (Hz)	Number of H	δ (ppm)
6, 6′	8.69 (ddd)	4.8, 2.0, 1.0	2	149.94
3, 3′	8.49 (ddd)	8.0, 1.0, 1.0	2	137.69
4, 4′	7.94 (ddd)	7.5, 8.0, 1.5	2	124.68
5, 5′	7.43 (ddd)	8.0, 5.0, 1.0	2	121.34
Quaternary carbon				156.65

ddd = doublet of doublet of doublet

Figure 16 showed the ^{1}H NMR of the bpy ligand. All the signals were well seperated. The bpy ligand had four equivalent protons on molecule. The protons of the H6 (H6′), H3 (H3′), H4 (H4′) and H5 (H5′) occured at 8.69 (ddd), 8.49 (ddd), 7.94 (ddd) and 7.43 (ddd) ppm, respectively. The assignment of signals were based on the data from of ^{1}H-^{1}H COSY NMR spectroscopy (Figure 17).

The chemical shift of proton H6 occurred at lower field than other protons because proton H6 was located next to the nitrogen atom. The signal of proton H3 appeared at lower field than proton H4 and H5 but higher field than proton H6. It showed as doublet of doublet of doublet (ddd) with *J*-coupling 8.0 (H4), 1.0 (H5), 1.0 (H6) Hz at 8.49 ppm.

The ^{13}C NMR signal assignments (Figure 18) were based on the data from ^{1}H-^{13}C HMQC NMR spectroscopy (Figure 19). The ^{13}C NMR spectrum of the bpy ligand displayed 4 resonance signals in aromatic region. The downfield resonance at 156.65 ppm was assigned to the quaternary carbon (C2, C2′). The methine carbons occurred at 149.94, 137.69, 124.68 and 121.34 ppm were assigned to C6 (6′), C3 (3′), C4 (4′) and C5 (5′) positions, respectively.

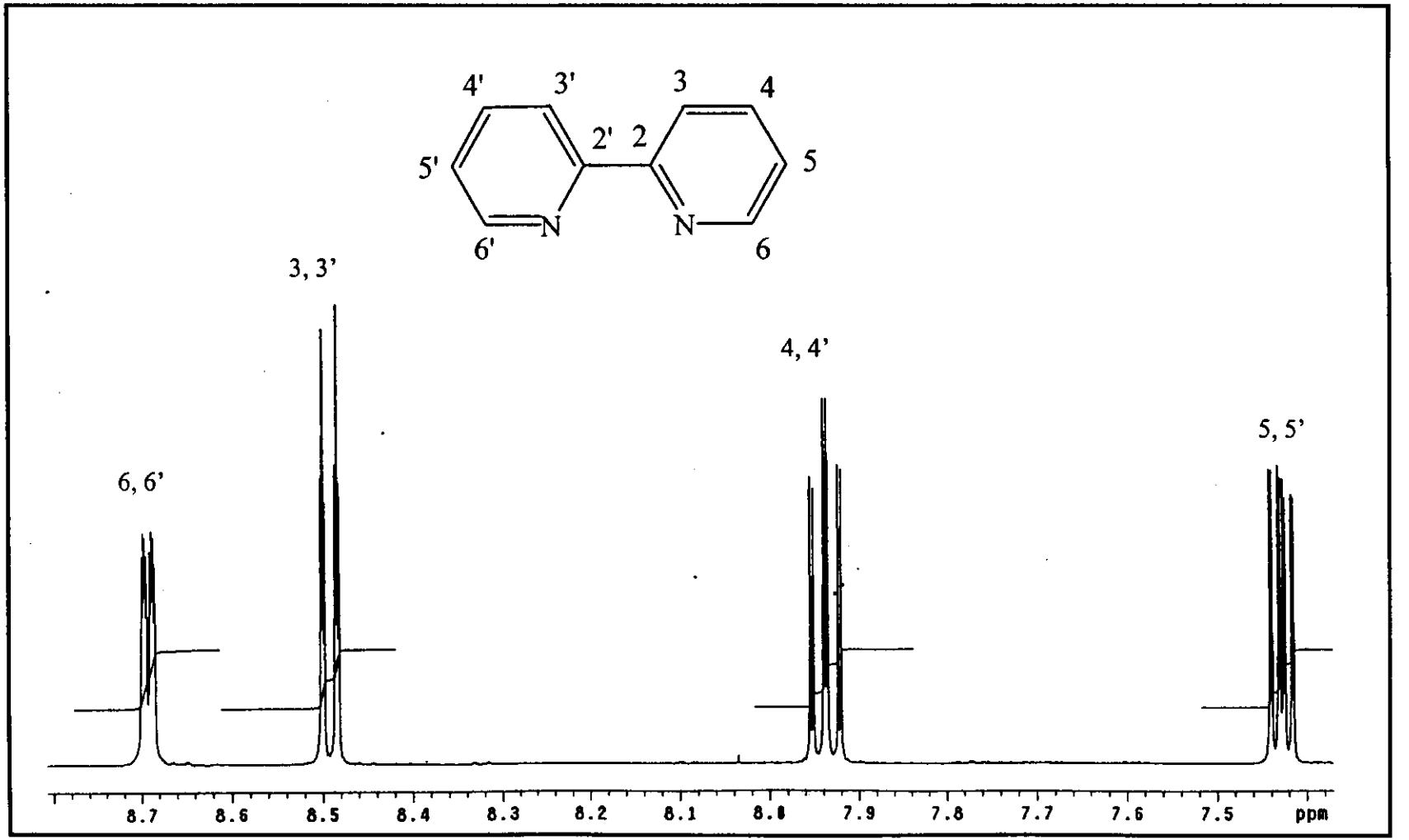

Figure 16 ^{1}H NMR spectrum of bpy in acetone-d_6

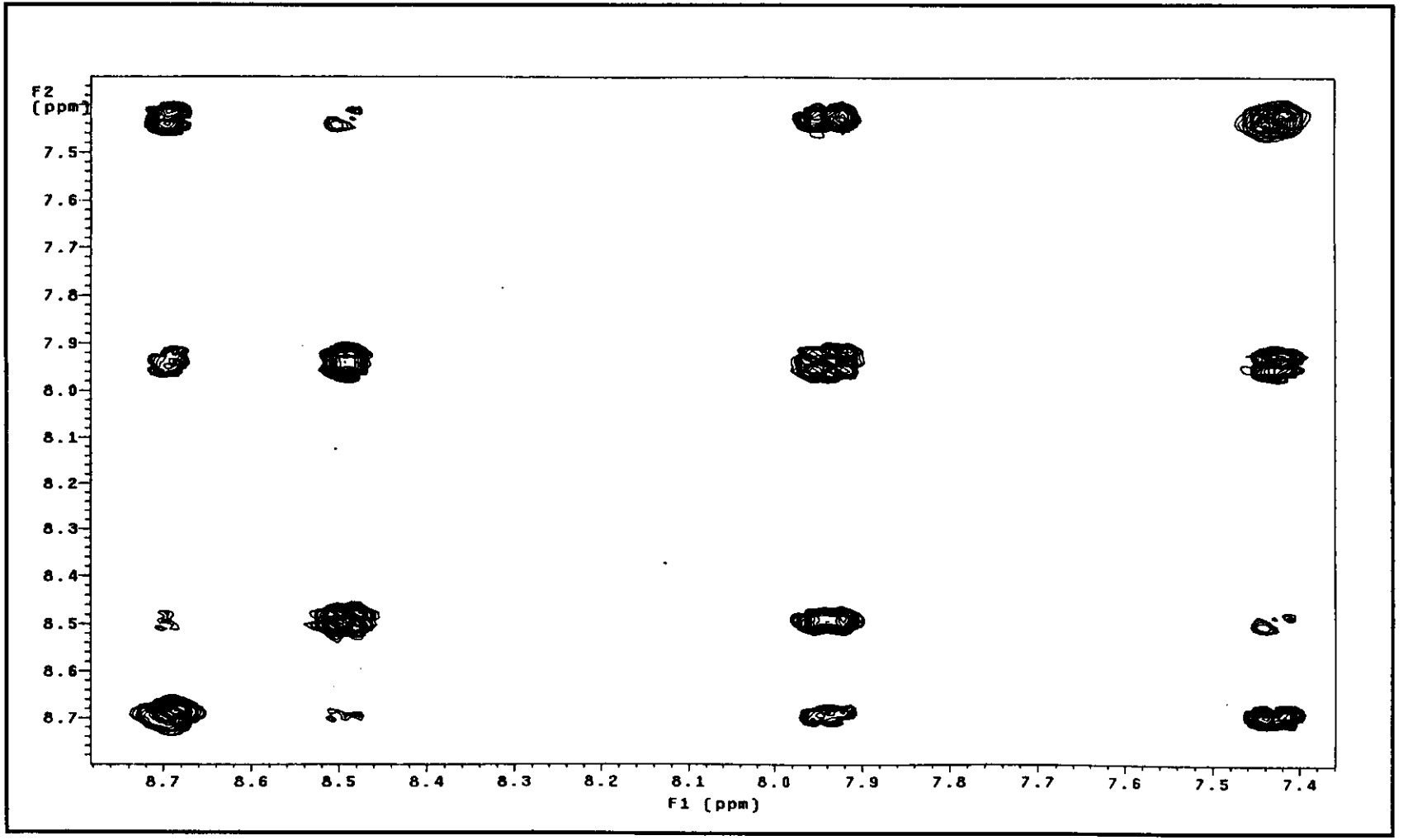

Figure 17 ^{1}H-^{1}H COSY NMR spectrum of bpy in acetone-d_6.

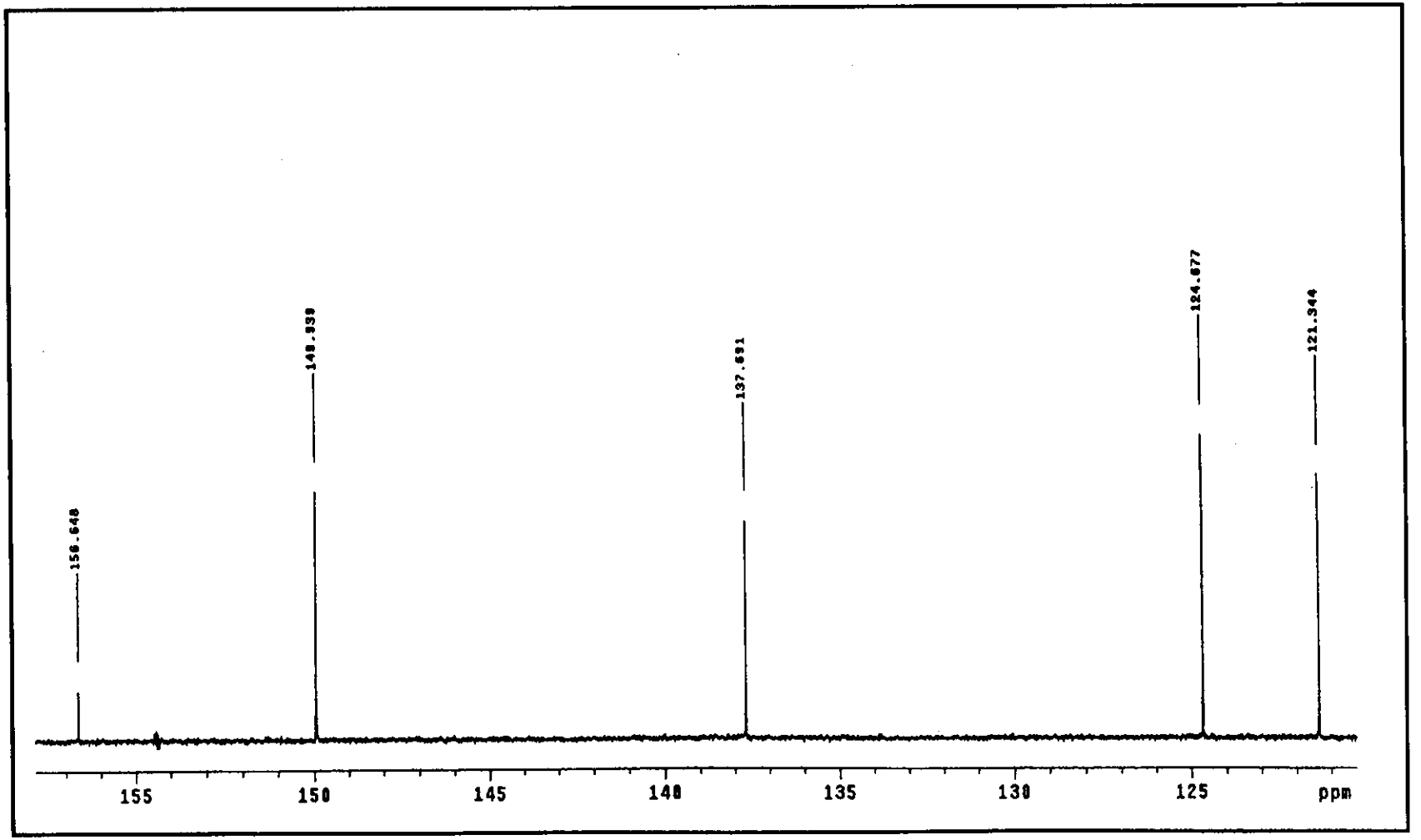

Figure 18 ^{13}C NMR spectrum of bpy in acetone-d_6.

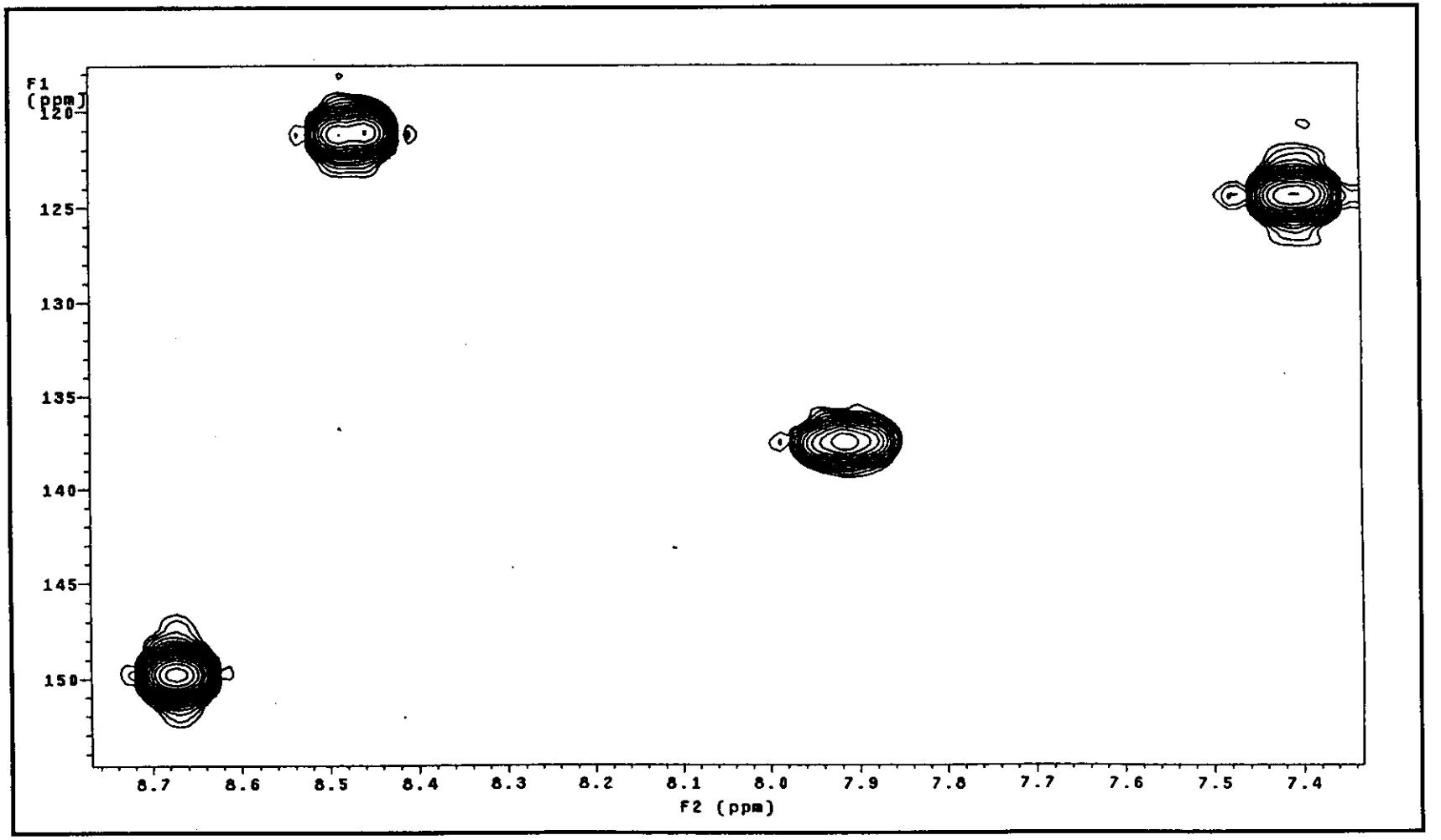

Figure 19 ^{1}H-^{13}C HMQC NMR spectrum of bpy in acetone-d_6.

Table 7 The NMR spectroscopic data of the phen ligand in acetone-d_6

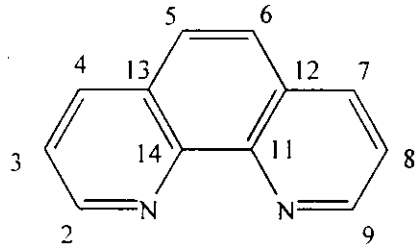

H-Position	^{1}H NMR			^{13}C NMR
	δ (ppm)	J (Hz)	Number of H	δ (ppm)
2, 9	9.18 (dd)	4.5, 1.5	2	150.76
4, 7	8.48 (dd)	8.5, 1.5	2	136.94
5, 6	7.98 (s)	-	2	127.40
3, 8	7.78 (dd)	8.0, 4.5	2	123.96
Quaternary carbon				146.76, 129.53

dd = doublet of doublet and s = singlet

The ^{1}H NMR spectrum of the phen ligand (Figure 20) in acetone-d_6 indicated again the presence of four signals. The phen ligand had four equivalent proton on molecule. The assignment of signals were based on the used of ^{1}H-^{1}H COSY NMR spectra (Figure 21).

The chemical shift of proton H2 occurred at lower field than other protons. It appeared doublet of doublet and splitted by proton H3 (J = 4.5 Hz) and H4 (J = 1.5Hz) at 9.18 ppm. The proton H3 was located between proton H2 and H4 and gave the coupling constant J = 4.5 and 8.0 Hz, respectively. The proton H4 occurred downfield than proton H5, which coupled with H3 (J = 8.5 Hz) and H2 (J = 1.5 Hz). The signal of proton H5 was observed at 7.98 ppm.

The ^{13}C NMR signal assignments (Figure 22) were based on the ^{1}H-^{13}C HMQC NMR spectra (Figure 23). The ^{13}C NMR spectrum of the phen ligand displayed 4 resonance signals in aromatic region. The downfield resonance at 146.76 ppm was assigned to quaternary carbon which was located near one of nitrogen. The signal at 129.53 ppm was assigned to quaternary carbon C12(14) which was not closed to nitrogen atom. The signals at 150.76, 136.94, 127.40 and 123.96 ppm were assigned to C2 (9), C4 (7), C5 (6) and C3 (8) positions, respectively.

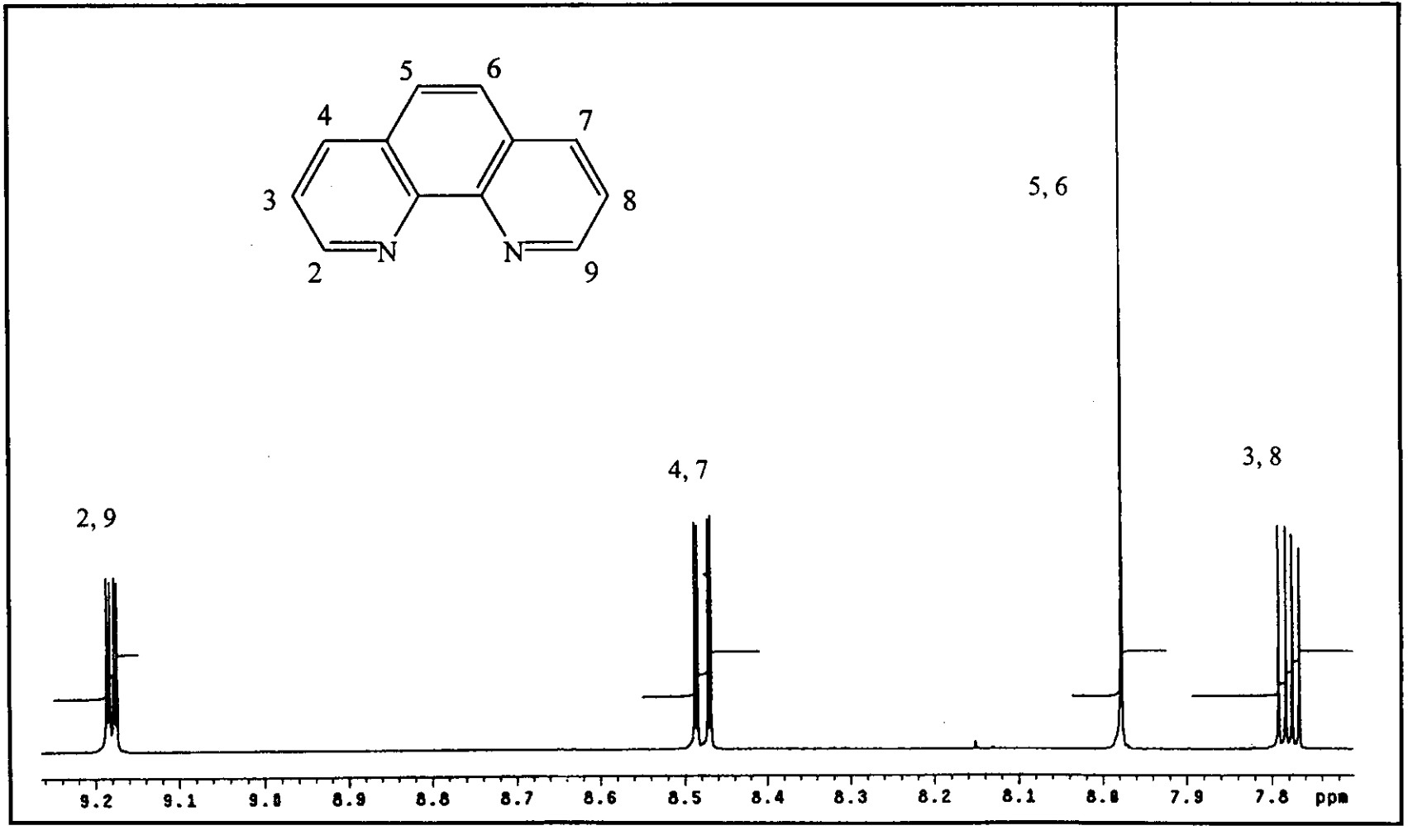

Figure 20 ^{1}H NMR spectrum of phen in acetone-d_6.

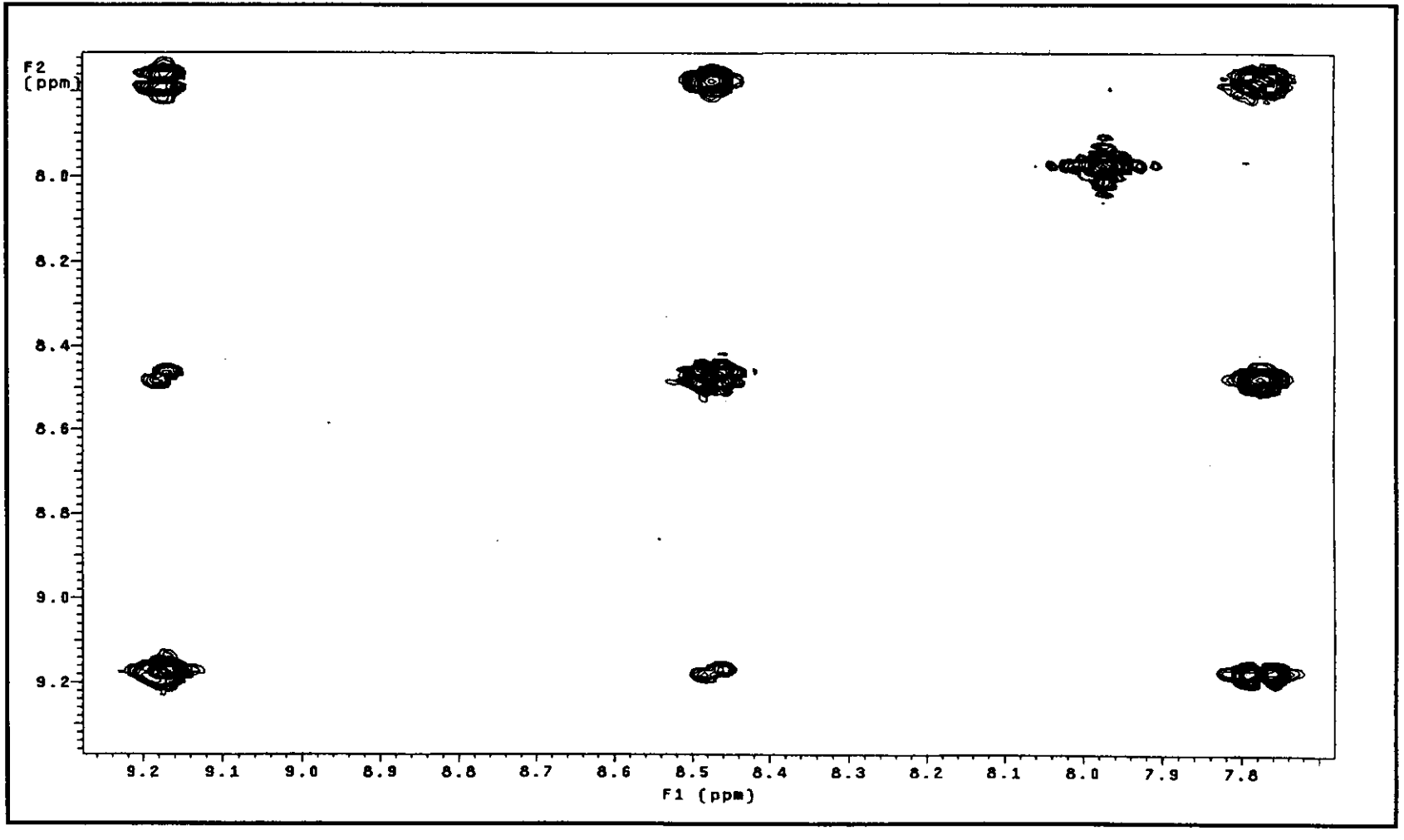

Figure 21 ^{1}H-^{1}H COSY NMR spectrum of phen in acetone-d_6.

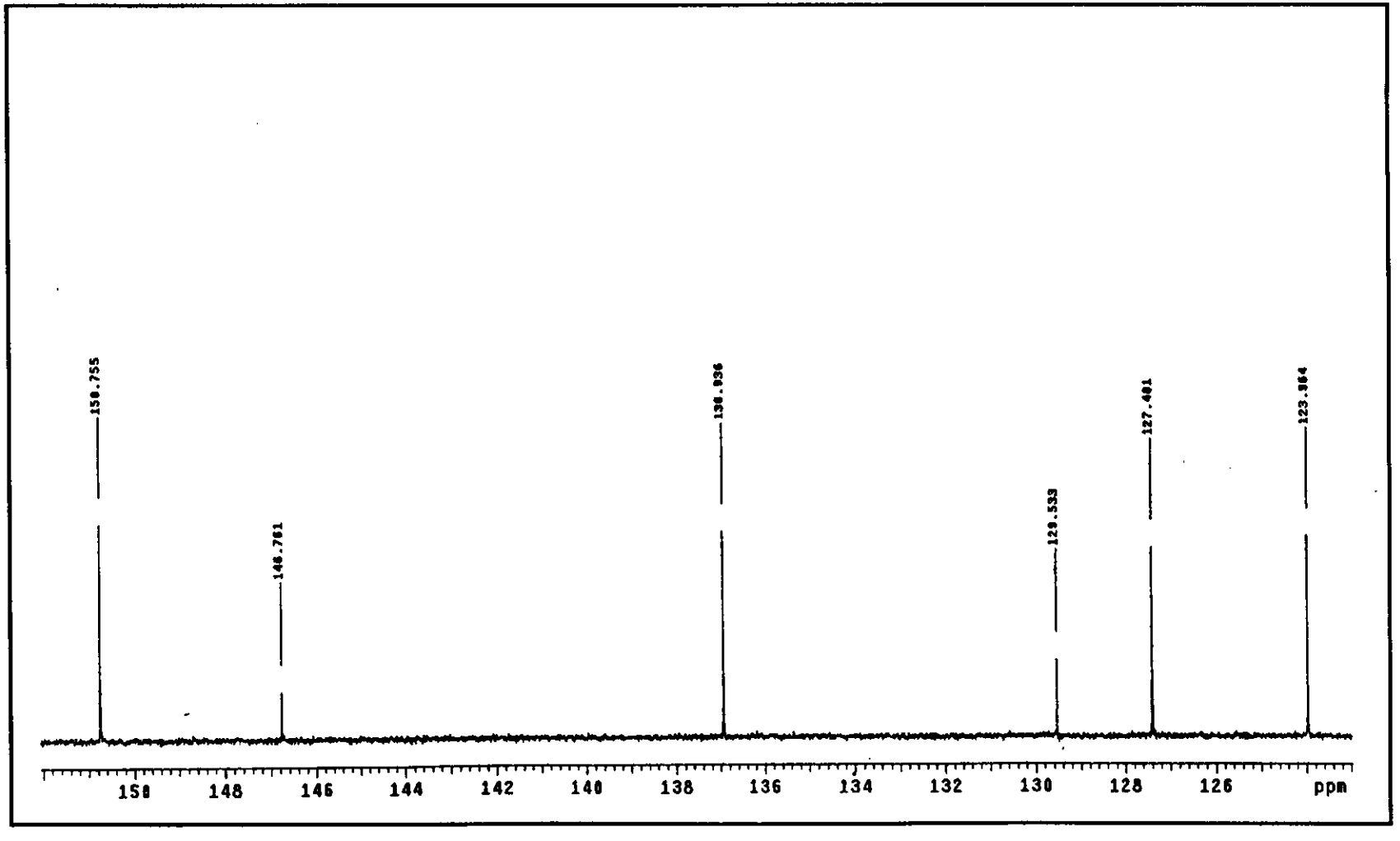

Figure 22 ^{13}C NMR spectrum of phen in acetone-d_6.

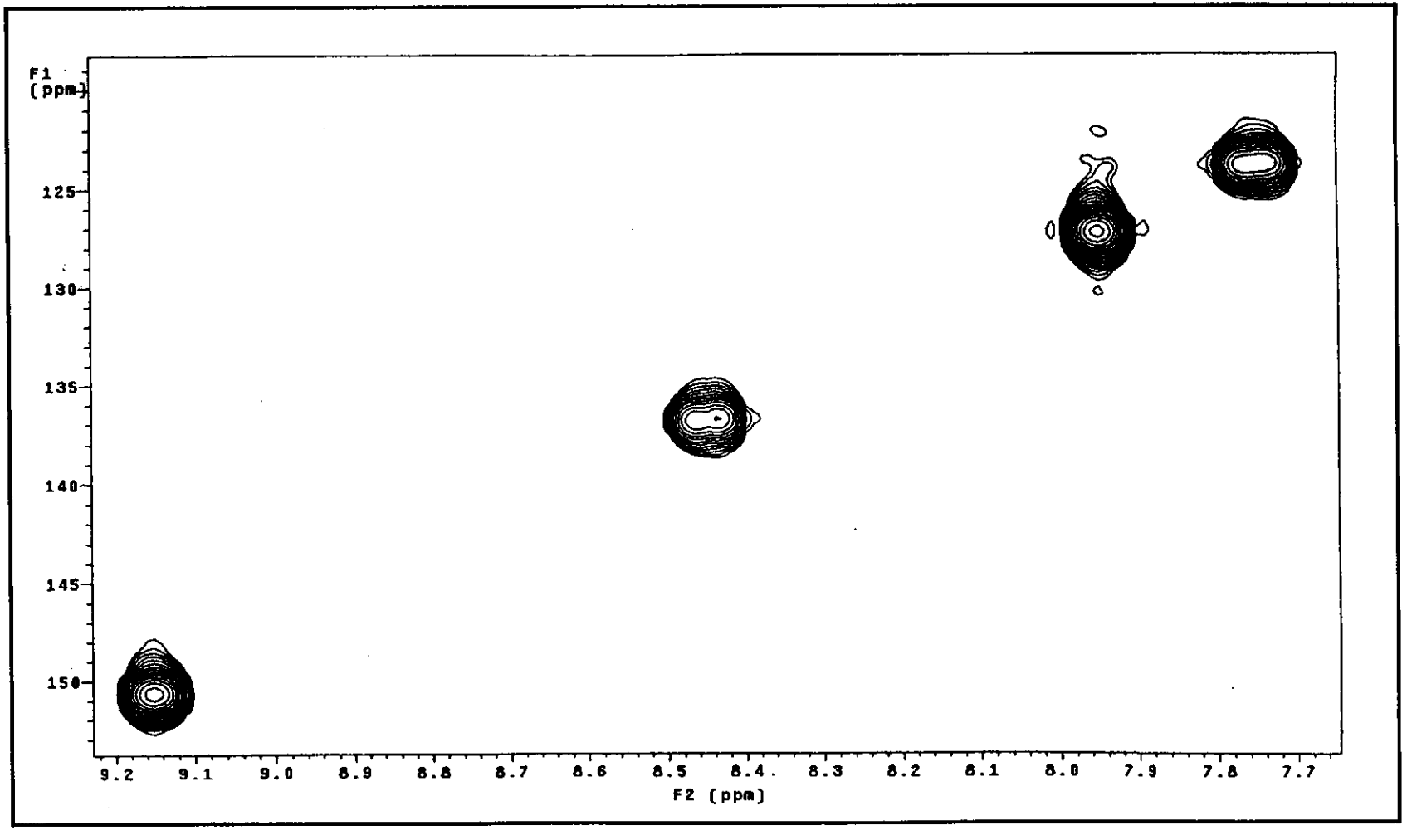

Figure 23 ^{1}H-^{13}C HMQC NMR spectrum of phen in acetone-d_6.

3.2.3 Cyclic voltammetry

Cyclic voltammetry is a technique to study the oxidation-reduction processes of the azpy and the azpym ligands. The cyclic voltammograms in acetonitrile solution of both ligands are shown in Figure 24 to 25, respectively (with half-wave potential). In addition, the potentials were compared to the potential of ferrocene couple ($E_{1/2}$ = 0 V, ΔE_p= 65 mV).

In this experiment, the different scan rates were used to examine the couple or redox reaction. The couple having equal anodic and cathodic current was referred to the reversible couple. In contrast, the unequal current was referred to the unequal transfer of the electron in the reduction and oxidation. This led to irreversible couple. The results of cyclic voltammetry are summarized in Table 8.

Table 8 Cyclic voltammetric data of the azpy and the azpym ligands in 0.1 M TBAH acetonitrile at scan rate 50 mV/s (ferrocene as an internal standard, ΔE_p = 65 mV)

Ligand	Oxidation		Reduction	
	E_{pa}, V	E_{pc}, V	E_{pa}, V	E_{pc}, V
Azpy	-	-	-1.47	-1.61
Azpym	-	-	-1.05	-1.32

E_{pa} = anodic peak and E_{pc} = cathodic peak

Reduction range

The cyclic voltammetry on azpy and azpym ligands were carried out in the range 0.0 to 2.0 V. The experiments showed two irreversible couples. The E_{pc} of the azpym ligand occurred closer to 0.0 V than the azpy ligand.

Oxidation range

The cyclic voltammograms of the azpy and the azpym showed no signal in the potential range 0.0 to + 1.3 V.

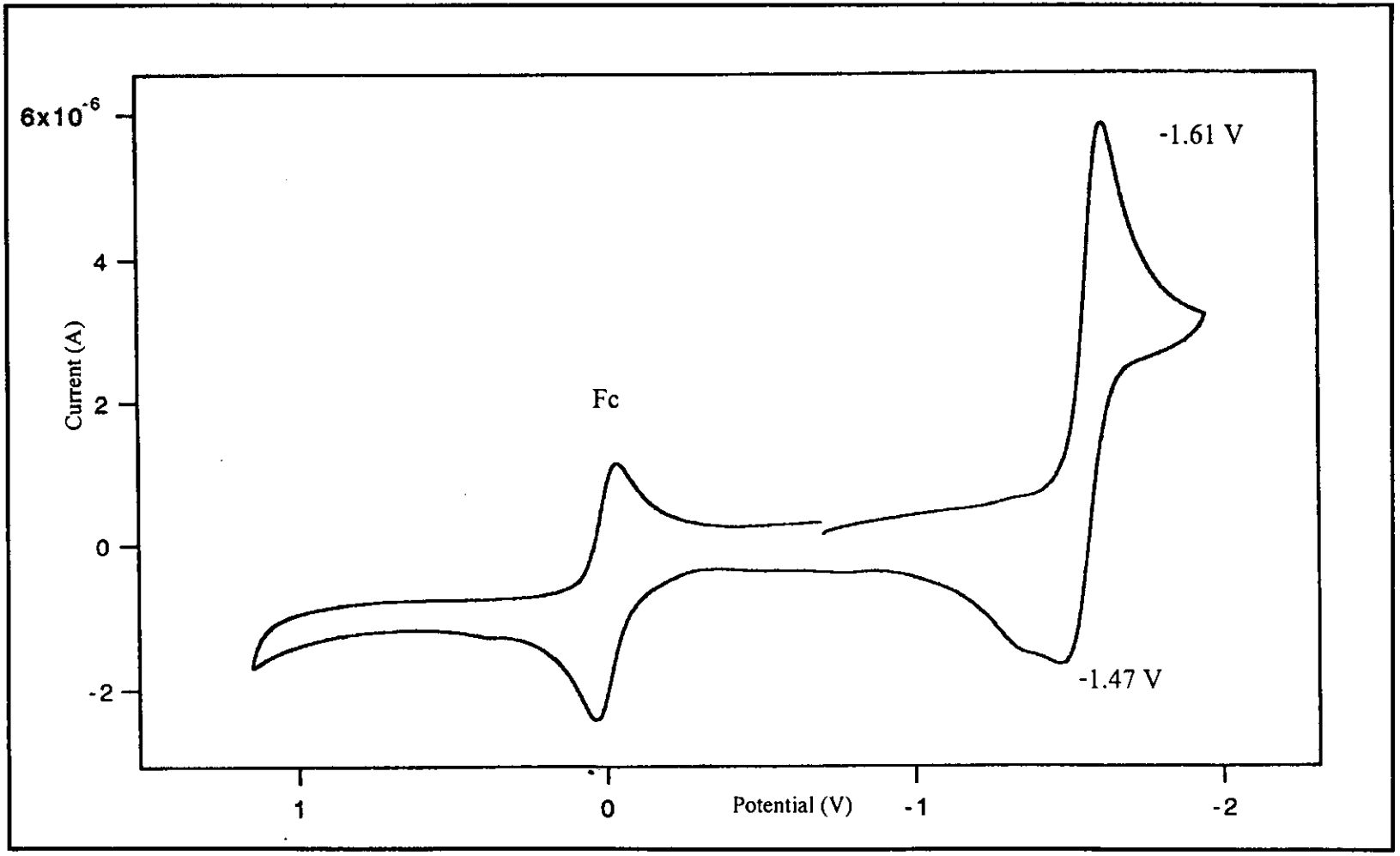

Figure 24 Cyclic voltammogram of azpy in 0.1 M TBAH CH_3CN at scan rate 50 mV/s.

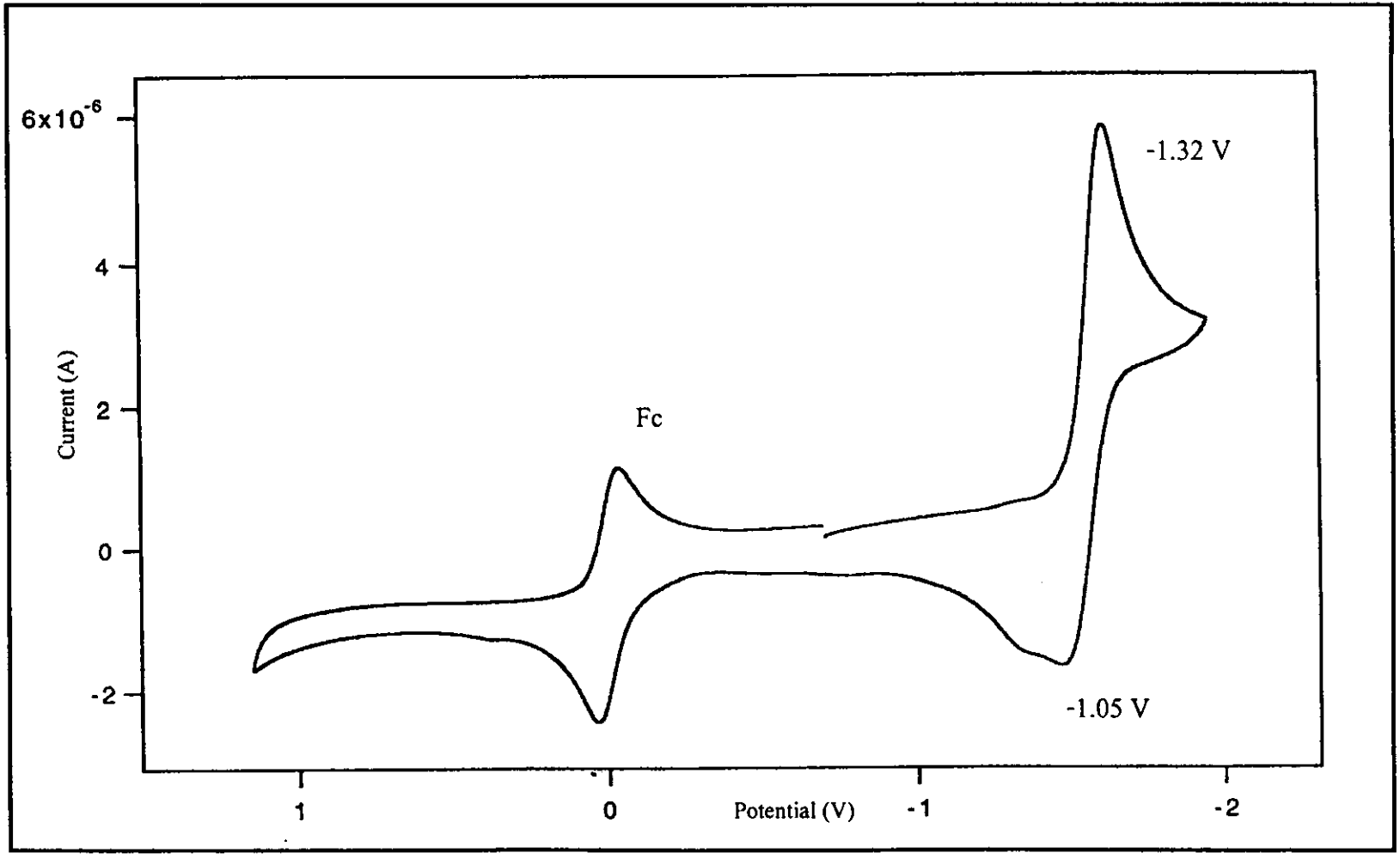

Figure 25 Cyclic voltammogram of azpym in 0.1 M TBAH CH_3CN at scan rate 50 mV/s.

3.3 Preparation and characterization of the $Ru(azpy)_2Cl_2$

The $Ru(azpy)_2Cl_2$ complex was synthesized from the reaction of $RuCl_3.3H_2O$ and azpy in ethanol. This complex occurred in three isomeric forms designated as *trans-cis-cis (tcc,* γ, with respect to chlorides, pyridines, and azo nitrogens respectively), *cis-trans-cis (ctc,* α) and *cis-cis-cis (ccc,* β). The order of elution from column chromatography is *tcc*-isomer, *ctc*-isomer, *ccc*-isomer.

The three isomers of $Ru(azpy)_2Cl_2$ complex were characterized by Elemental Analysis, FAB-mass spectrometry, Infrared spectroscopy and Nuclear Magnetic Resonance spectroscopy.

Only one isomer, *ctc*-$Ru(azpy)_2Cl_2$ which used as precursor for synthesis the $[Ru(azpy)_2L]^{2+}$ complexes, was also characterized by UV-Visible absorption spectroscopy and Cyclic voltammetry.

3.3.1 Elemental analysis

Elemental analysis is a technique to confirm composition of C, H, N in complexes. The analytical data of *tcc*, *ctc*, *ccc*-$Ru(azpy)_2Cl_2$ complexes corresponded to the calculated values. The elemental analysis data are listed in Table 9.

Table 9 Elemental analysis data of three isomers of $Ru(azpy)_2Cl_2$

Complexes	%C		%N		%H	
	Calc.	Found	Calc.	Found	Calc.	Found
tcc-$Ru(azpy)_2Cl_2$	49.08	47.84	15.61	15.00	3.37	3.37
ctc-$Ru(azpy)_2Cl_2$	49.08	48.97	15.61	15.62	3.37	3.62
ccc-$Ru(azpy)_2Cl_2$	49.08	49.64	15.61	15.83	3.37	3.50

3.3.2 The FAB mass spectrometry

The FAB mass spectrometry is a technique to study molecular mass of all Complexes.The FAB mass spectra of *tcc*, *ctc*, *ccc*-$[Ru(azpy)_2Cl_2]$ complexes are shown in Figure 26 to 28. The results of FAB mass spectra with the corresponding relative abundance are summarized in Table 10.

Table 10 FAB mass spectrometric data of the three isomers of $Ru(azpy)_2Cl_2$

Complexes	m/z	Stoichiometry	Equivalent Species	Rel. Abun.
tcc-$Ru(azpy)_2Cl_2$	538	$[Ru(azpy)_2Cl_2]$	[M]	50
	503	$[Ru(azpy)_2Cl]^+$	$[M-Cl]^+$	26
	307	$[Ru(azpy)]^{2+} + Na^+$	$[M\text{-azpy-}2Cl]^{2+} + Na^+$	100
ctc-$Ru(azpy)_2Cl_2$	561	$[Ru(azpy)_2Cl_2] + Na^+$	$[M] + Na^+$	30
	538	$[Ru(azpy)_2Cl_2]$	[M]	65
	503	$[Ru(azpy)_2Cl]^+$	$[M-Cl]^+$	100
	467	$[Ru(azpy)_2]^{2+}$	$[M-2Cl]^{2+}$	33

Table 10 (continued)

Complexes	m/z	Stoichiometry	Equivalent Species	Rel. Abun.
ccc -$Ru(azpy)_2Cl_2$	561	$[Ru(azpy)_2Cl_2] + Na^+$	$[M] + Na^+$	42
	538	$[Ru(azpy)_2Cl_2]$	[M]	94
	503	$[Ru(azpy)_2Cl]^+$	$[M-Cl]^+$	100
	467	$[Ru(azpy)_2]^{2+}$	$[M-2Cl]^{2+}$	40

M= Molecular weight (MW) of $Ru(azpy)_2Cl_2$

MW of $Ru(azpy)_2Cl_2$ = 538.7 g/mol

Parent ion peaks and expected fragments of the complexes were detected. The molecular weight of $Ru(azpy)_2Cl_2$ was 538.7 g/mol. In the FAB mass spectrum of *tcc*-$Ru(azpy)_2Cl_2$ complex (Figure 30), a strong peak at m/z = 307 (100%) was observed and attributed to the $[Ru(azpy)]^{2+}$+ Na^+ cation (Figure 31) and the peak at m/z = 538 (50%) was assigned to $Ru(azpy)_2Cl_2$. The *ctc*-isomer (Figure 31) showed the main peak at m/z = 503 (100%) which was assigned to the loss of chloride atom. The peak at m/z = 538 (65%) corresponded to $Ru(azpy)_2Cl_2$. The *ccc*-isomer gave the same result.

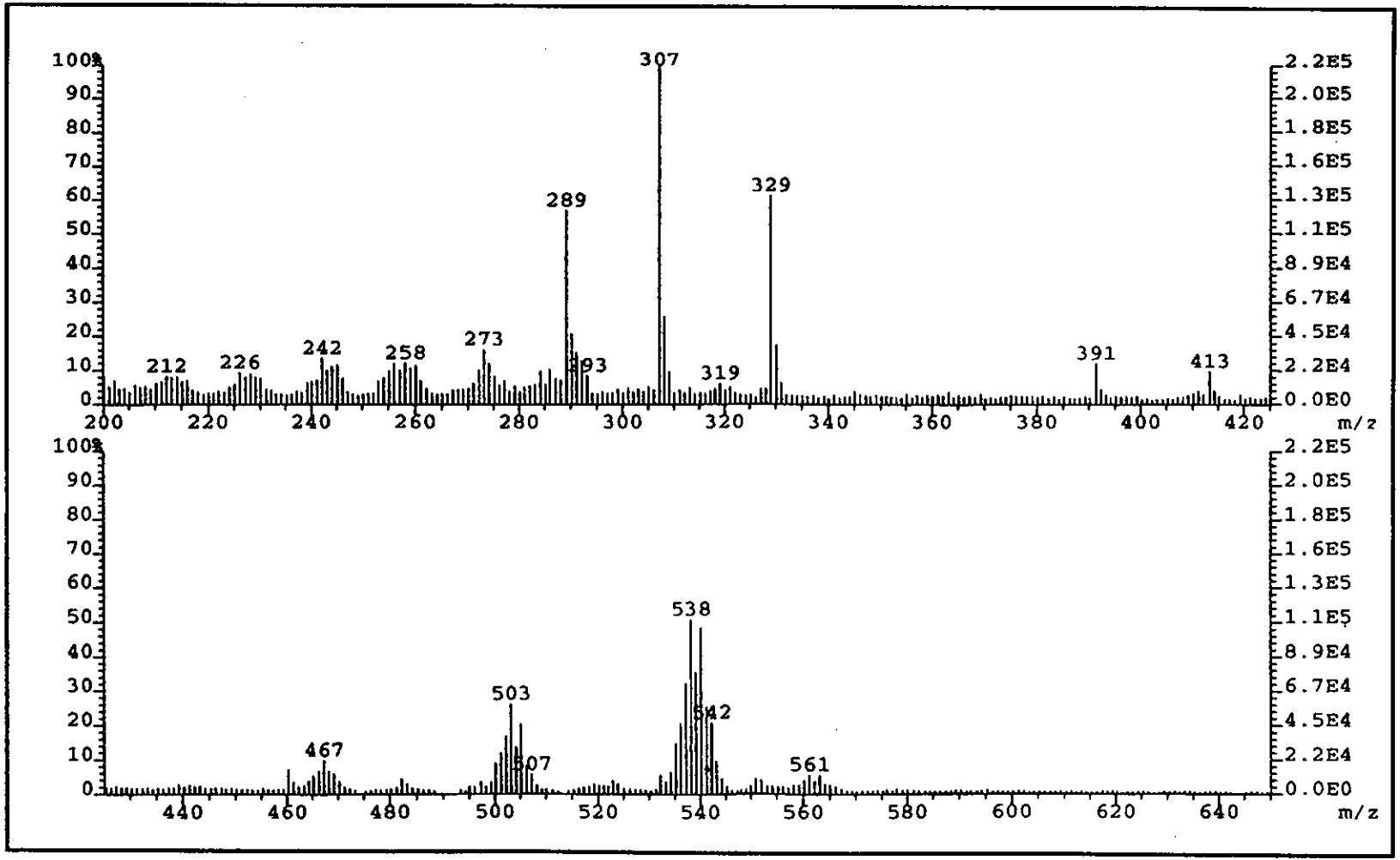

Figure 26 FAB mass spectrum of *tcc*-Ru(azpy)$_2$Cl$_2$.

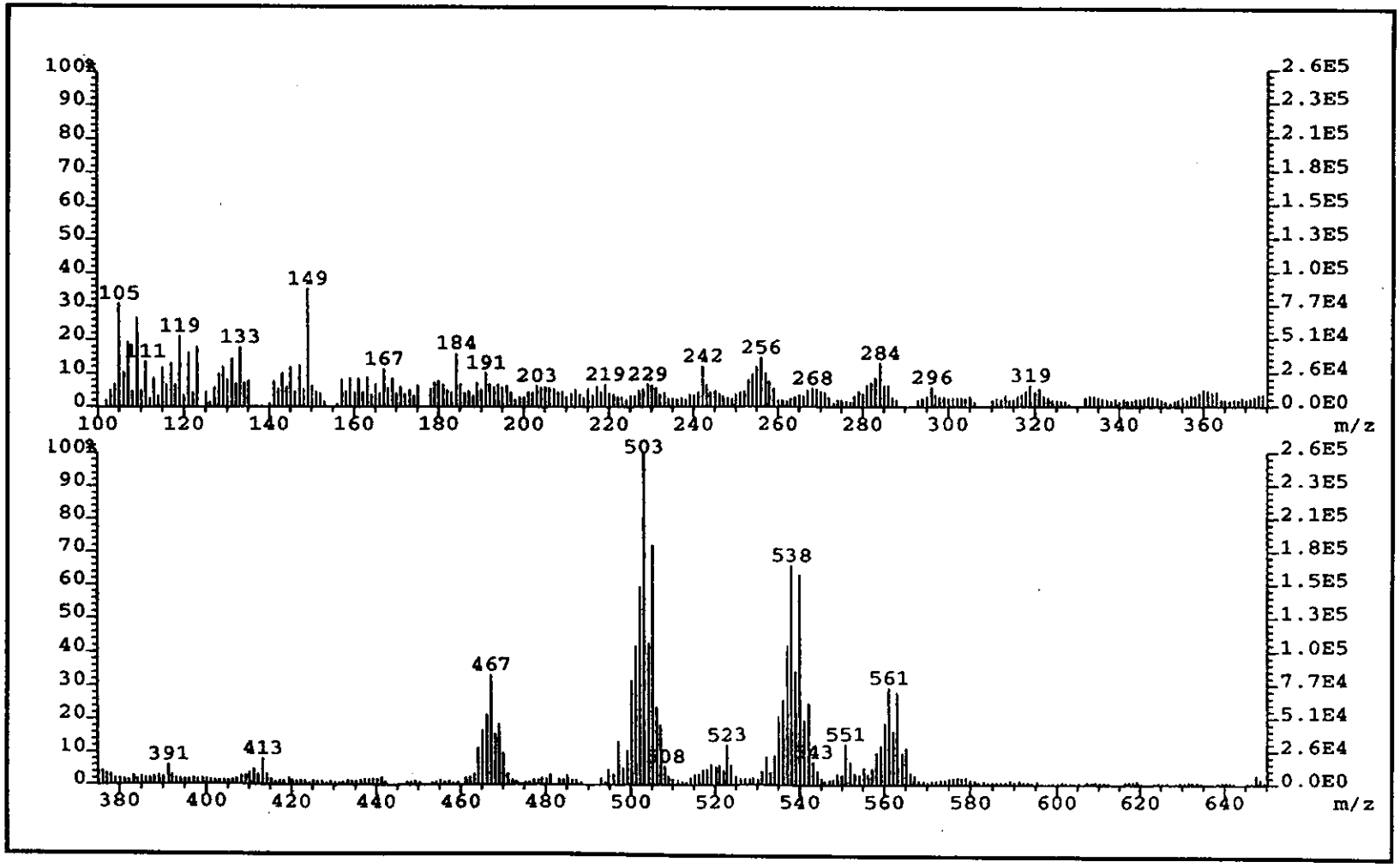

Figure 27 FAB mass spectrum of *ctc*-Ru(azpy)$_2$Cl$_2$.

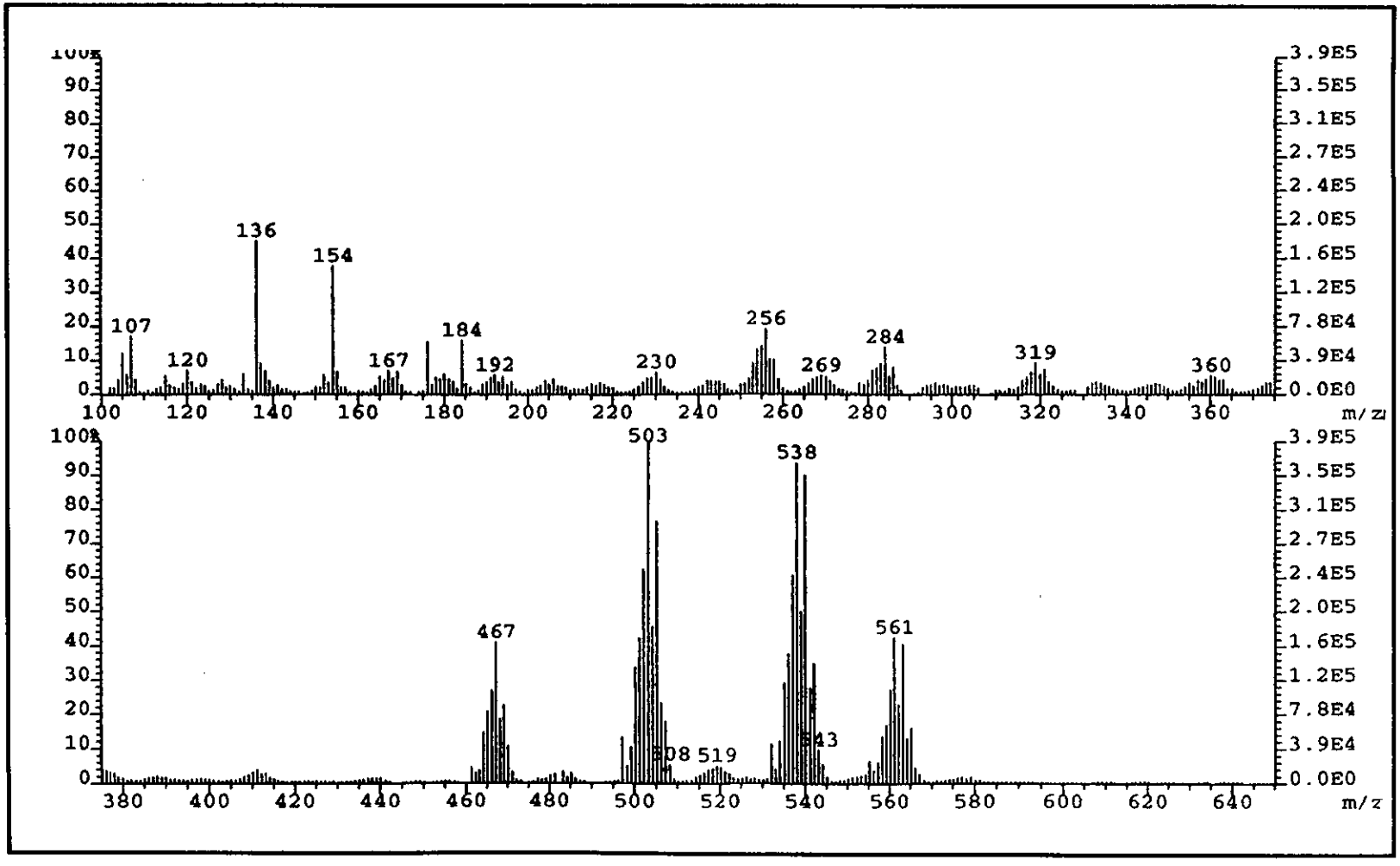

Figure 28 FAB mass spectrum of *ccc*-Ru(azpy)$_2$Cl$_2$.

3.3.3 Infrared spectroscopy

The Infrared spectroscopy is a technique to study functional group in complexes. The infrared spectra of *tcc*, *ctc*, *ccc*-$Ru(azpy)_2Cl_2$ were appeared in the range 1800-370 cm^{-1}. The infrared spectroscopic data were shown in Table 11. The infrared spectra of complexes were shown in Figure 29 to 31.

Table 11 Infrared spectroscopic data of three isomers of $Ru(azpy)_2Cl_2$

Vibrational modes	Frequencies (cm^{-1})		
	tcc-$Ru(azpy)_2Cl_2$	*ctc*-$Ru(azpy)_2Cl_2$	*ccc*-$Ru(azpy)_2Cl_2$
N=N (azo)stretching	1289 (s)	1322 (s)	1317 (s)
C=C stretching and C=N stretching	1599 (m) 1482 (m) 1465 (m) 1451 (m)	1598 (m) 1480 (m) 1449 (m)	1599 (m) 1482 (m) 1451 (s)
C-H out of plane bending	778 (m) 746 (m) 696 (m)	780 (m) 761 (m) 696 (m)	783 (s) 743 (m) 691 (s)

S = strong, m =medium

The vibrations of interest were four C=C, C=N stretching modes which were observed between 1450-1600 $cm^{-1}$and a N=N stretching mode near 1420 cm^{-1}. All isomers of $Ru(azpy)_2Cl_2$ complexes gave similar N=N stretching frequencies. In frared spectra of *tcc*-$Ru(azpy)_2Cl_2$, *ctc*-$Ru(azpy)_2Cl_2$ and *ccc*-$Ru(azpy)_2Cl_2$ showed the N=N

stretching vibration at 1289, 1322 and 1317 cm^{-1}, respectively. (An azo mode in free azpy occurred at 1421 cm^{-1}). The shift to lower energy in the complexes indicated less double-bond character in the N=N group. This was strong evidence for substantial π-back bonding to ruthenium through azo nitrogen.

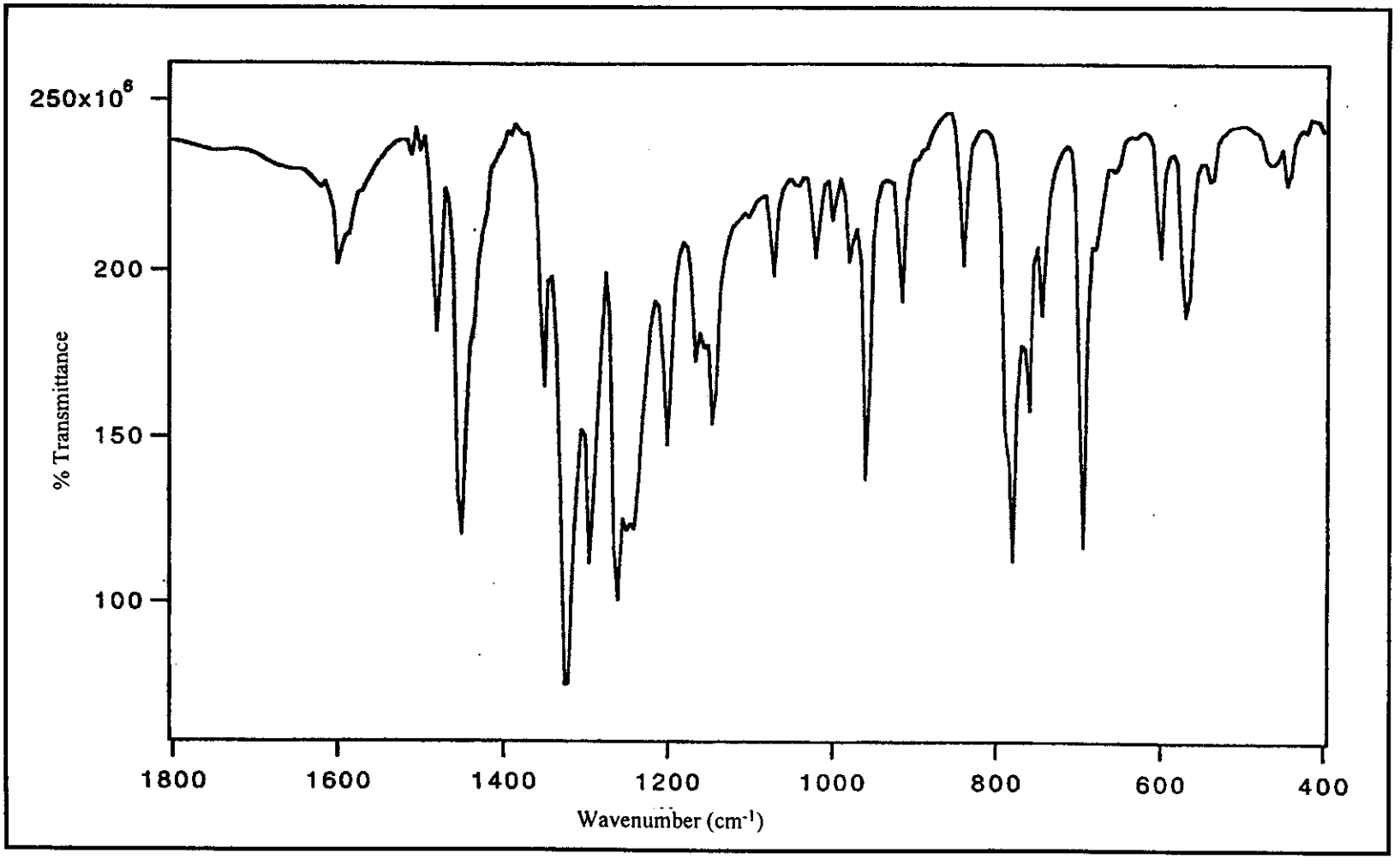

Figure 29 IR spectrum of *tcc*-Ru(azpy)$_2$Cl$_2$.

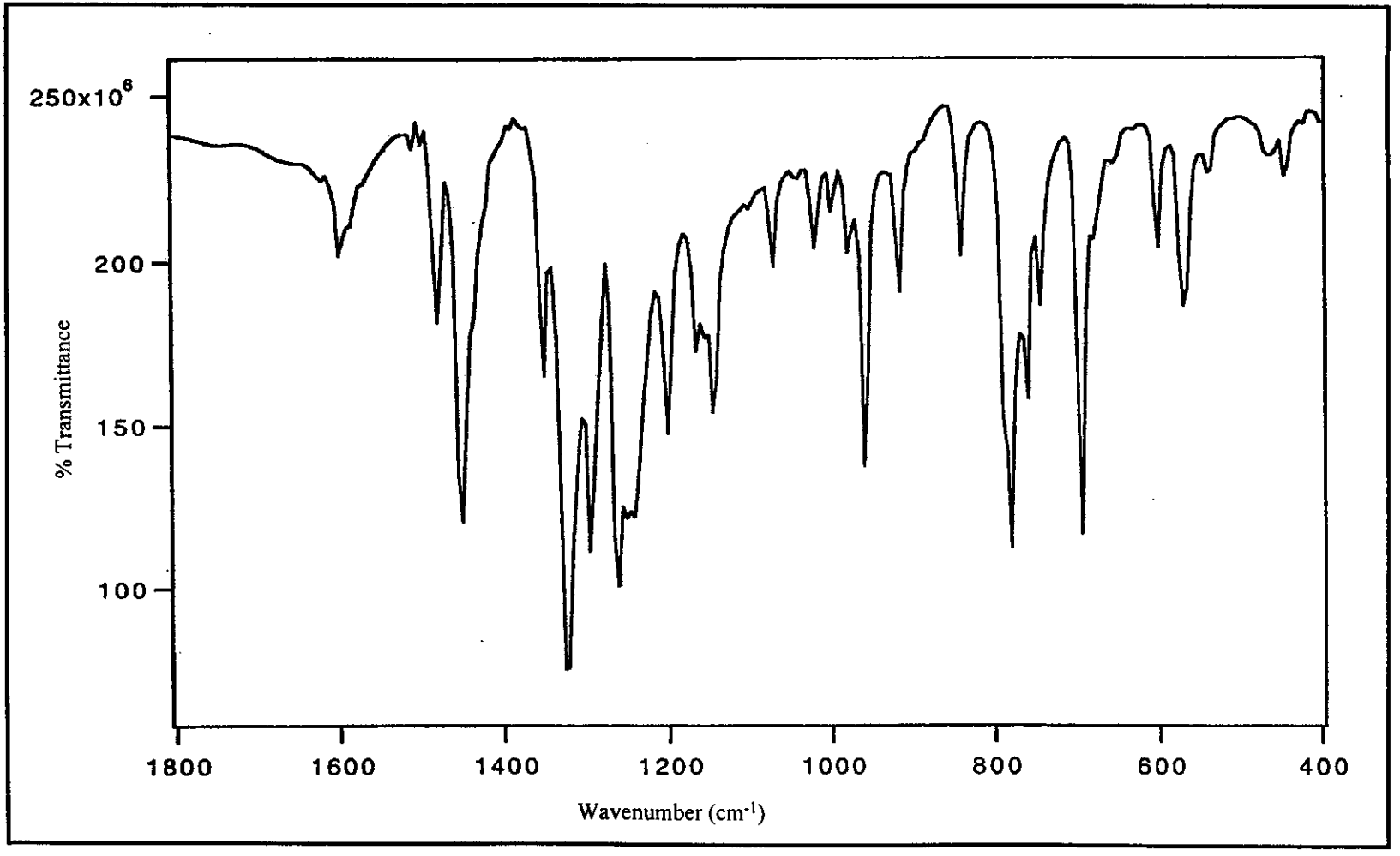

Figure 30 IR spectrum of *ctc*-$Ru(azpy)_2Cl_2$.

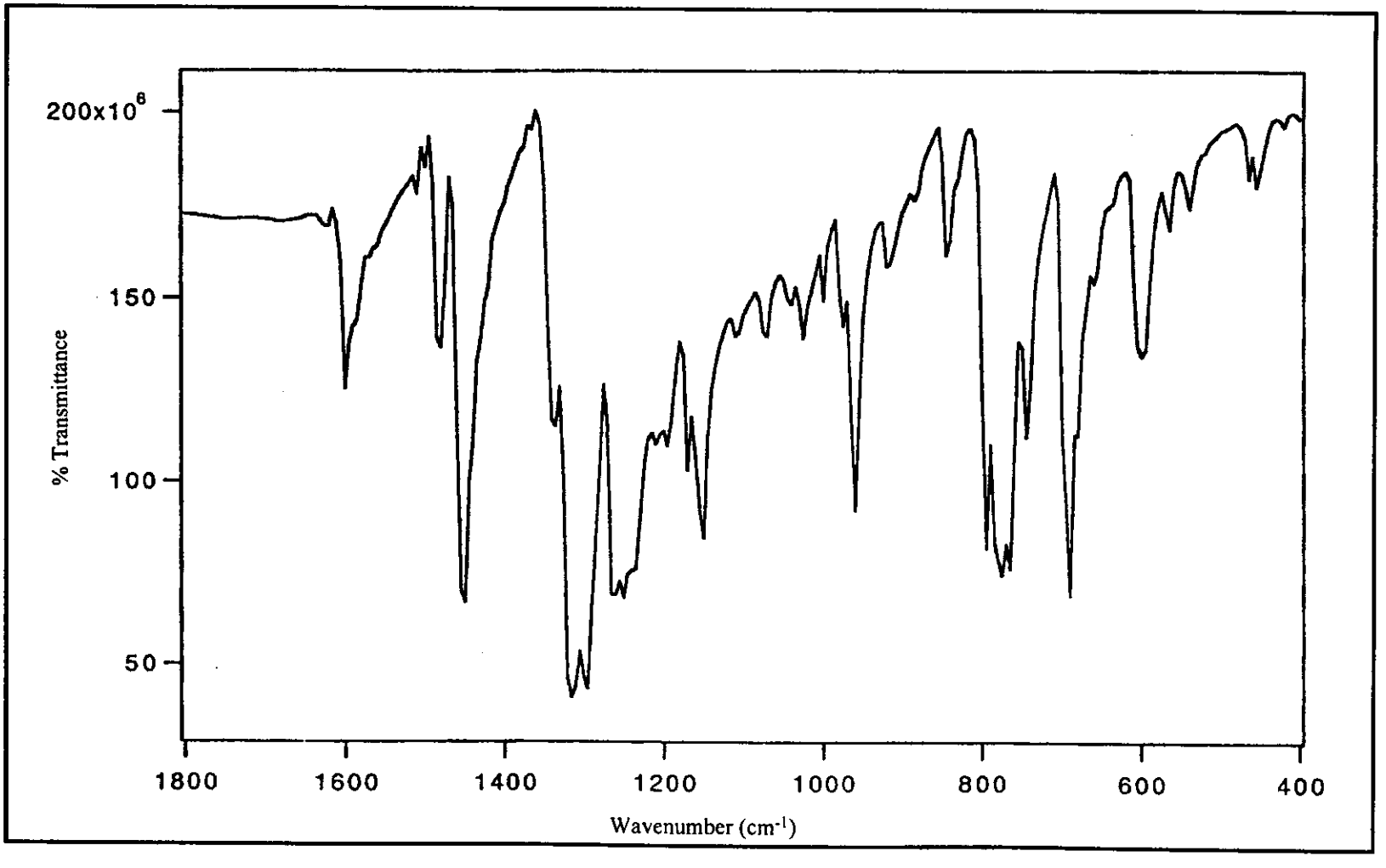

Figure 31 IR spectrum of *ccc*-$Ru(azpy)_2Cl_2$.

3.3.4 Nuclear Magnetic Resonance spectroscopy

The NMR spectroscopy is a technique to support the molecular configuration. The experiments were carried out in acetone-d_6. TMS was used an internal reference. The signals assignment of proton and carbon were made on the basis of peak integration, coupling constants and ^{1}H-^{1}H COSY and ^{1}H-^{13}C HMQC experiments. The ^{1}H NMR spectra of *tcc* and *ctc*-Ru(azpy)$_2$Cl$_2$ showed only one set of ligands peaks, indicating two equivalent ligands, therefore the complex must be symmetric. The isomer *tcc*-Ru(azpy)$_2$Cl$_2$ and *ctc*-Ru(azpy)$_2$Cl$_2$ have C_{2v} and C_2 symmetry, respectively but isomer *ccc*-Ru(azpy)$_2$Cl$_2$ have less symmetry (C_1). The chemical shift data and corresponding assignments are presented on Table 12 to 14.

(a) *tcc*-Ru(azpy)$_2$Cl$_2$ complex

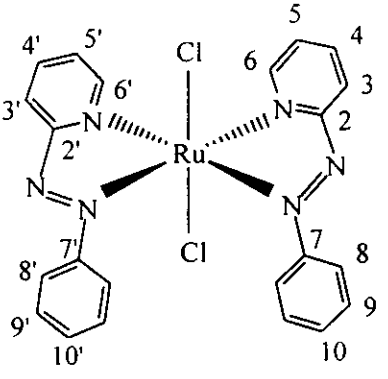

The ^{1}H NMR spectrum of *tcc*-Ru(azpy)$_2$Cl$_2$ (Figure 32) showed only one set of azpy peak, indicating two equivalent azpy ligands so the complex must be symmetric due to its C_{2v} axis. The pattern of ^{1}H NMR signals of *tcc*-Ru(azpy)$_2$Cl$_2$ was similar to that in the free ligands, but differ in chemical shifts. The chemical shift of proton H6 in metal complex occurred downfield more than free ligand because this

proton was closer to the coordination center. The assignment was made with the use of ^{1}H-^{1}H COSY NMR spectroscopy (Figure 33).

The ^{13}C NMR spectrum of this complex (Figure 34) showed 8 resonance signals. The assignment was based on the ^{1}H-^{13}C HMQC NMR spectroscopy (Figure 35). The downfield resonance at 166.02 ppm was assigned to quaternary carbon (C2). The chemical shift at 147.39 ppm belonged to quaternary carbon (C7). The methine carbon occurring at 150.09, 124.44, 141.52, 124.42, 123.13, 129.66 and 128.21 ppm were assigned to carbon in C6 (6′), C3 (3′), C4 (4′), C5 (5′), C8 (8′), C10 (10′) and C9 (9′) positions, respectively. The chemical shift data and corresponding assingnments were presented on Table 12.

Table 12 The NMR spectroscopic data of *tcc*-$Ru(azpy)_2Cl_2$ in acetone-d_6

H-Position	^{1}H NMR			^{13}C NMR
	δ (ppm)	*J* (Hz)	Number of H	δ (ppm)
6, 6′	9.15 (dd)	6.0, 1.0	2	150.09
3, 3′	8.65 (ddd)	7.5, 1.0, 1.0	2	124.44
4, 4′	8.39 (ddd)	8.0, 8.0, 1.5	2	141.52
5, 5′	8.01 (ddd)	7.5, 6.0, 1.0	2	124.42
8, 8′	7.55 (dd)	8.5, 1.5	4	123.13
10, 10′	7.22 (dd)	7.5, 1.5	2	129.66
9, 9′	7.03 (dd)	7.0, 7.0	4	128.21
Quaternary carbon				166.02, 147.39

dd = doublet of doublet, ddd = doublet of doublet of doublet

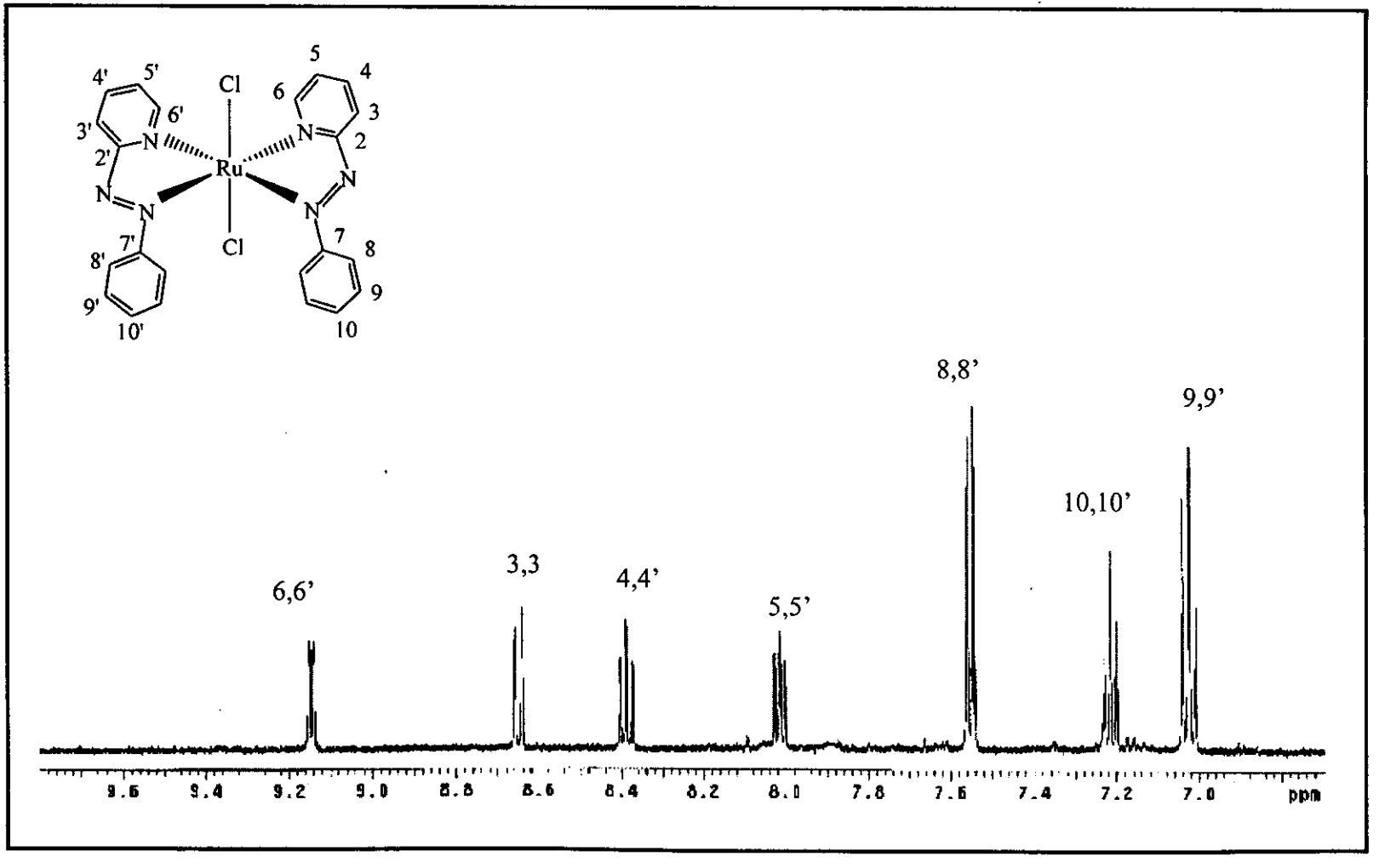

Figure 32 ^{1}H NMR spectrum of *tcc*-Ru(azpy)$_2$Cl$_2$ in acetone-d_6.

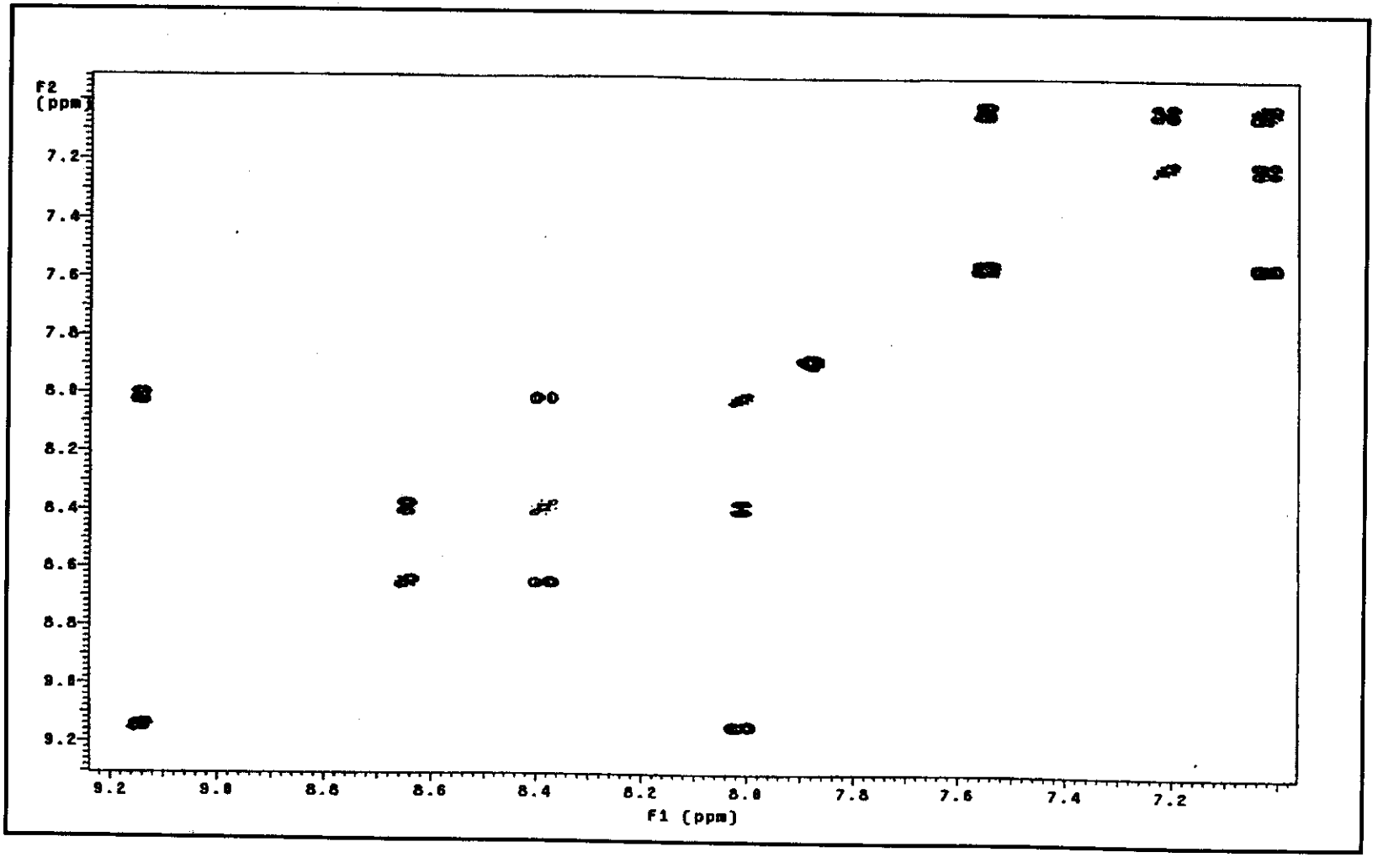

Figure 33 ^{1}H-^{1}H COSY NMR spectrum of *tcc*-$Ru(azpy)_2Cl_2$ in acetone-d_6.

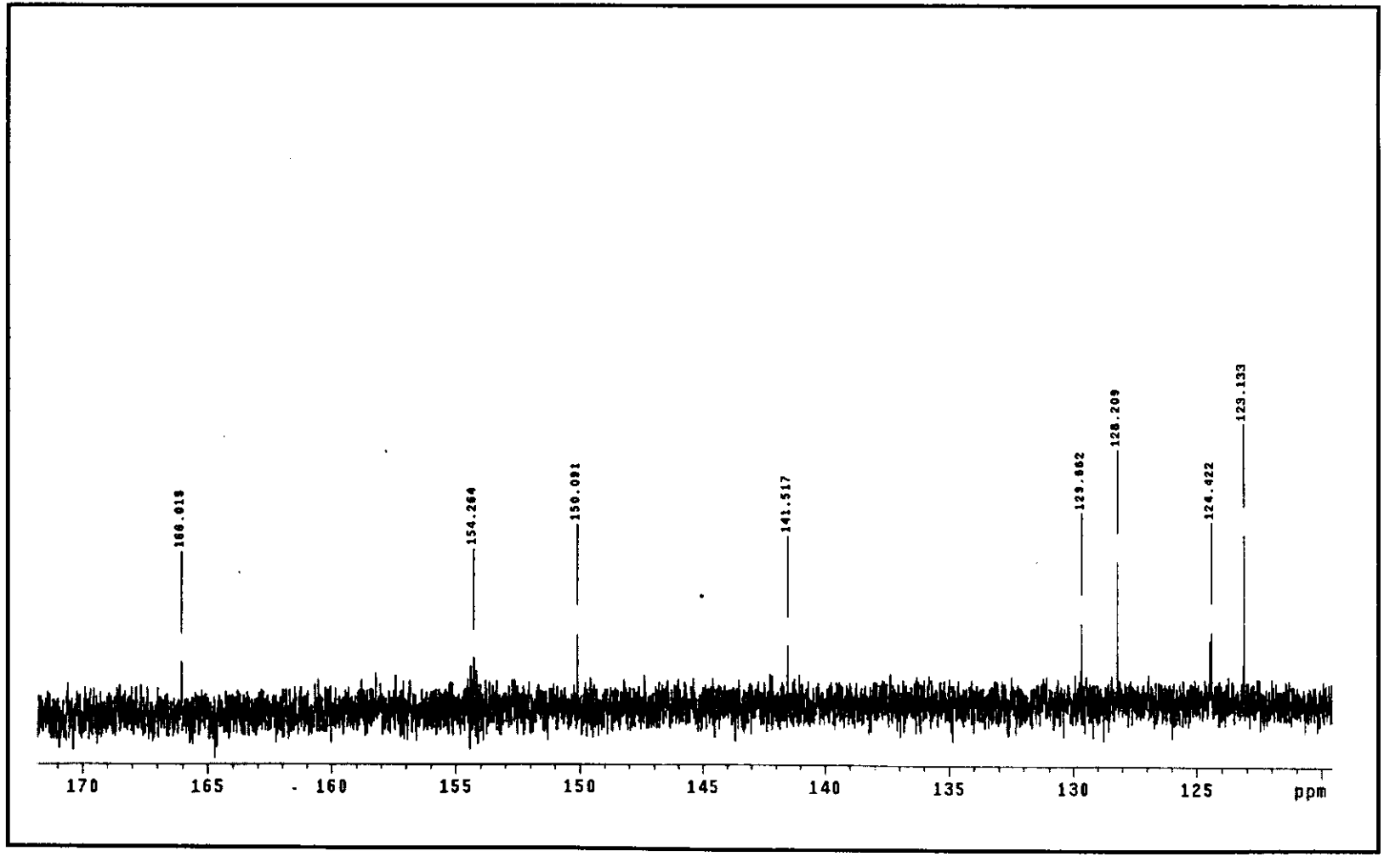

Figure 34 ^{13}C NMR spectrum of *tcc*-$Ru(azpy)_2Cl_2$ in acetone-d_6.

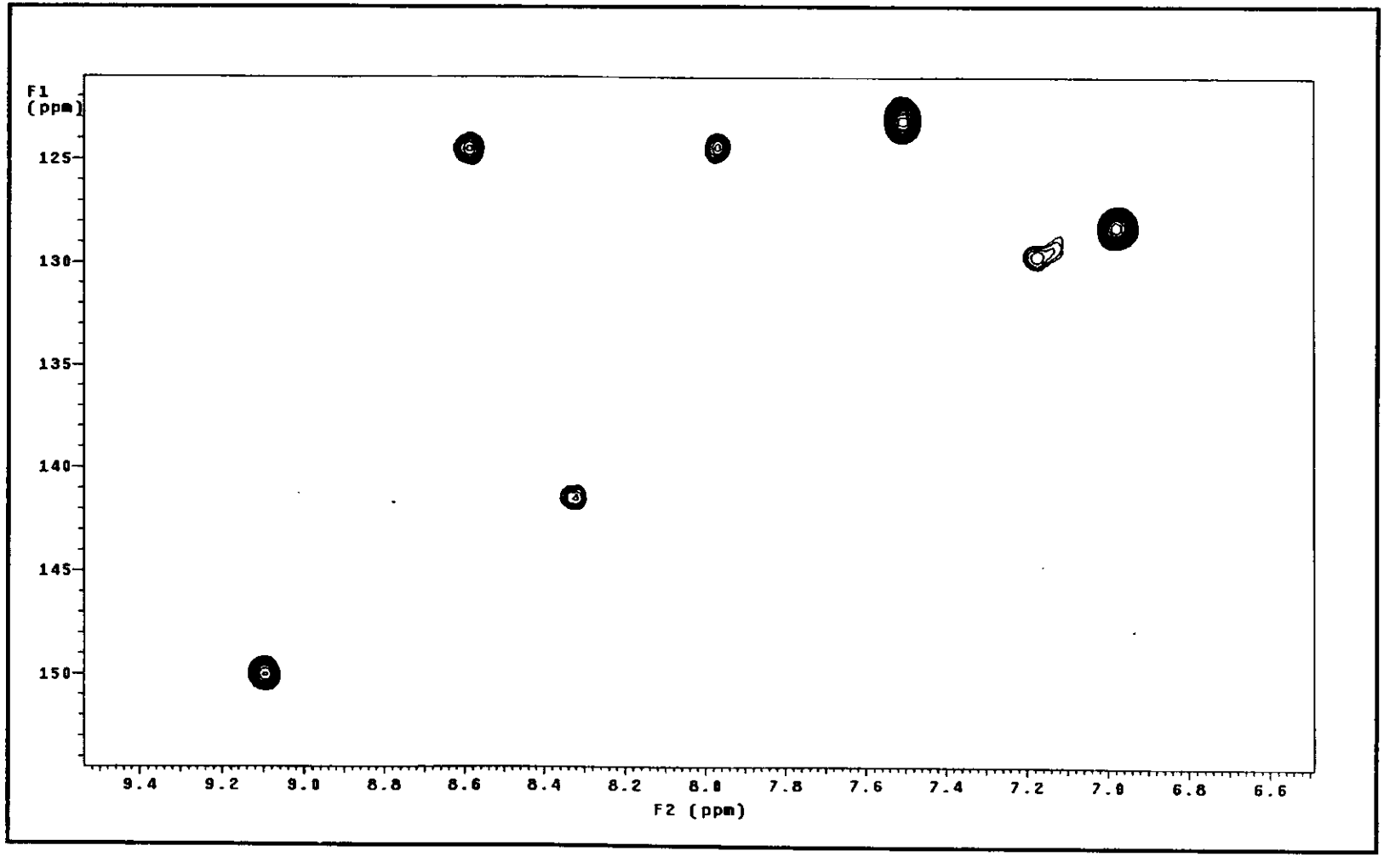

Figure 35 ^{1}H-^{13}C HMQC NMR spectrum of *tcc*-$Ru(azpy)_2Cl_2$ in acetone-d_6.

(b) *ctc*-Ru(azpy)$_2$Cl$_2$ complex

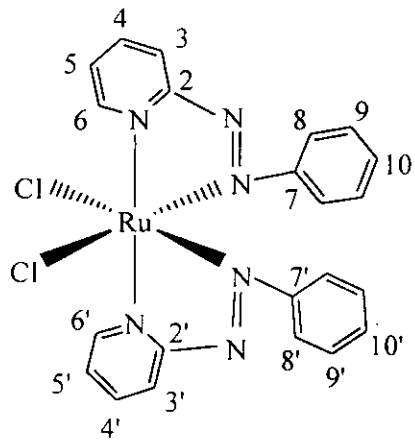

The ^{1}H NMR spectrum of *ctc*-Ru(azpy)$_2$Cl$_2$ (Figure 36) showed only one set of the azpy peak. The complex must be symmetric therefore the signal showed one set of ligand peaks. The ^{1}H NMR spectrum showed 7 resonance signals. The signal of proton H6, 6′ and H4,4′ and H5,5′ were shifted to downfield compared to the free ligands. It was due to coordination to ruthenium(II) center and steric effect of structure. The assignment was made with the use of ^{1}H-^{1}H COSY NMR spectroscopy (Figure 37).

The ^{13}C NMR spectrum of this complex (Figure 38) showed 8 resonance signals. The assignment was based on the ^{1}H-^{13}C HMQC NMR spectroscopy (Figure 39). The downfield resonance at 167.53 and 151.81 ppm were assigned to quaternary carbons (C2 and C7 respectively). The methine carbon occurring at 156.27, 127.18, 138.58, 125.92, 130.80, 129.22 and 122.75 ppm were assigned to carbon C6 (6′), C3 (3′), C4 (4′), C5 (5′), C10 (10′), C9 (9′) and C8 (8′) positions, respectively. The chemical shift data and corresponding assignnments were presented in Table 13.

Table 13 The NMR spectroscopic data of *ctc*-$Ru(azpy)_2Cl_2$ in acetone-d_6

H-Position	^{1}H NMR			^{13}C NMR
	δ (ppm)	J (Hz)	Number of H	δ (ppm)
6, 6′	9.37 (dd)	5.8, 1.0	2	156.27
3, 3′	8.61 (dd)	8.0, 0.5	2	127.18
4, 4′	8.22 (ddd)	7.5, 8.0, 1.5	2	138.58
5, 5′	7.77 (ddd)	7.5, 6.0, 1.5	2	125.92
10, 10′	7.36 (dd)	8.0, 1.0	2	130.80
9, 9′	7.23 (dd)	8.0, 8.5	4	129.22
8, 8′	6.93 (dd)	8.5, 1.0	4	122.75
Quaternary carbon				167.53, 151.81

dd = doublet of doublet, ddd = doublet of doublet of doublet

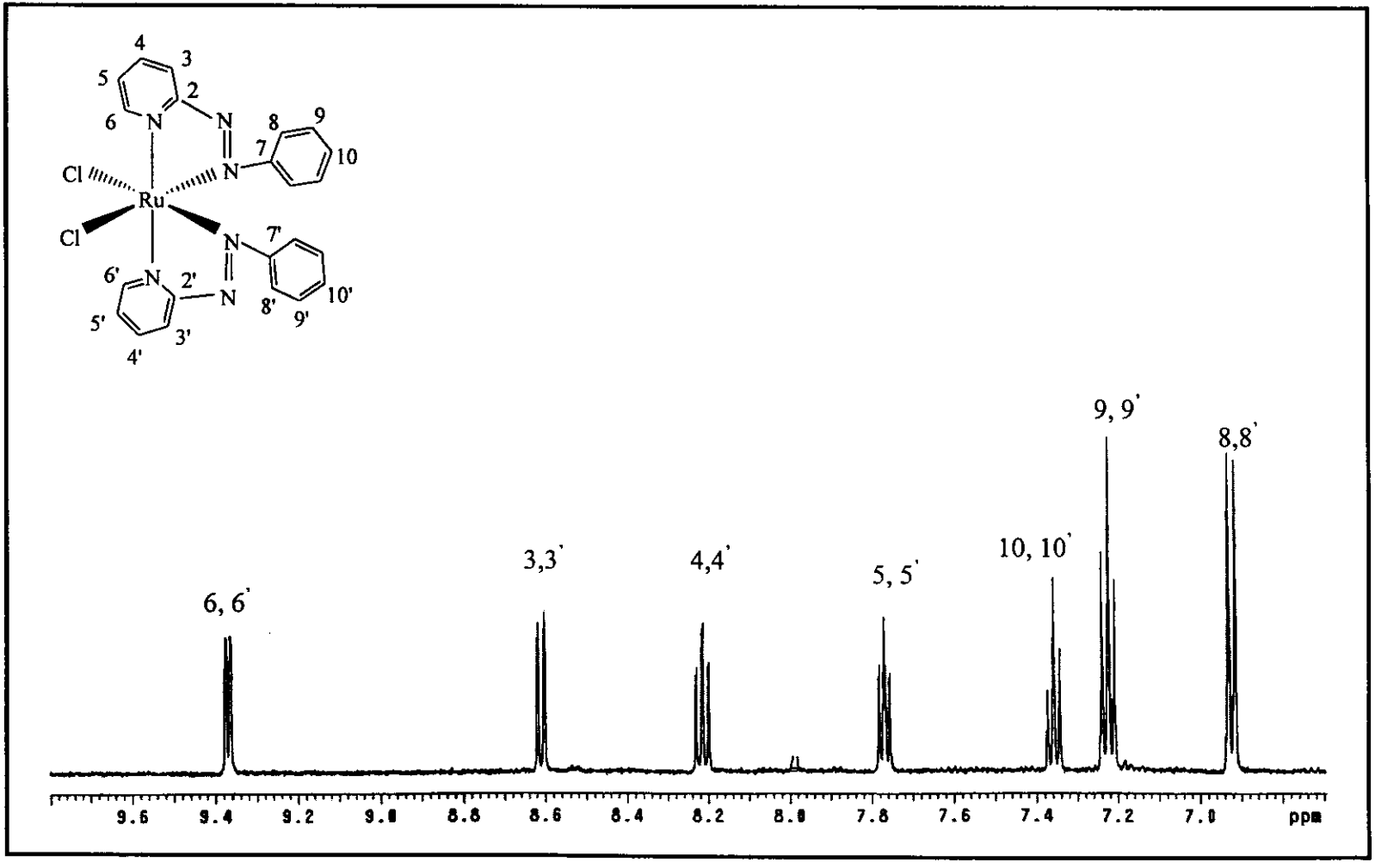

Figure 36 ^{1}H NMR spectrum of *ctc*-Ru(azpy)$_2$Cl$_2$ in acetone-d_6.

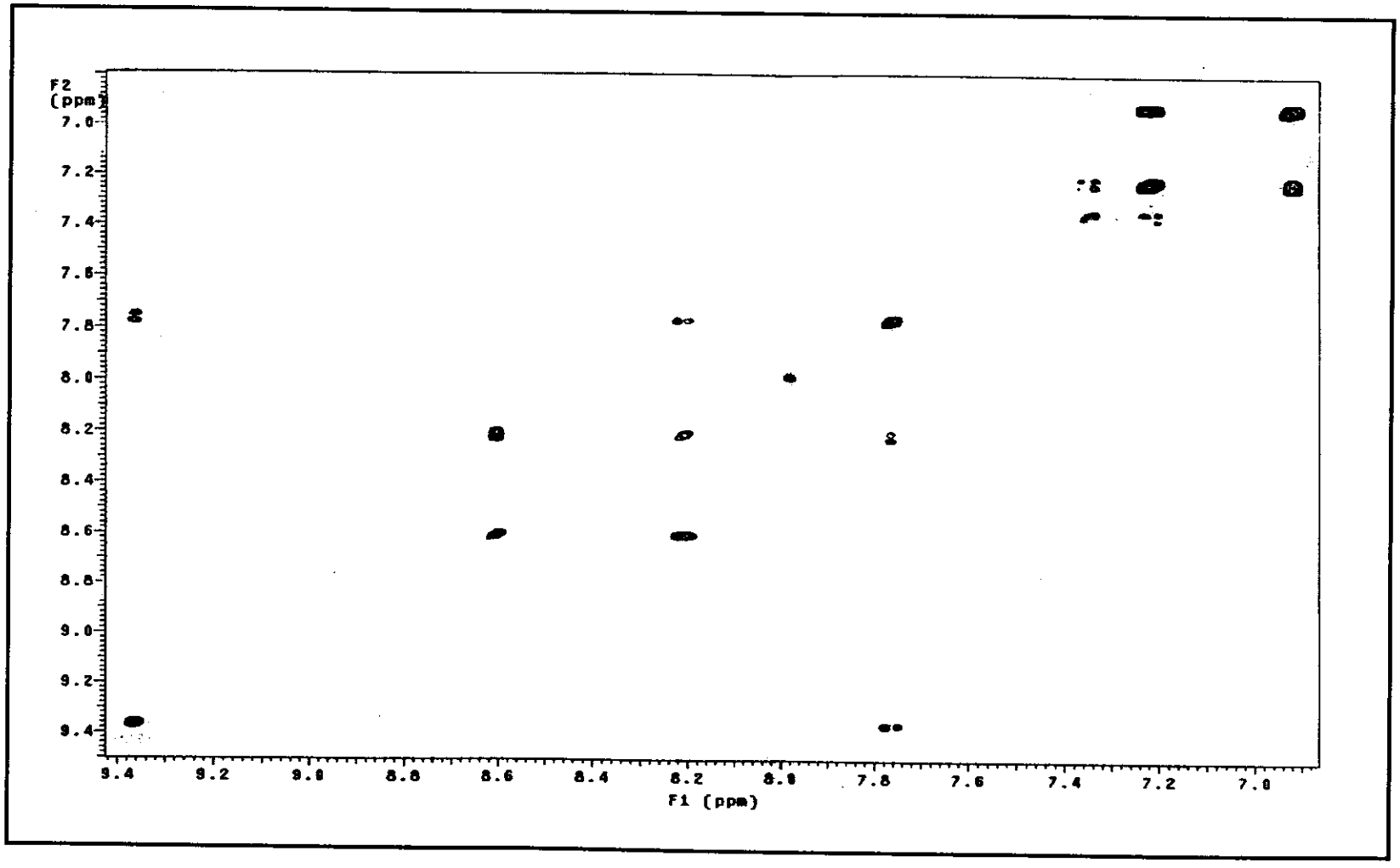

Figure 37 ^{1}H-^{1}H COSY NMR spectrum of *ctc*-$Ru(azpy)_2Cl_2$ in acetone-d_6

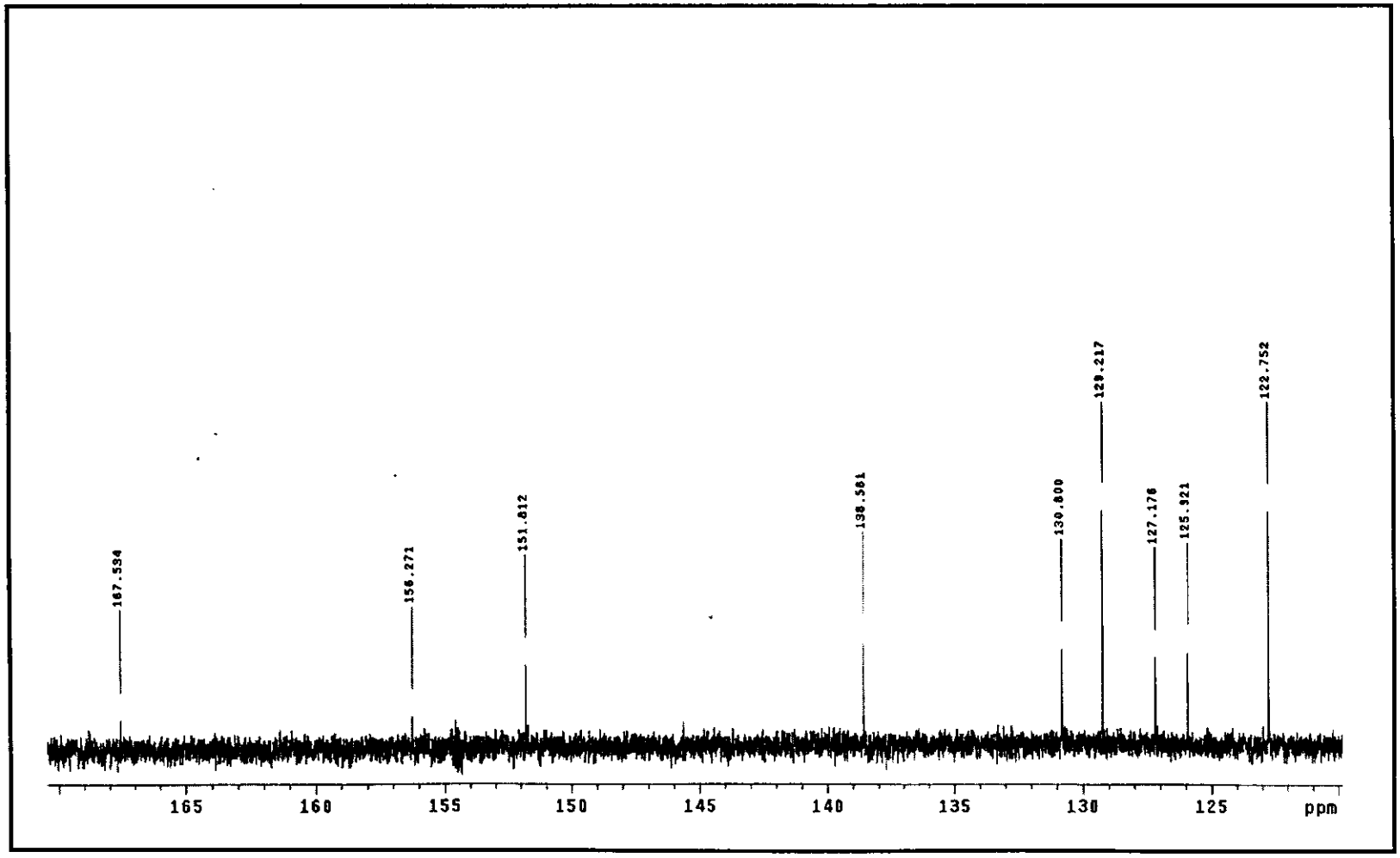

Figure 38 ^{13}C NMR spectrum of *ctc*-$Ru(azpy)_2Cl_2$ in acetone-d_6

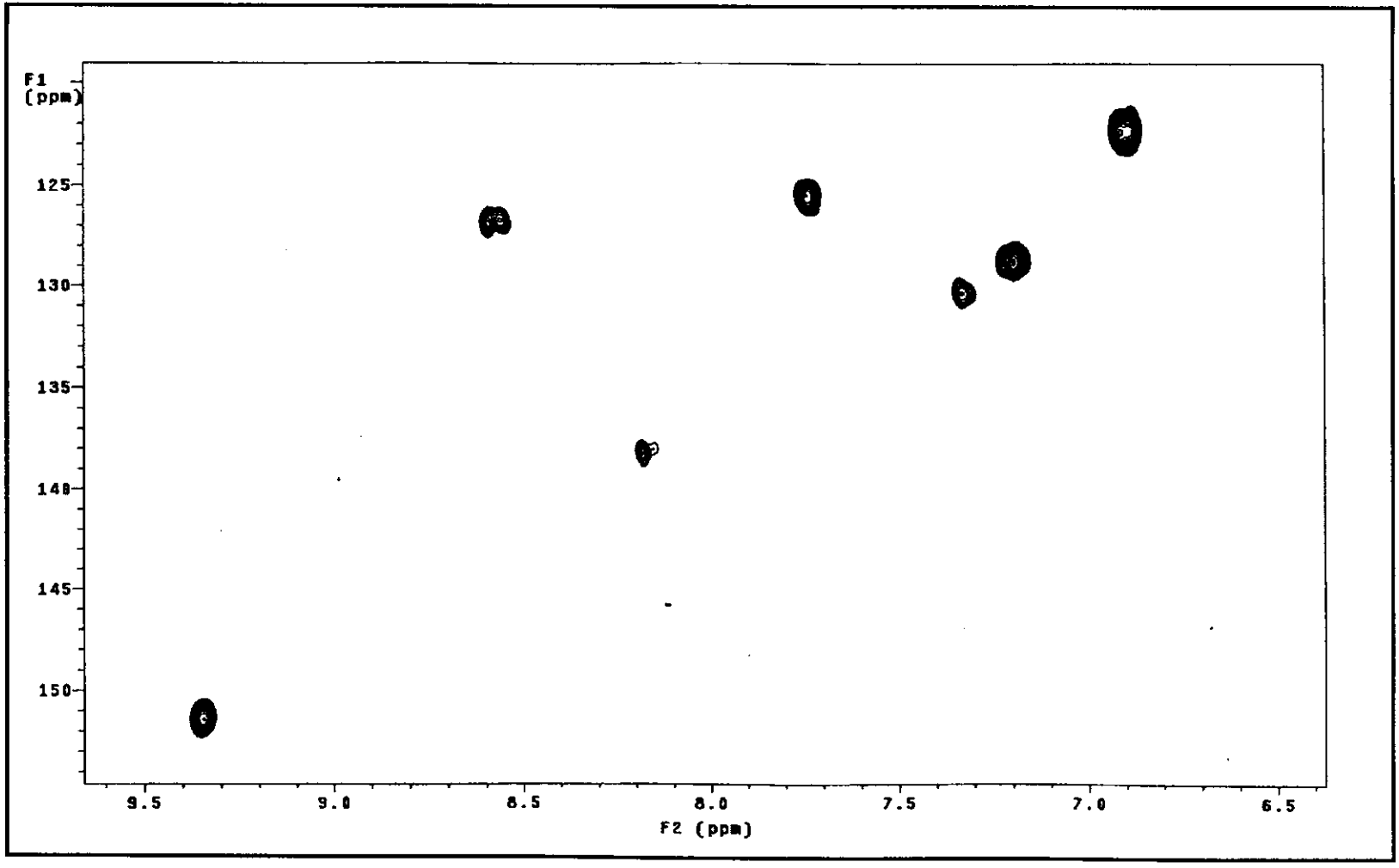

Figure 39 ^{1}H-^{13}C HMQC NMR spectrum of *ctc*-$Ru(azpy)_2Cl_2$ in acetone-d_6

(c) *ccc*-Ru(azpy)$_2$Cl$_2$ complex

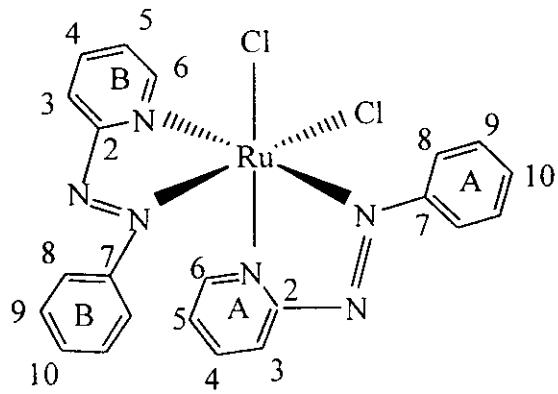

The ^{1}H NMR spectrum of *ccc*-Ru(azpy)$_2$Cl$_2$ (Figure 40) showed 14 resonance signals. The ^{1}H NMR signals of *ccc*-Ru(azpy)$_2$Cl$_2$ complex showed two set of azpy ligands with had different chemical shifts. The signal of proton H6 on pyridine (B) ring exhibited chemical shift at 9.69 ppm which was downfield more than proton H6 (7.49 ppm) on pyridine (A) ring. It was due to the effecting from Cl and nitrogen on pyridine ring in cis position. The different of chemical shift of proton H8 on phenyl (A) ring (7.89 ppm) with proton H8 on phenyl (B) ring (6.73 ppm) was due to phenyl ring (A) and Cl in the cis position. The assignment was based on the used of ^{1}H-^{1}H COSY NMR spectroscopy (Figure 41).

The ^{13}C NMR spectrum of this complex (Figure 42) showed 18 resonance signals in the aromatic region. The assignment was based on the ^{1}H-^{13}C HMQC NMR spectroscopy (Figure 43). The quaternary carbon (C2) which was located near two electron withdrawing nitrogen occurred at 167.01 and 165.79 ppm. The signals at 157.67 and 155.85 ppm were assigned to quaternary carbons (C7), which located near one electron withdrawing nitrogen. The methine carbon showed 14 signals. The chemical shift data and corresponding assingnments were presented in Table 14.

Table 14 The NMR spectroscopic data of *ccc*-$Ru(azpy)_2Cl_2$ in acetone-d_6

H-Position	^{1}H NMR			^{13}C NMR
	δ (ppm)	*J* (Hz)	Number of H	δ (ppm)
6 (B)	9.69 (ddd)	5.5, 1.5, 0.5	1	149.90
3 (B)	8.66 (ddd)	8.0, 1.3, 0.5	1	126.57
3 (A)	8.55 (ddd)	8.0, 1.3, 0.5	1	124.59
4 (B)	8.40 (ddd)	8.0, 7.5, 1.5	1	139.62
4 (A)	8.18 (ddd)	8.0, 7.5, 1.5	1	139.35
5 (B)	8.08 (ddd)	8.0, 5.5, 1.0	1	126.24
8 (A)	7.89 (dd)	9.0, 1.0	2	126.24
5 (A)	7.56 (dd)	8.0, 5.5, 1.5	1	124.95
10(A)	7.54 (dd)	7.5, 1.0	1	130.78
6 (A)	7.49 (ddd)	6.0, 1.8, 0.5	1	149.62
10 (B)	7.45 (dd)	7.5, 1.0	1	129.87
9 (A)	7.42 (dd)	8.0, 8.5	2	128.84
9 (B)	7.29 (dd)	8.0, 8.0	2	127.41
8 (B)	6.73 (dd)	8.5, 1.0	2	121.50
Quaternary Carbon				167.01, 165.79 157.67, 155.85

dd = doublet of doublet, ddd = doublet of doublet of doublet

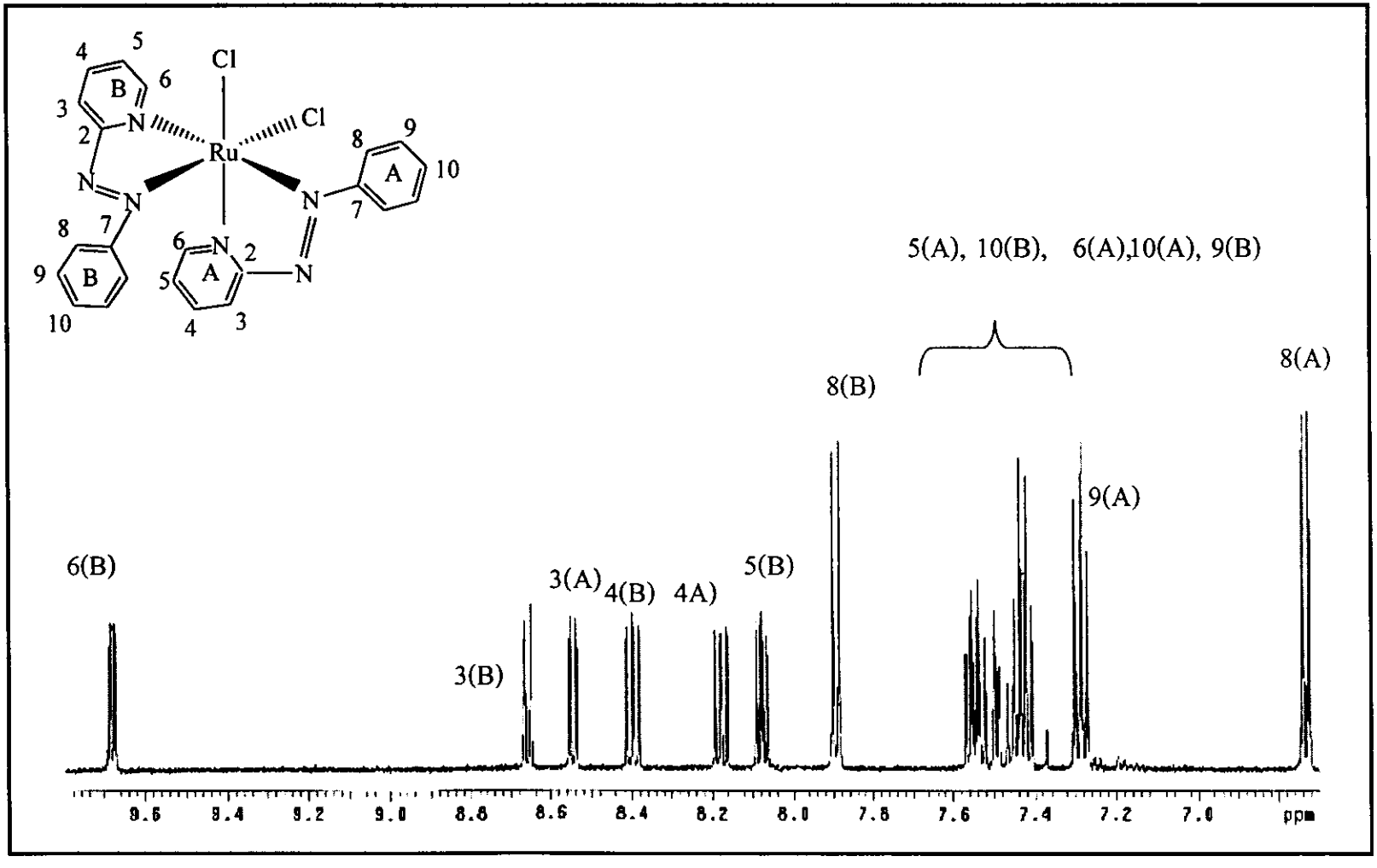

Figure 40 ^{1}H NMR spectrum of *ccc*-Ru(azpy)$_2$Cl$_2$ in acetone-d_6.

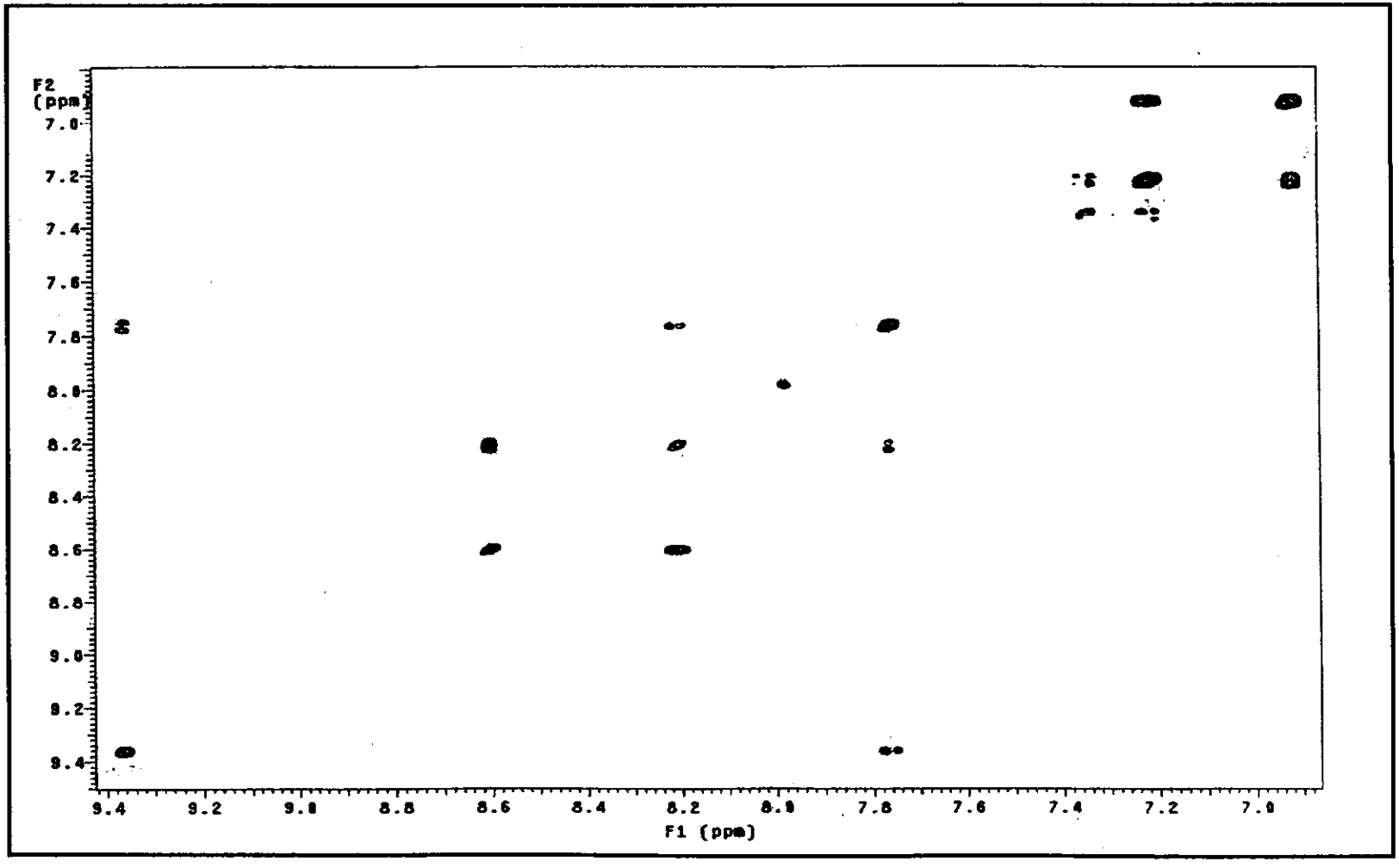

Figure 41 ^{1}H-^{1}H COSY NMR spectrum of *ccc*-$Ru(azpy)_2Cl_2$ in acetone-d_6

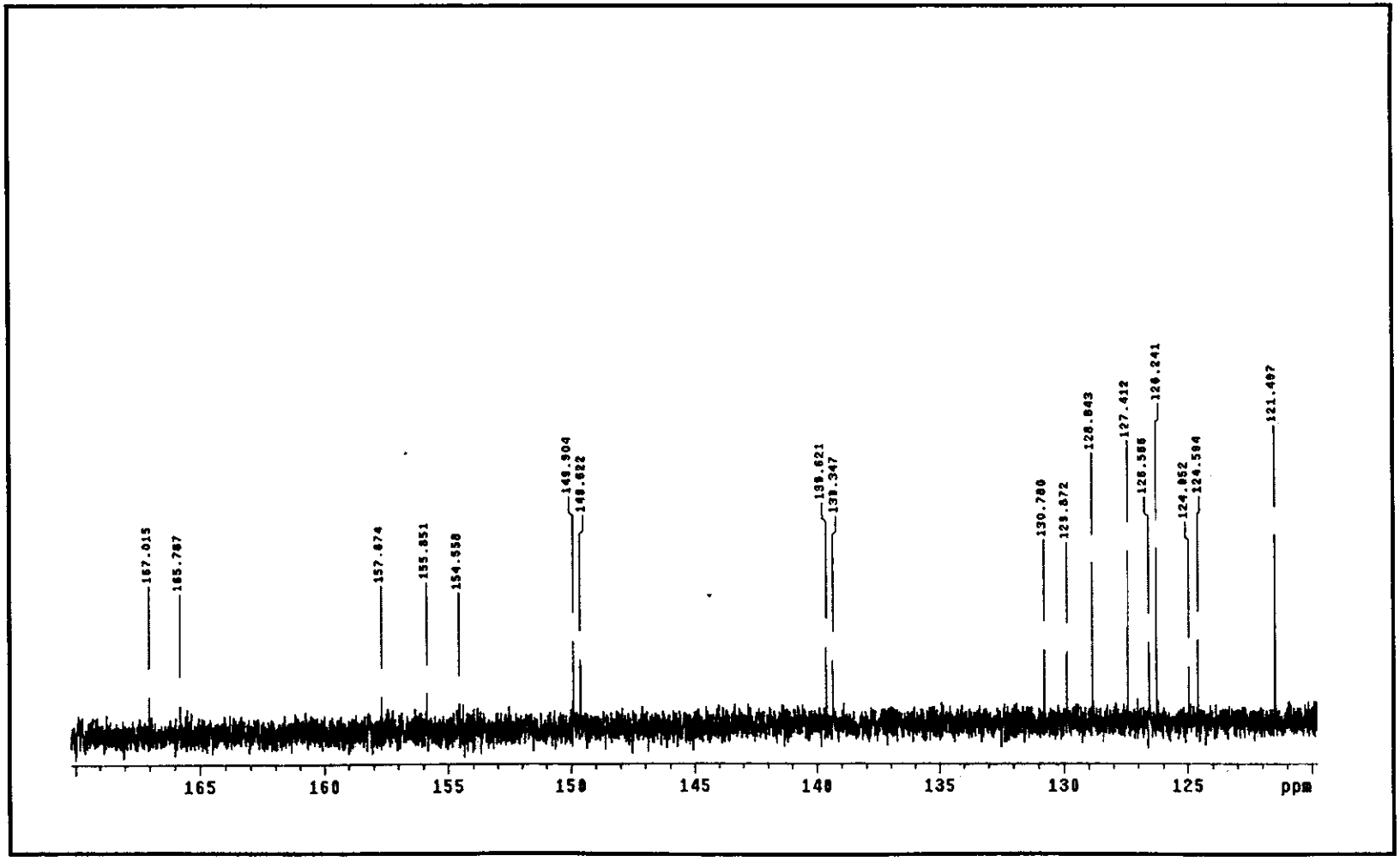

Figure 42 ^{13}C NMR spectrum of *ccc*-$Ru(azpy)_2Cl_2$ in acetone-d_6.

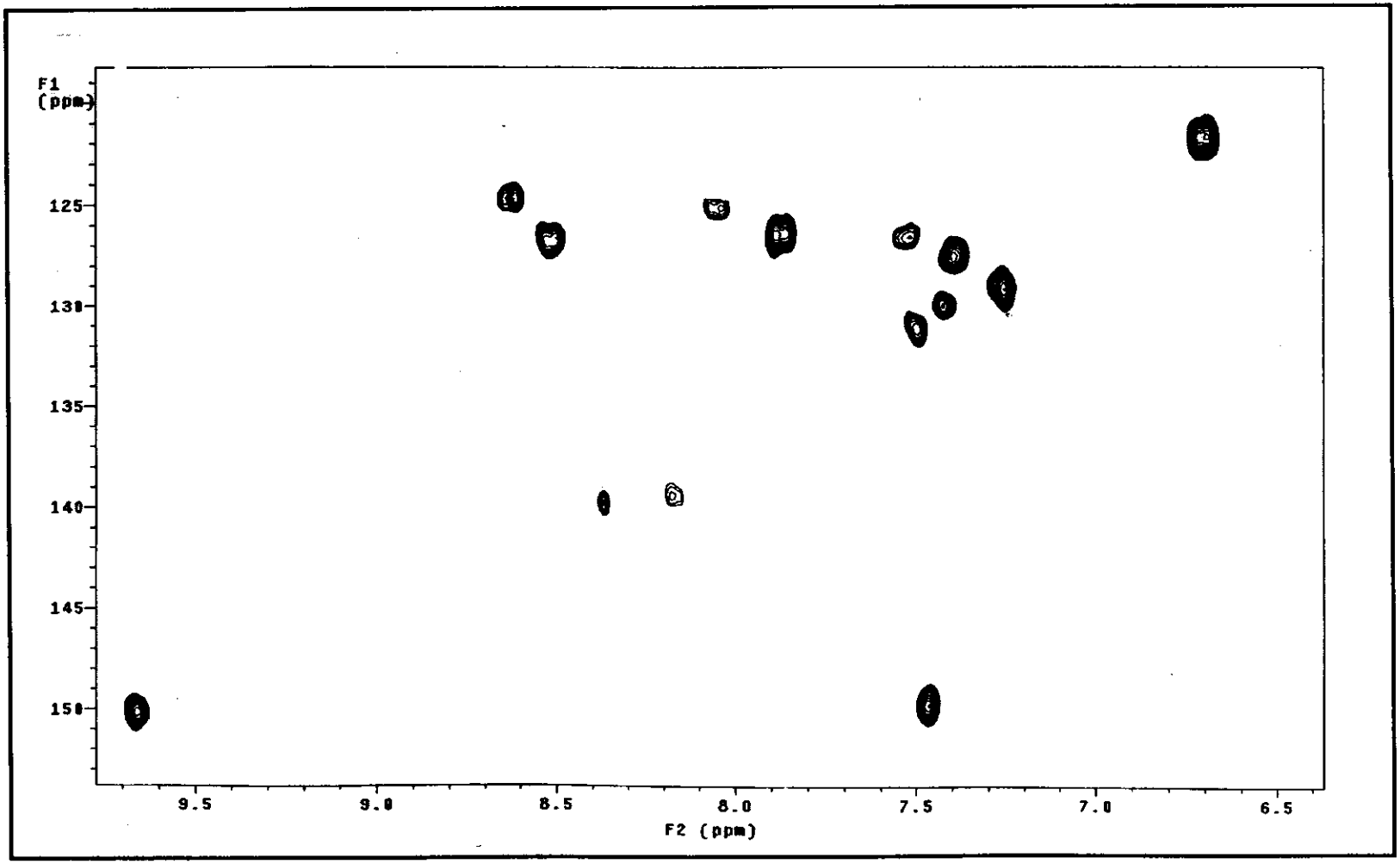

Figure 43 ^{1}H-^{13}C HMQC NMR spectrum of *ccc*-$Ru(azpy)_2Cl_2$ in acetone-d_6.

3.3.5 UV-Visible absorption spectroscopy

UV-Visible absorption spectroscopy is a technique to study the electronic transitions of the complexes. The UV-Visible absorption spectrum the complex of *ctc*-$Ru(azpy)_2Cl_2$ in acetonitrile are shown in Figure 44. In addition, their absorption spectra were studied in dimethyl sulfoxide (DMSO), dichloromethane, ethanol, and methanol and the data are summarized in Table 15.

Table 15 The UV-Visible absorption spectroscopic data of *ctc*-$Ru(azpy)_2Cl_2$

Complex	λ_{max} nm, (ε^ax10^{-4} $M^{-1}cm^{-1}$)				
	DMSO	CH_3CN	CH_2Cl_2	MeOH	EtOH
ctc-$Ru(azpy)_2Cl_2$	318 (2.6)	317 (2.6)	318 (2.6)	315 (2.1)	317 (1.5)
	593 (1.1)	584 (1.2)	582 (1.1)	575 (1.0)	580 (0.7)

[a]Molar Extinction coefficient

The absorption spectra of *ctc*-$Ru(azpy)_2Cl_2$ were obtained in both ultraviolet (200-400 nm) and visible regions (400-800 nm). The complexes exhibited transition in UV region due to intraligand charge transfer transition, $\pi \rightarrow \pi^*$ whereas the band in the visible region were assinged to metal-to-ligand charge-transfer transitions (MLCT) involving transfer of an electron from the metal d orbitals to π^* orbitals of the ligands with high molar extinction coefficient (ε, 10^{-4} M^{-1} cm^{-1}).

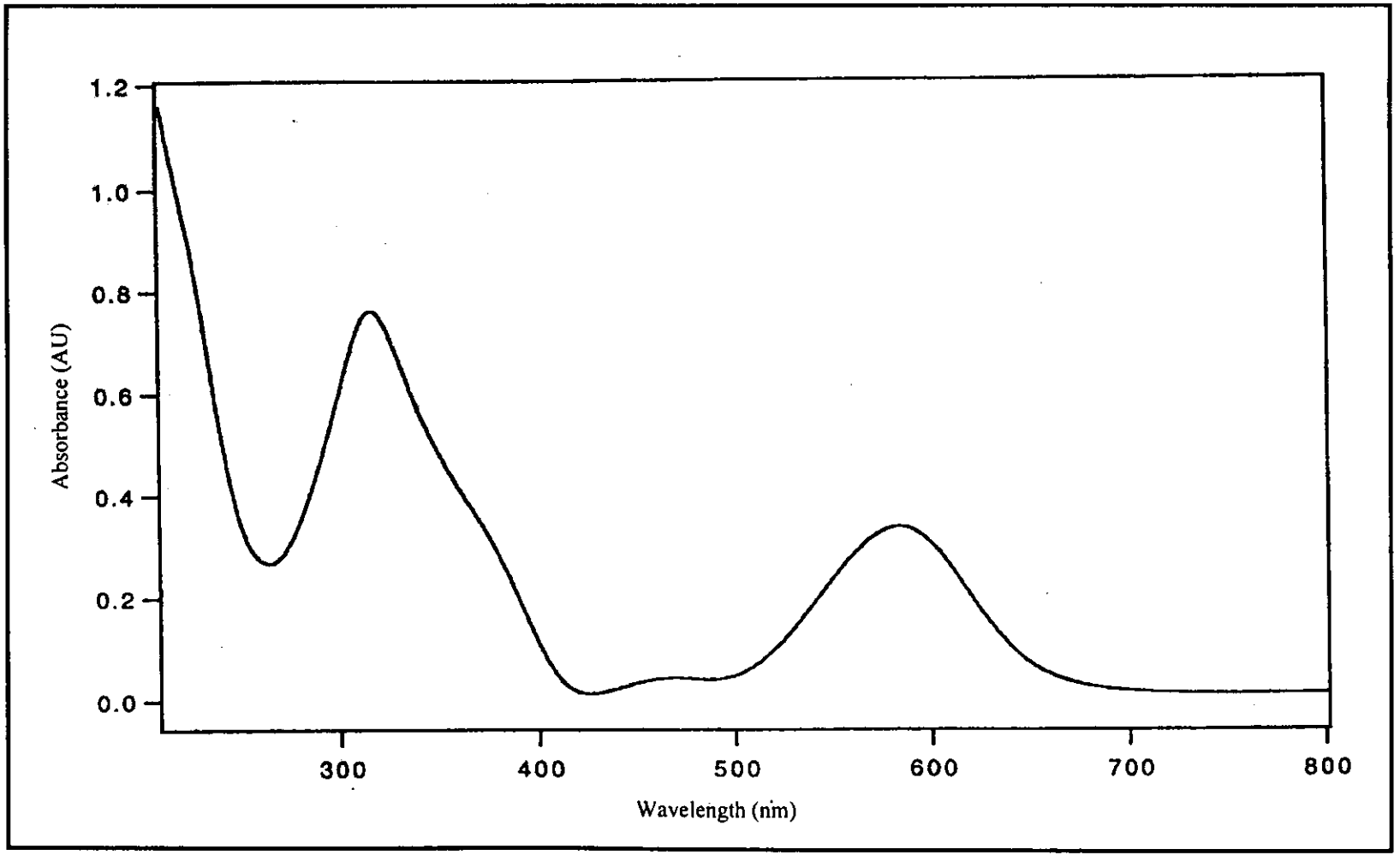

Figure 44 UV-Visible absorption spectrum of *ctc*-$Ru(azpy)_2Cl_2$ in CH_3CN.

3.3.6 Cyclic voltammetry

Cyclic voltammetry is a technique to study redox properties of the complex of *ctc*-$Ru(azpy)_2Cl_2$. The electron transfer properties of this complex were shown in Figure 49 with corresponding half-wave potentials. The cyclic voltammogram of complexes displayed metal oxidation in the oxidation range and ligand reduction in the reduction range. In addition, the potentials were compared to the potential of ferrocene couple ($E_{1/2}$ = 0 V, ΔE_p= 65 mV).

A glassy carbon working electrode, platinum wire auxillary electrode, and platinum reference electrode were used in three-electrode configuration.

Table 16 Cyclic voltammetric data of *ctc*-$Ru(azpy)_2Cl_2$ in 0.1 M TBAH acetonitrile at scan rate 50 mV/s (ferrocene as an internal standard, ΔE_p = 65 mV)

Complex	$E_{1/2}$, V (ΔE, mV)	
	Oxidation	Reduction
ctc-$Ru(azpy)_2Cl_2$	+0.73 (88)	-0.94 (64)
		-1.04[a]
		-1.79

[a]cathodic peak

Oxidation Potential

In the potential range from 0 to +0.9 V, one reversible oxidative response was observed. The Ru(II)/Ru(III) couple was reversible in *ctc*-$Ru(azpy)_2Cl_2$ with one electron transfer in comparison with ferrocene couple.

Reduction Potential

In the potential range from 0 to -2.0 V, three couples appeared. The peak at -0.94 and -1.79 V were reversible couple at higher scan rates. Whereas, the peak at -1.04 V was irreversible (Figure 45).

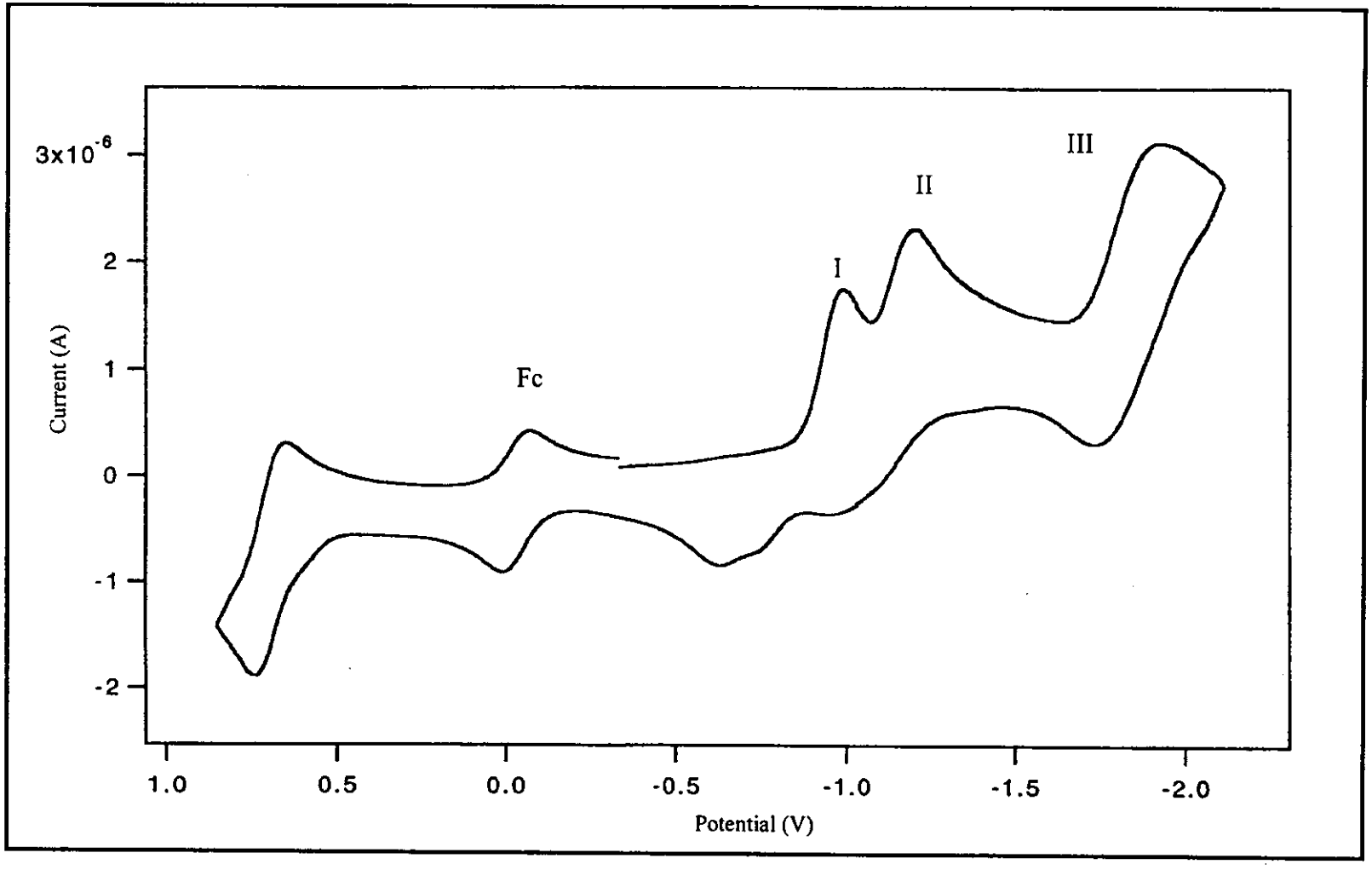

Figure 45 Cyclic voltammogram of *ctc*-$Ru(azpy)_2Cl_2$ in 0.1 M TBAH CH_3CN at scan rate 50 mV/s.

3.4 Preparation of the $[Ru(azpy)_2L]^{2+}$

The $[Ru(azpy)_2L]^{2+}$ complexes were prepared by reaction between $AgNO_3$, *ctc*-$Ru(azpy)_2Cl_2$ and ligands (azpy, azpym, bpy and phen), in mixture of ethanol-water (3:1 v/v) with stirring and refluxing, followed by the addition of excess NH_4PF_6 or NH_4BF_4. The physical properties of all complexes are listed in Table 17.

Table 17 The physical properties of complexes

Complex	Physical properties	
	Color	Melting point (°C)
$[Ru(azpy)_3](PF_6)_2$	Red-brown	292-293
$[Ru(azpy)_2azpym](PF_6)_2$	Red-brown	286-287
$[Ru(azpy)_2bpy](PF_6)_2$	Red	296-297
$[Ru(azpy)_2phen](BF_4)_2$	Red	335-336

The complexes were highly soluble in polar solvents such as acetonitrile, acetone, dimethyl sulfoxide (DMSO), *N,N*-dimethylformamide (DMF). They were moderately soluble in methanol, ethanol, dichloromethane and insoluble in hexane, ethyl acetate, and benzene.

3.5 Characterization of $[Ru(azpy)_2L]^{2+}$

The chemistries of $[Ru(azpy)_2L]^{2+}$ complexes (L = azpy, azpym, bpy and phen) were studied by Elemental Analysis, FAB mass spectrometry, Infrared

Spectroscopy, UV-Visible absorption spectroscopy, Nuclear Magnetic Resonance spectroscopy, Cyclic voltammetry, and X-ray Crystallography.

3.5.1 Elemental analysis

The elements in the complexes were confirmed by this method. The analytical data of all the complexes consistent with the calculated values. Results from elemental analysis are shown in Table 18.

Table 18 Elemental analysis data of $[Ru(azpy)_2L]^{2+}$ (L = azpy, azpym, bpy and phen)

Complex	%C		%N		%H	
	Calc.	Found	Calc.	Found	Calc.	Found
$[Ru(azpy)_3](PF_6)_2$	42.15	42.04	13.40	13.07	2.89	2.99
$[Ru(azpy)azpym](PF_6)_2$	40.81	41.70	14.88	14.64	2.78	3.07
$[Ru(azpy)bpy](PF_6)_2$	42.07	41.79	12.26	11.67	2.87	2.88
$[Ru(azpy)phen](BF_4)_2$	49.72	47.65	13.64	13.05	3.19	2.80

3.5.2 FAB mass spectrometry

The FAB mass spectrometric data for the $[Ru(azpy)_2 L]^{2+}$ complexes (L = azpy, azpym, bpy and phen) are shown in Figure 46 to 49. The important FAB mass spectrometric data of complexes with the corresponding relative abundance are listed in Table 19.

Table 19 FAB mass spectrometric data of $[Ru(azpy)_2L]^{2+}$ (L =azpy, azpym, bpy and phen)

Complexes	m/z	Stoichiometry	Equivalent species	Rel. Abun.
$[Ru(azpy)_3](PF_6)_2$	651	$[Ru(azpy)_3]^{2-}$	$[M-2(PF_6)]^{2+}$	100
$[Ru(azpy)_2azpym](PF_6)_2$	652	$[Ru(azpy)_2azpym]^{2+}$	$[M-2(PF_6)]^{2+}$	100
$[Ru(azpy)_2bpy](PF_6)_2$	624	$[Ru(azpy)_2bpy]^{2+}$	$[M-2(PF_6)]^{2+}$	100
$[Ru(azpy)_2phen](BF_4)_2$	648	$[Ru(azpy)_2phen]^{2+}$	$[M-2(BF_4)]^{2+}$	100

M = Molecular weight (MW) of each complex

MW of $[Ru(azpy)_3](PF_6)_2$ = 940.66 g/mol

MW of $[Ru(azpy)_2azpym](PF_6)_2$ = 941.20 g/mol

MW of $[Ru(azpy)_2bpy](PF_6)_2$ = 913.64 g/mol

MW of $[Ru(azpy)_2phen](BF_4)_2$ = 821.07 g/mol

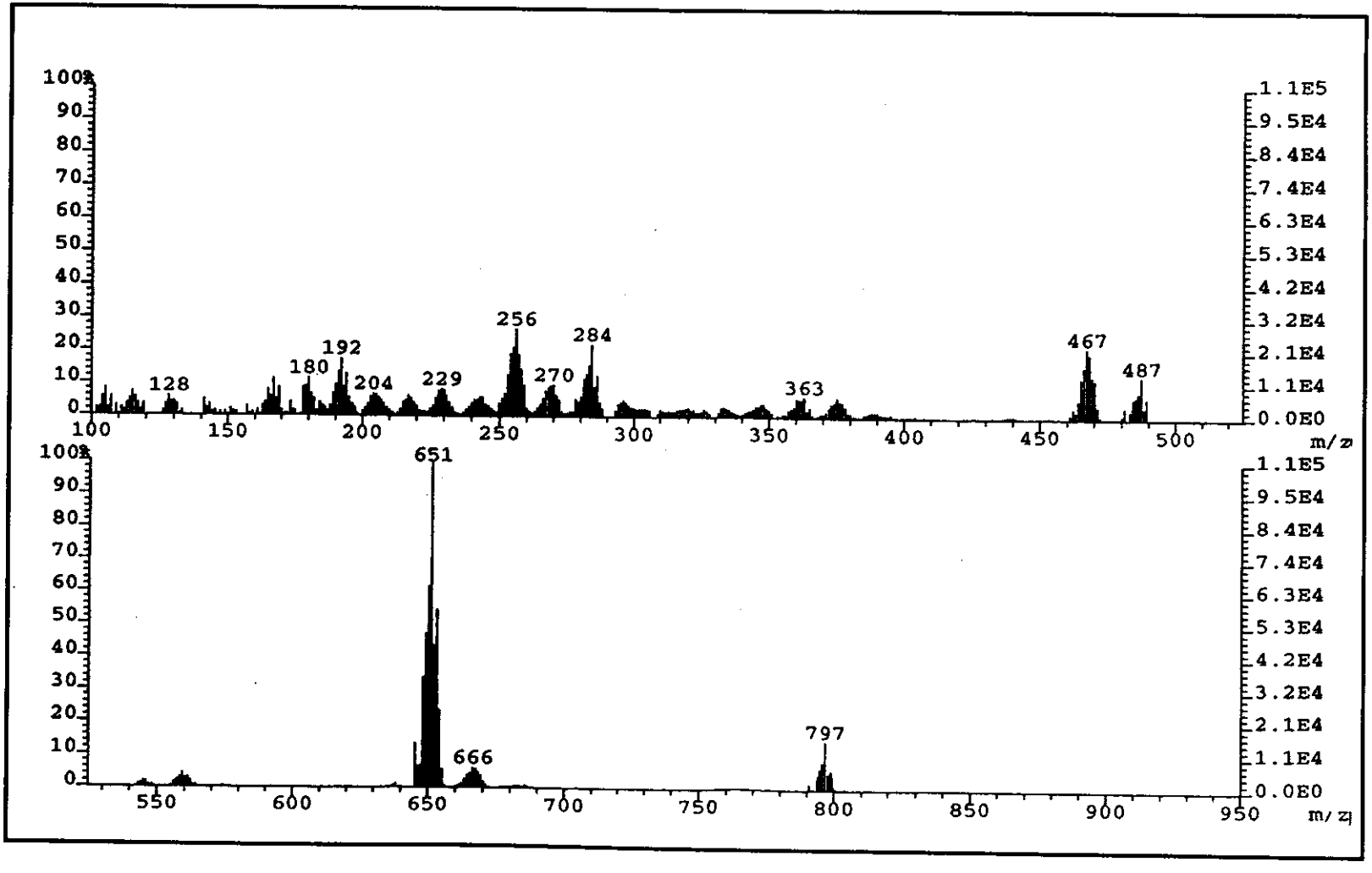

Figure 46 FAB mass spectrum of $[Ru(azpy)_3](PF_6)_2$.

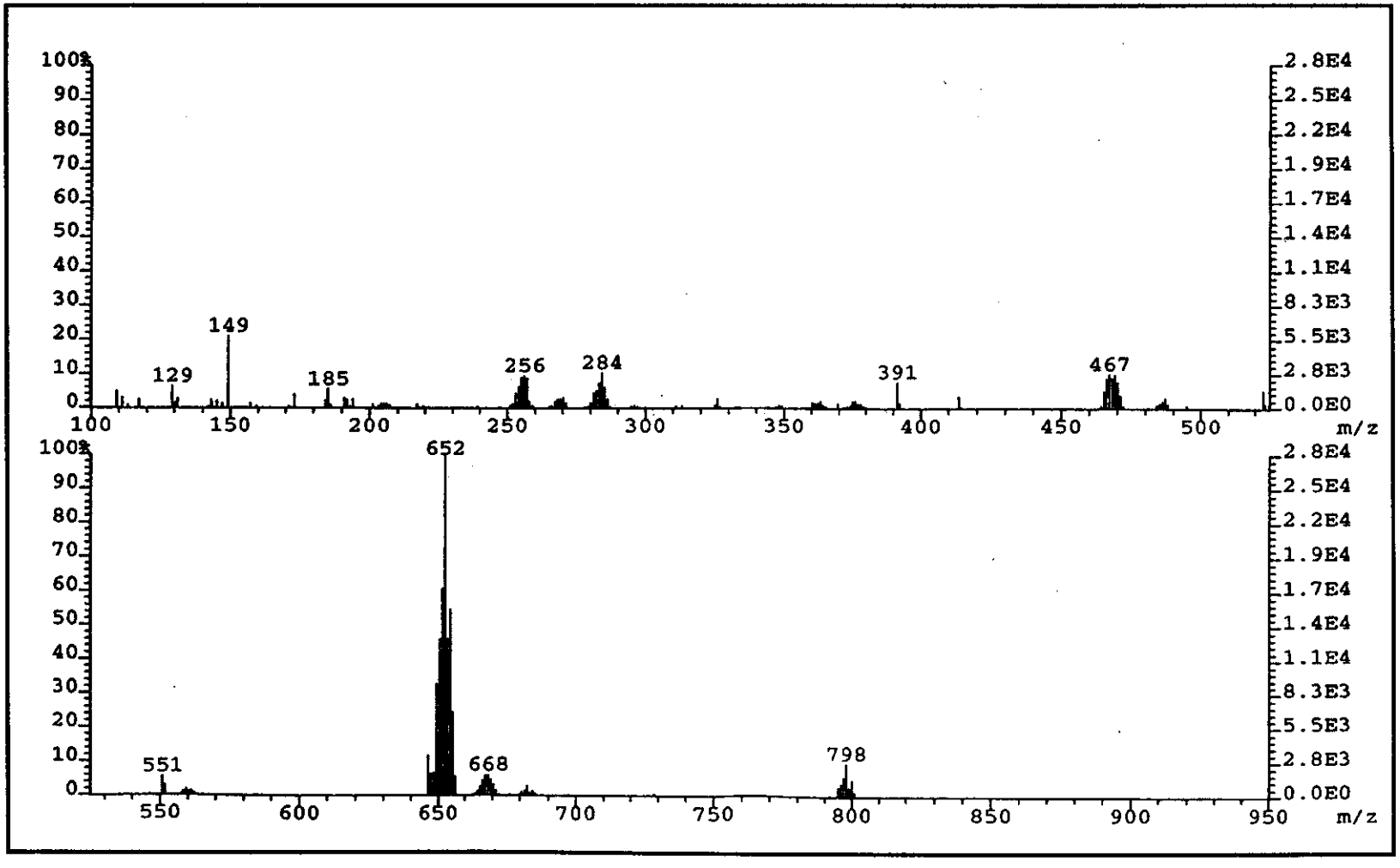

Figure 47 FAB mass spectrum of $[Ru(azpy)_2azpym](PF_6)_2$.

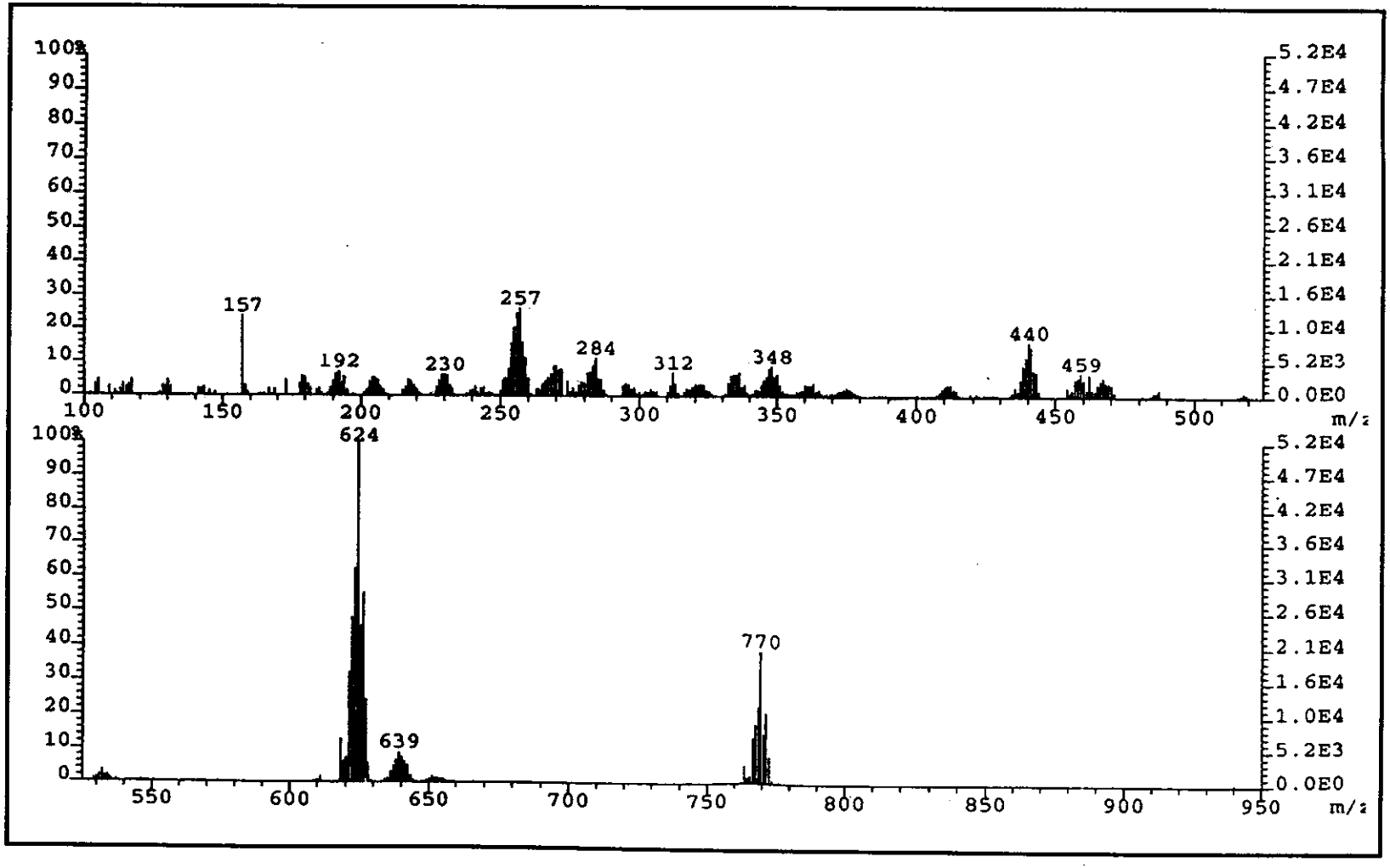

Figure 48 FAB mass spectrum of $[Ru(azpy)_2bpy](PF_6)_2$.

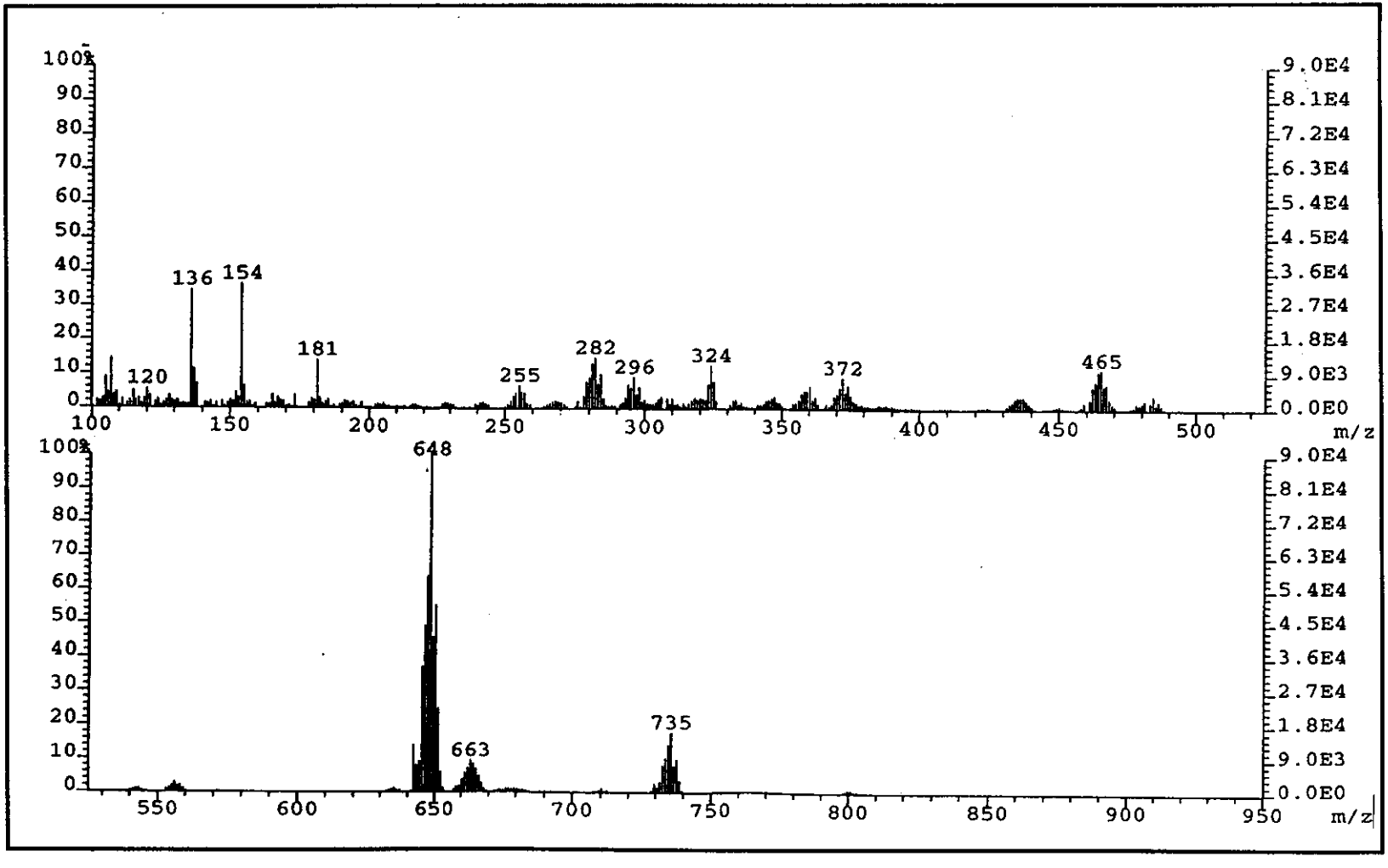

Figure 49 FAB mass spectrum of $[Ru(azpy)_2phen](PF_6)_2$.

3.5.3 Infrared spectroscopy

Infrared spectra of the $[Ru(azpy)_2L]^{2+}$ (L =azpy, azpym, bpy and phen) were recorded in the range of 1800-370 cm^{-1} with KBr disc. It exhibited several bands with variable intensities. The infrared spectra are shown in Figure 50 to 53 and the spectroscopic data are listed in Table 20.

Table 20 Infrared spectroscopic data of $[Ru(azpy)_2L]^{2+}$ (L = azpy, azpym, bpy and phen)

Vibrational modes	Wavenumber (cm^{-1}) of $[Ru(azpy)_2L]^{2+}$ (L = ligand)			
	azpy	azpym	bpy	phen
N=N(azo) stretching	1360 (s)	1358 (s)	1351 (s)	1354 (s)
C=N stretcching C=C stretching	1603 (m) 1455 (m)	1585 (m) 1456 (m)	1604 (m) 1449 (m)	1603 (m) 1454 (m) 1430 (m)
C-H out of plane bending	777 (s) 741 (m) 692 (s)	781 (s) 740 (m) 693 (s)	781 (s) 761 (s) 695 (s)	783 (s) 744 (s) 695 (s)

s= strong, m = medium

Infrared spectra of all $[Ru(azpy)_2L]^{2+}$ complexes showed vibrations of different intensities below 1,600 cm^{-1}. The bands near 1600 cm^{-1} was assigned to the

stretching vibration of monosubstituted benzene ring (Santra and Lahiri, 1998). The free azpy exhibited a sharp band at 1421 cm^{-1} corresponded to N=N stretching mode. In the complexes, the N=N stretching frequency of the coordinated ligand was appreciably lowered (1351-1360 cm^{-1}) compared to that of free ligand (1421 cm^{-1}). This was a good indication of N-coordination.

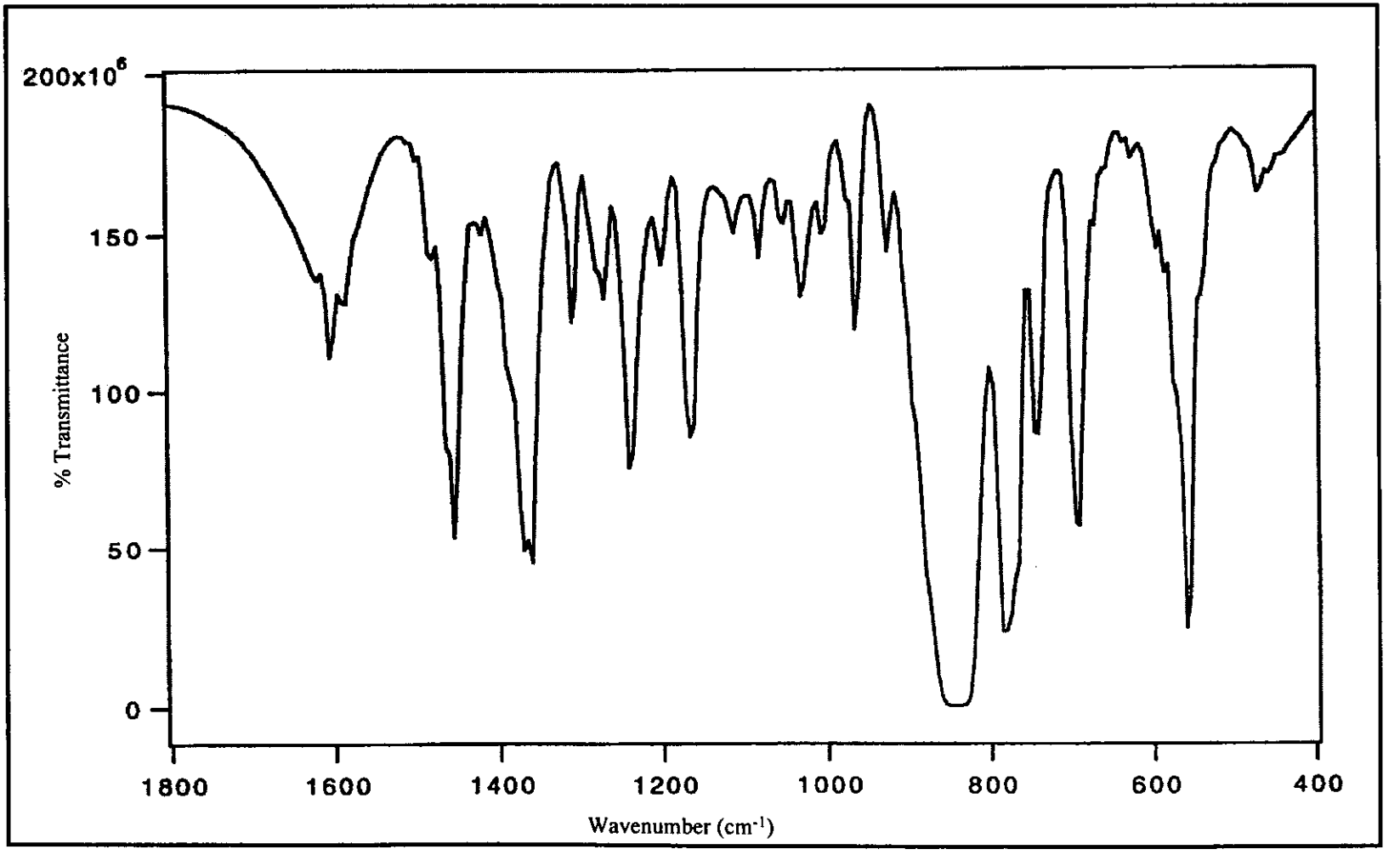

Figure 50 IR spectrum of $[Ru(azpy)_3](PF_6)_2$.

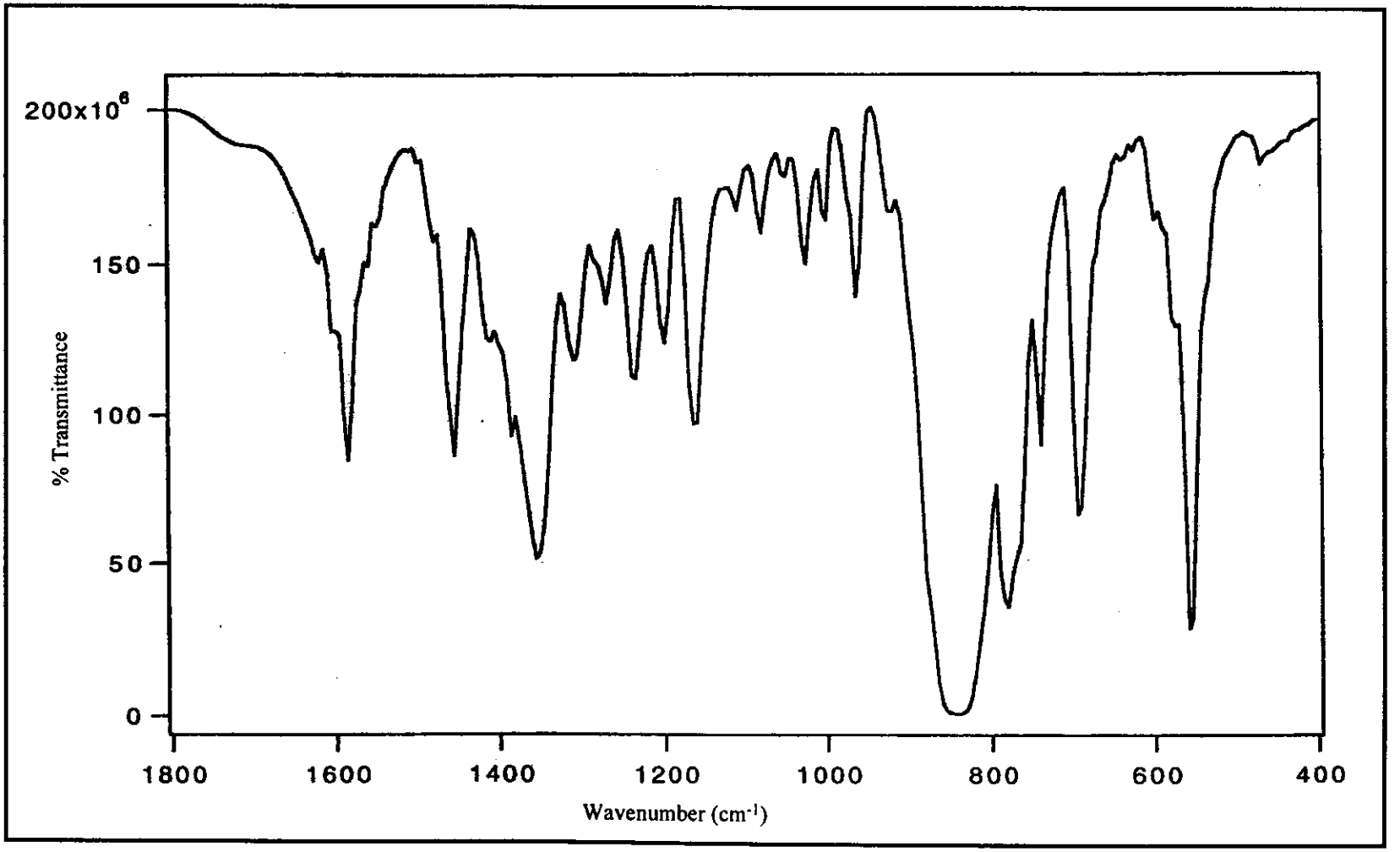

Figure 51 IR spectrum of $[Ru(azpy)_2azpym](PF_6)_2$.

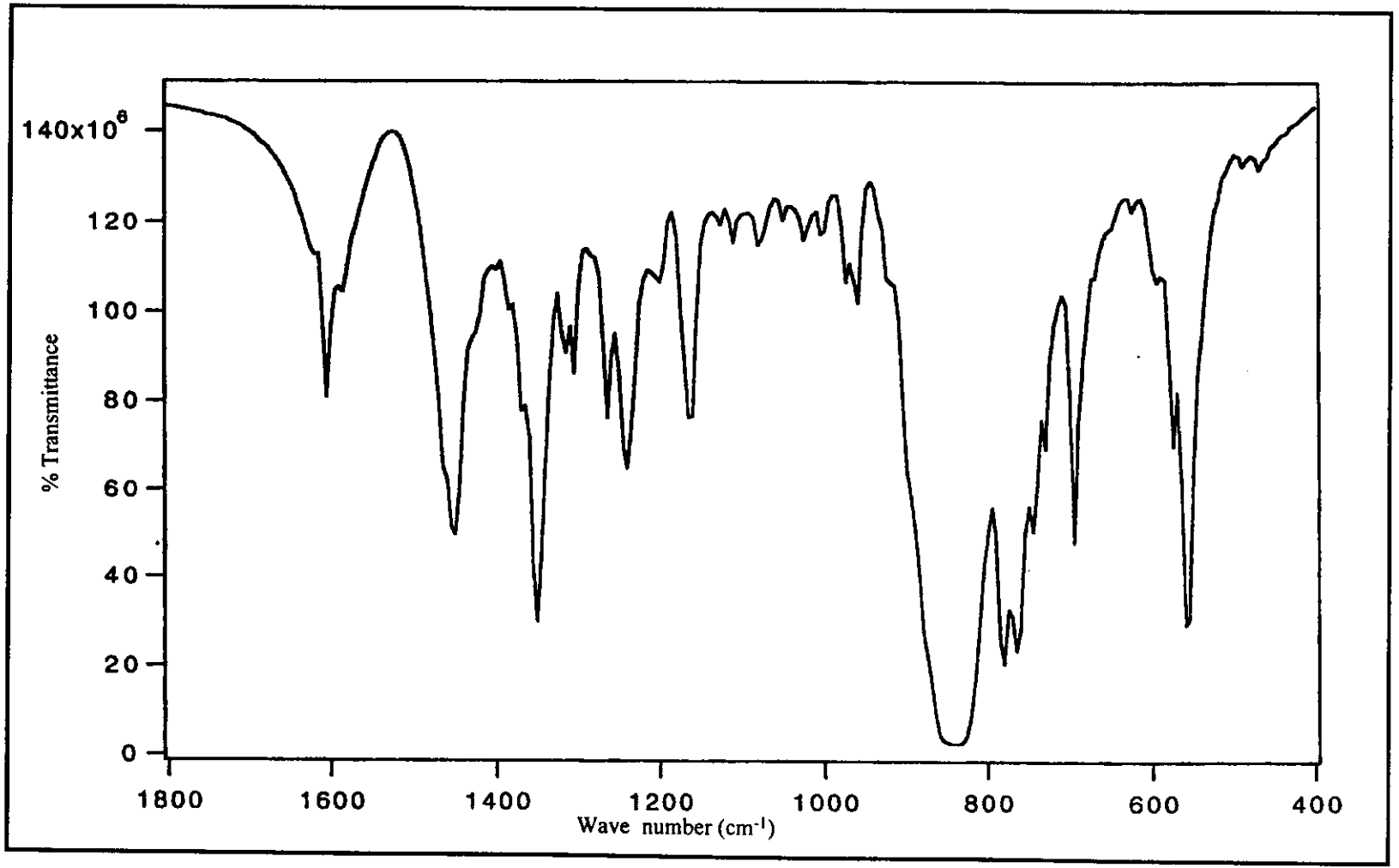

Figure 52 IR spectrum of $[Ru(azpy)_2bpy](PF_6)_2$.

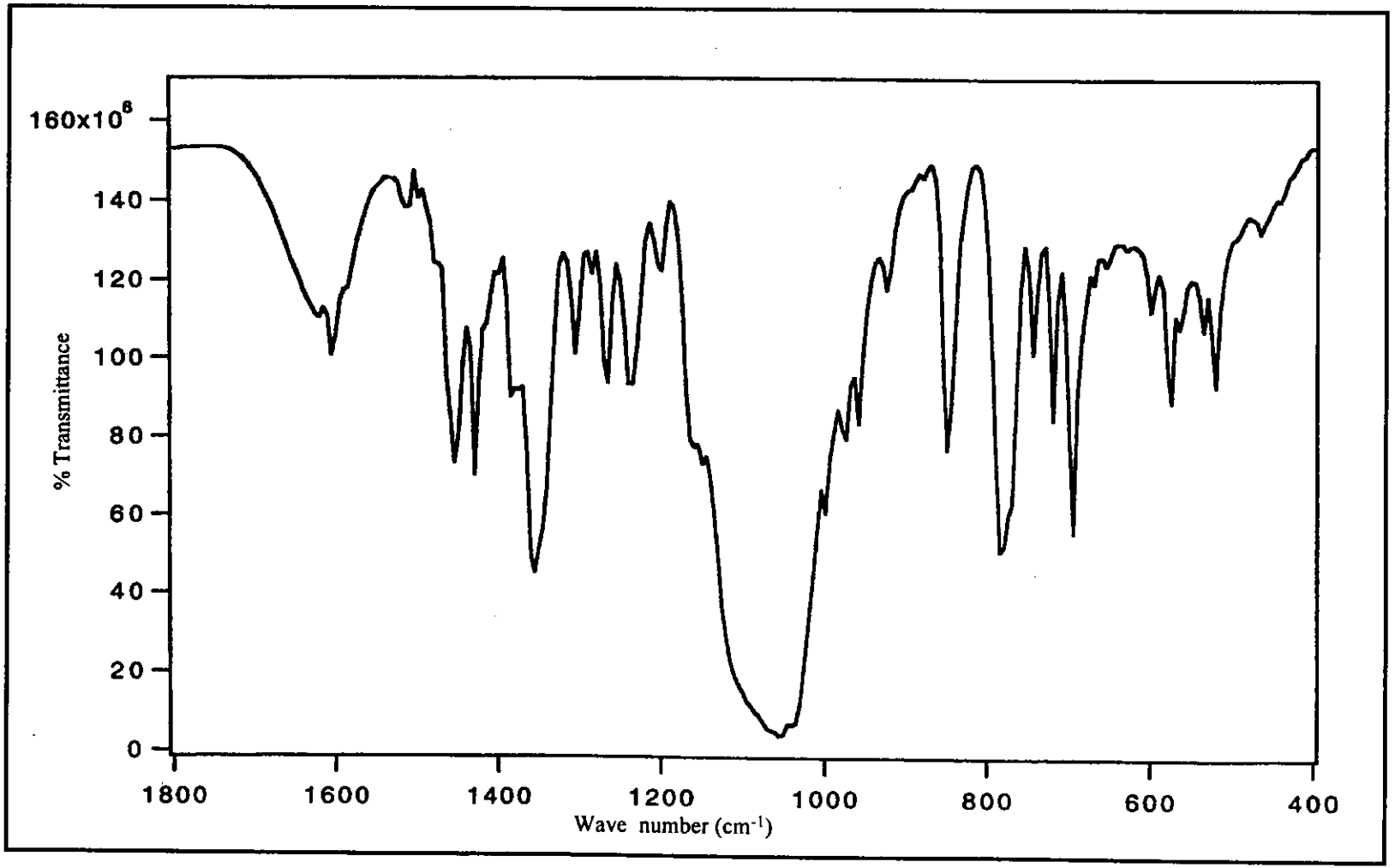

Figure 53 IR spectrum of $[Ru(azpy)_2phen](BF_4)_2$.

3.5.4 UV-Visible absorption spectroscopy

The UV-Visible spectral data of complexes in acetonitrile exhibited in the range 200-800 nm. In addition, their absorption spectra were studied in dimethyl sulfoxide (DMSO), dichloromethane, ethanol and methanol. The absorption spectra in DMSO displayed two absorption bands and in the other solvents showed three absorption bands. The absorption data are listed in Table 21 and representative spectrum are shown in Figure 54 to 57.

Table 21 UV Visible absorption spectroscopic data of $[Ru(azpy)_2L]^{2+}$

(L =azpy, azpym, bpy and phen)

Complex	λ_{max} nm, ($\varepsilon^a x10^{-4}$ $M^{-1}cm^{-1}$)				
	DMSO	CH_3CN	MeOH	EtOH	CH_2Cl_2
$[Ru(azpy)_3]^{2+}$	371 (3.1)	276 (3.0)	276 (2.3)	278 (1.9)	278 (2.1)
	502 (1.3)	372 (3.6)	369 (3.4)	373 (3.0)	380 (3.5)
		494 (1.3)	486 (1.3)	494 (1.1)	487 (1.3)
$[Ru(azpy)_2azpym]^{2+}$	370 (3.1)	273 (2.8)	273 (2.2)	277 (1.7)	272 (2.3)
	487 (1.3)	372 (3.3)	370 (3.3)	370 (2.7)	380 (3.9)
		487 (1.1)	490 (1.2)	494 (1.0)	487 (1.4)
$[Ru(azpy)_2bpy]^{2+}$	370 (2.6)	281 (2.8)	282 (3.1)	260 (1.7)	283 (3.4)
	521 (1.4)	369 (1.8)	370 (2.4)	370 (2.3)	376 (2.8)
		517 (1.1)	514 (1.1)	516 (0.7)	518 (1.3)
$[Ru(azpy)_2phen]^{2+}$	369 (2.2)	260 (4.1)	260 (3.9)	260 (2.9)	260 (3.7)
	521 (1.1)	367 (2.4)	369 (2.5)	371 (1.9)	376 (2.5)
		516 (1.1)	514 (1.2)	516 (0.9)	518 (1.1)

[a]Molar Extinction coefficient

In the UV region (200-400 nm), the very intense bands were presumably due to intra-ligand, $\pi \rightarrow \pi^*$ transitions.

In the visible region (400-800 nm), the $[Ru(azpy)_2L]^{2+}$ complexes (L = azpy, azpym, bpy and phen) exhibited only one intense bands. In this region may be due to a metal-to-ligand charge-transfer transition (MLCT). The absorption bands of all complexes were not shifted when polarity of solvents was increased.

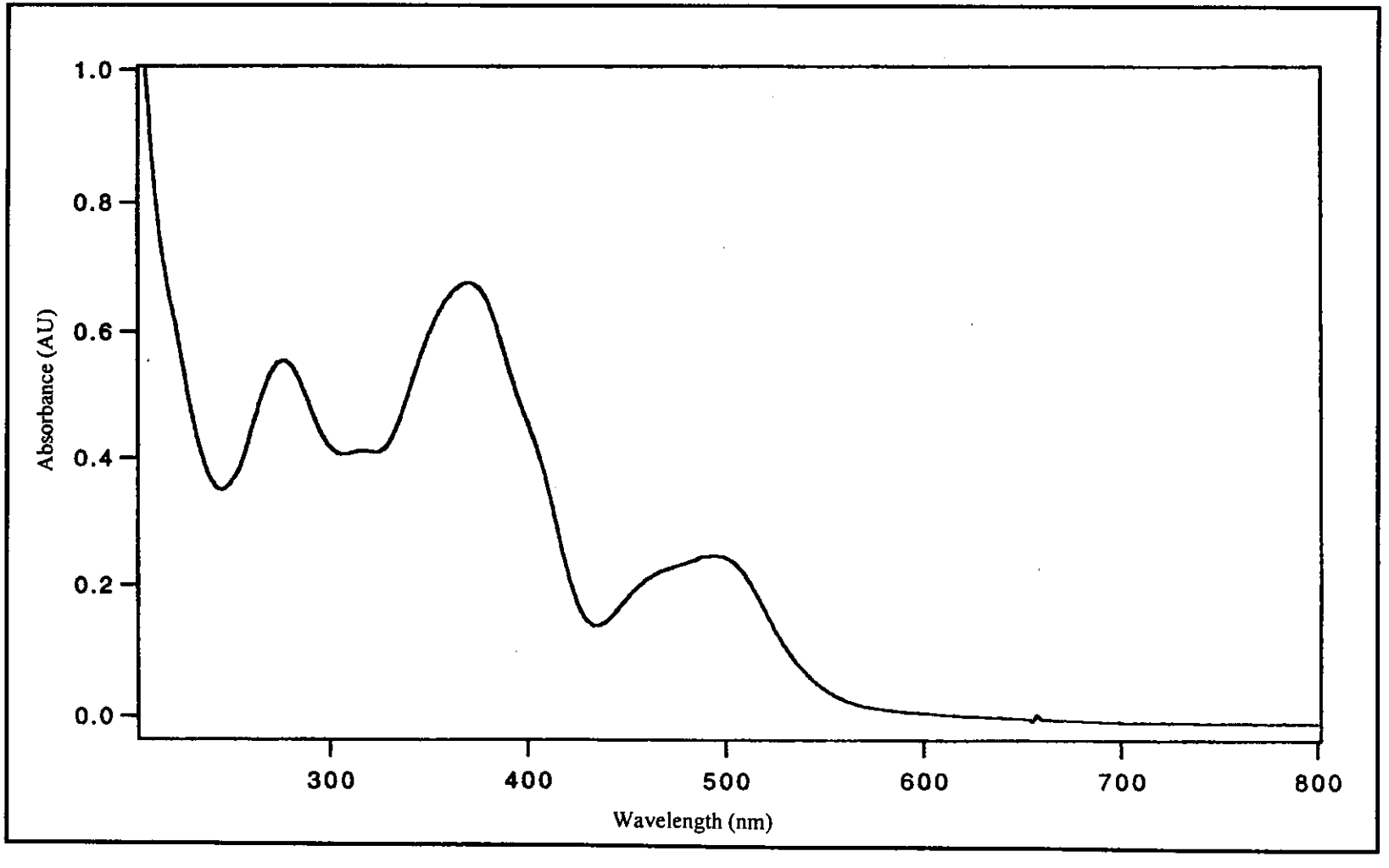

Figure 54 UV-Visible absorption spectrum of $[Ru(azpy)_3](PF_6)_2$ in CH_3CN.

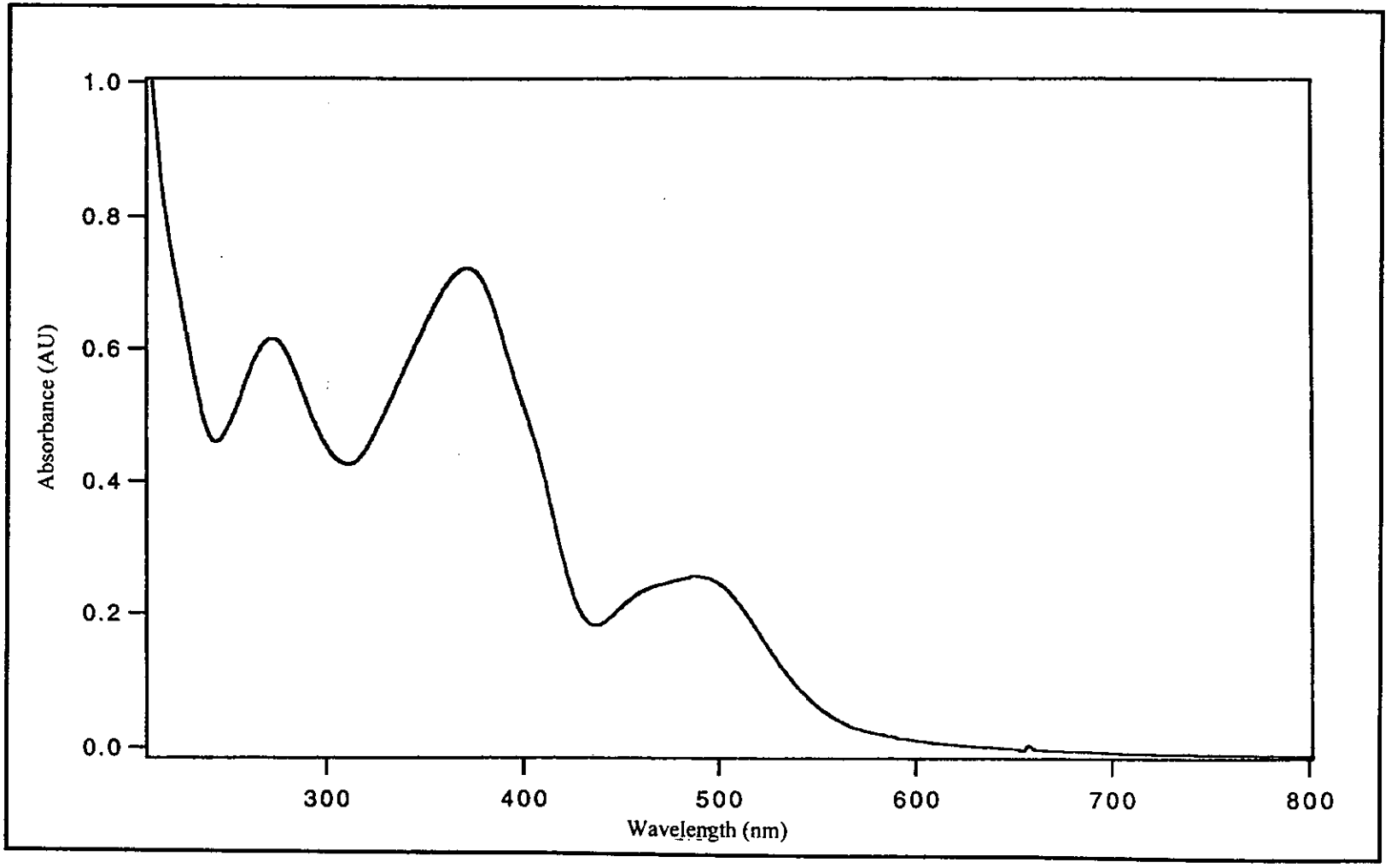

Figure 55 UV-Visible absorption spectrum of $[Ru(azpy)_2azpym](PF_6)_2$ in CH_3CN.

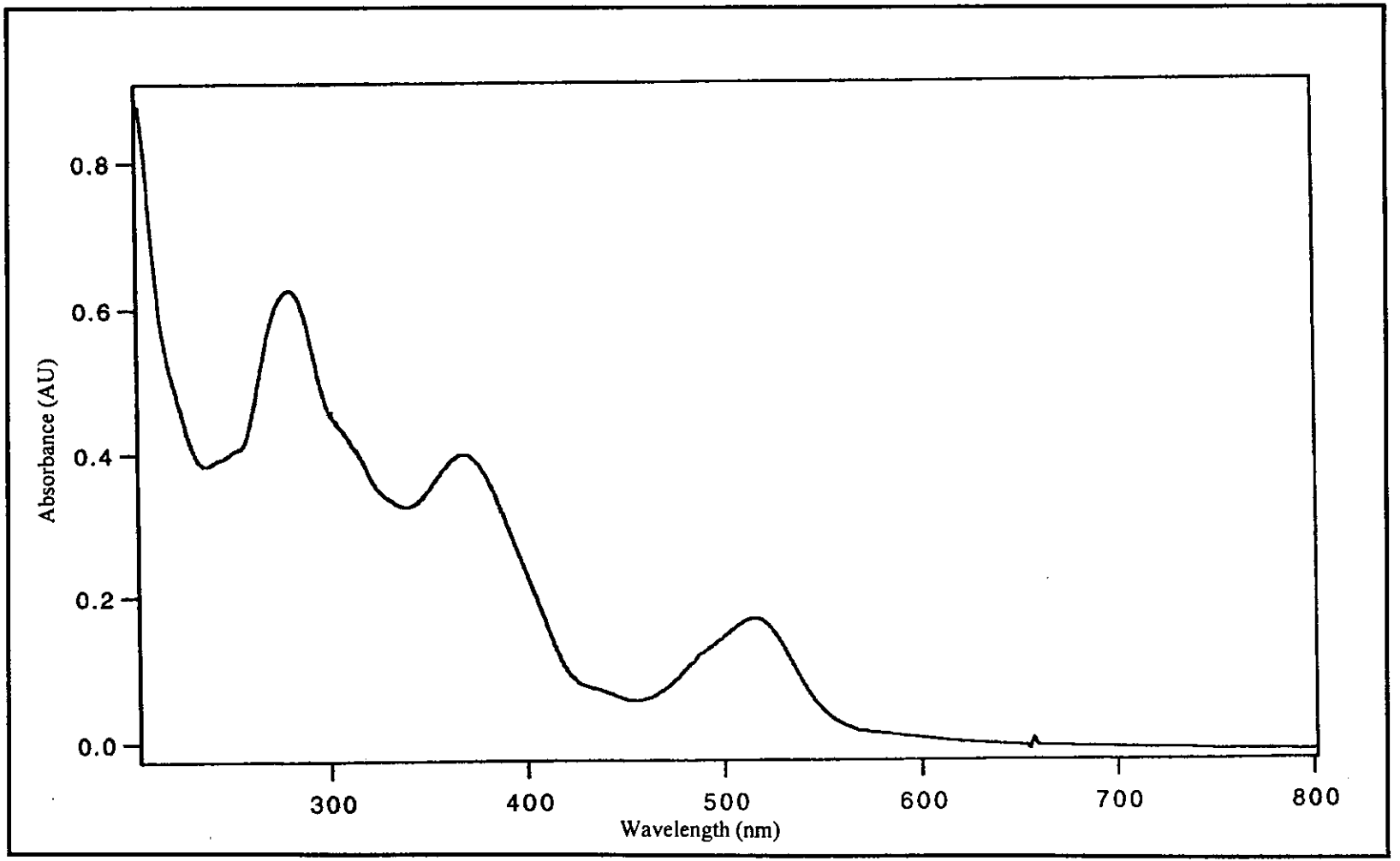

Figure 56 UV-Visible absorption spectrum of $[Ru(azpy)_2bpy](PF_6)_2$ in CH_3CN.

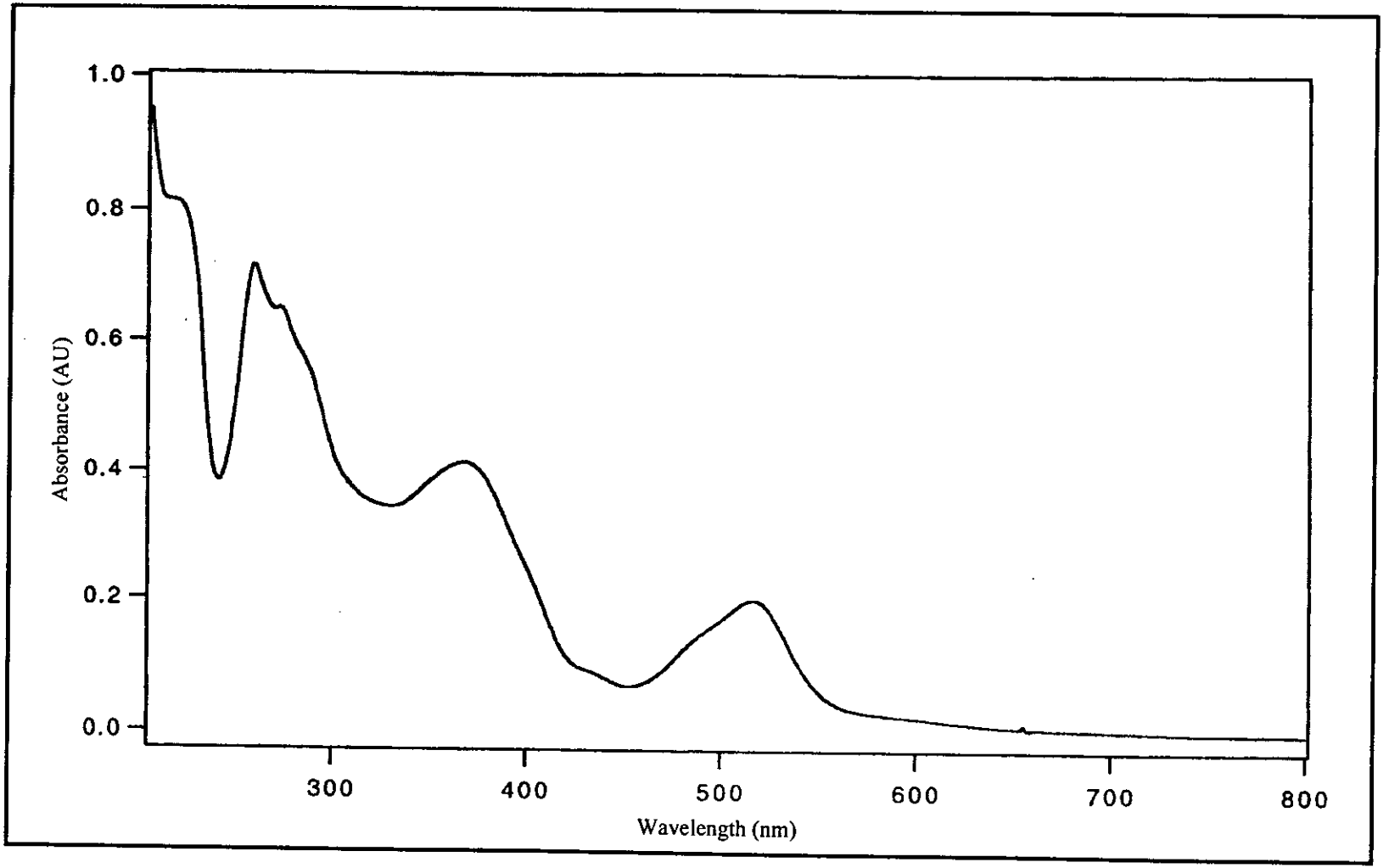

Figure 57 UV-Visible absorption spectrum of $[Ru(azpy)_2phen](BF_4)_2$ in CH_3CN.

3.5.5 Nuclear Magnetic Resonance spectroscopy

The NMR spectra of each complex prepared in acetone-d_6. Tetramethylsilane (TMS, $(CH_3)_4Si$) was used as an internal reference. The ^1H NMR spectra the complexes of $[Ru(azpy)_2L]^{2+}$ contained several overlapping resonance in aromatic region, owing to a large number of similar protons of these complex. The individual proton resonance were assigned on the basis of its relative intensity, spin-spin structure and ^1H-^1H COSY NMR spectroscopy. The ^{13}C NMR assignments were based on the ^1H-^{13}C HMQC NMR spectra. The NMR spectroscopic data of $[Ru(azpy)_2L]^{2+}$ complexes are presented in Table 22 to 25.

(a) $[Ru(azpy)_3](PF_6)_2$ complex

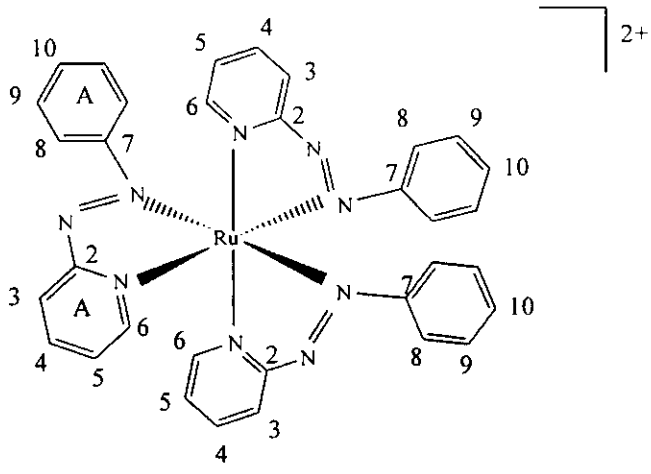

Since the $[Ru(azpy)_3](PF_6)_2$ complex was unsymmetrically, resulting in twenty-one resonances in the ^1H NMR spectrum (Figure 58), seven from each azpy ligand in the region of 9.20-7.02 ppm. The proton of pyridine ring (A) appeared at lower field than other pyridine ring. The pyridine protons (3H-6H) exhibited at

downfield than phenyl protons (8H-10H). The ^{1}H-^{1}H COSY spectrum was shown in Figure 59.

The ^{13}C NMR signal assignments (Figure 60) were based on the ^{1}H-^{13}C HMQC spectrum (Figure 61). The ^{13}C NMR spectrum showed twenty-two methine carbons, and six quaternary carbons. The chemical shifts were downfield of the free ligands position. The chemical shift data and proton, carbon assignments of this complex are summarized in Table 22.

Table 22 The NMR spectroscopic data of $[Ru(azpy)_3](PF_6)_2$ in acetone-d_6 solution

H-Position	^{1}H NMR			^{13}C NMR
	δ (ppm)	J (Hz)	Number of H	δ (ppm)
3 (A)	9.28 (d)	8.0	1	130.78
6 (A)	8.81 (d)	5.0	1	153.10
3	8.75 (d)	8.0	1	130.78
3	8.71 (d)	8.0	1	130.78
4 (A)	8.70 (dd)	7.5, 8.0	1	143.12
6	8.63 (d)	5.5	1	151.03
4	8.56 (ddd)	8.0, 8.0	1	143.05
4	8.45 (ddd)	7.5, 8.0, 1.0	1	143.12
6	8.36 (d)	5.5	1	152.38
5 (A)	7.99 (m)	-	1	130.78
5	7.99 (m)	-	1	130.78
5	7.92 (m)	-	1	130.78
10	7.65 (dd)	7.5, 1.5	1	134.79
10	7.60 (m)	-	1	130.21
9	7.54 (dd)	8.0, 8.0	2	130.21

Table 22 (continued)

H-Position	^{1}H NMR			^{13}C NMR
	δ (ppm)	*J* (Hz)	Number of H	δ (ppm)
10	7.52 (dd)	8.5, 1.5	1	130.21
9	7.45 (dd)	8.0, 7.5	2	130.21
8	7.37 (d)	7.5	2	123.92
8	7.34 (d)	8.5	2	123.92
9	7.31 (dd)	8.0, 7.5	2	130.21
8	7.02 (d)	8.0	2	123.92
Quaternary Carbon	164.60, 163.62, 156.08, 142.35, 132.23, 132.56			

d = doublet, dd = doublet of doublet, ddd = doublet of doublet of doublet

and m = multiplet

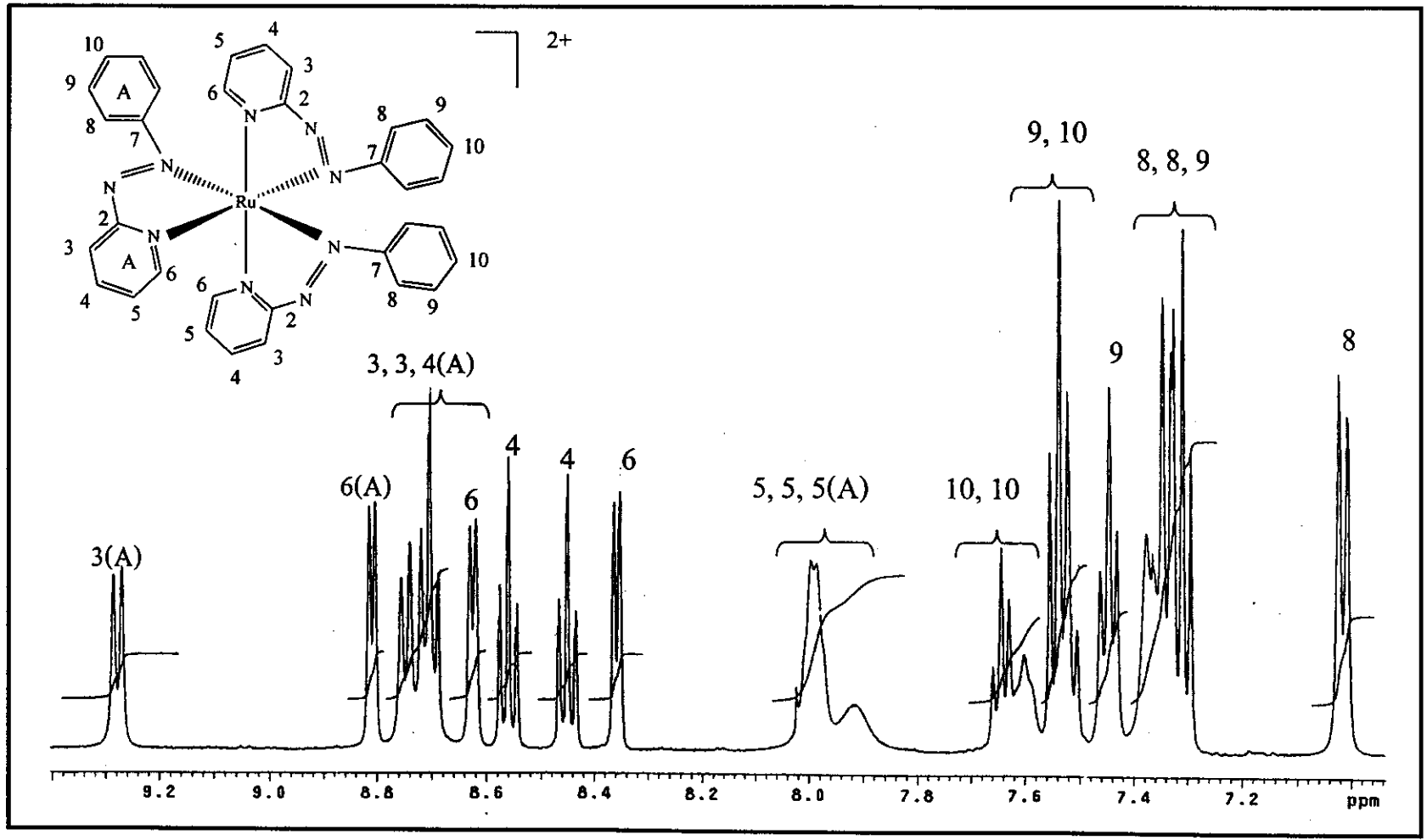

Figure 58 ^{1}H NMR spectrum of $[Ru(azpy)_3](PF_6)_2$ in acetone-d_6.

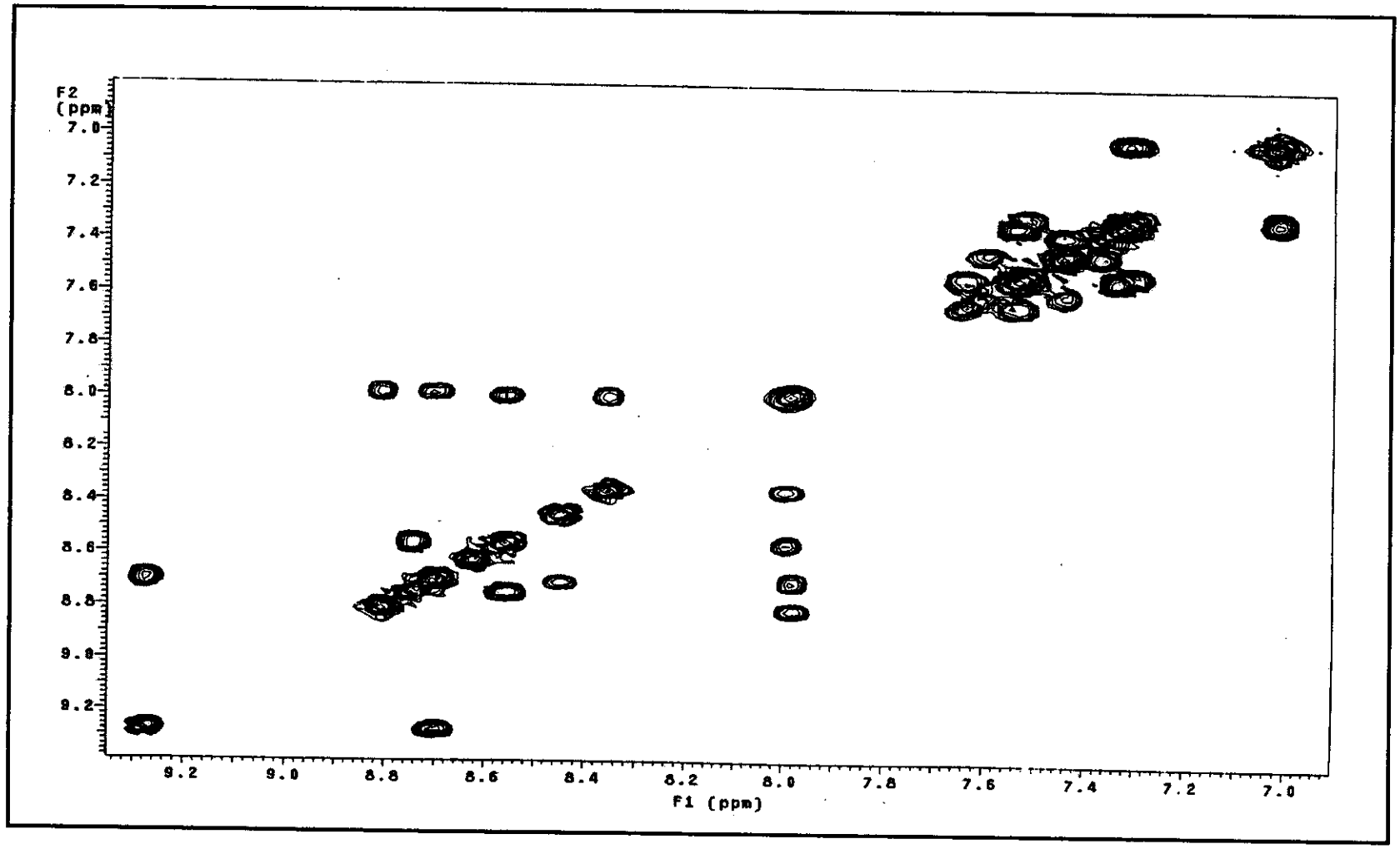

Figure 59 ^{1}H-^{1}H COSY NMR spectrum of $[Ru(azpy)_3](PF_6)_2$ in acetone-d_6

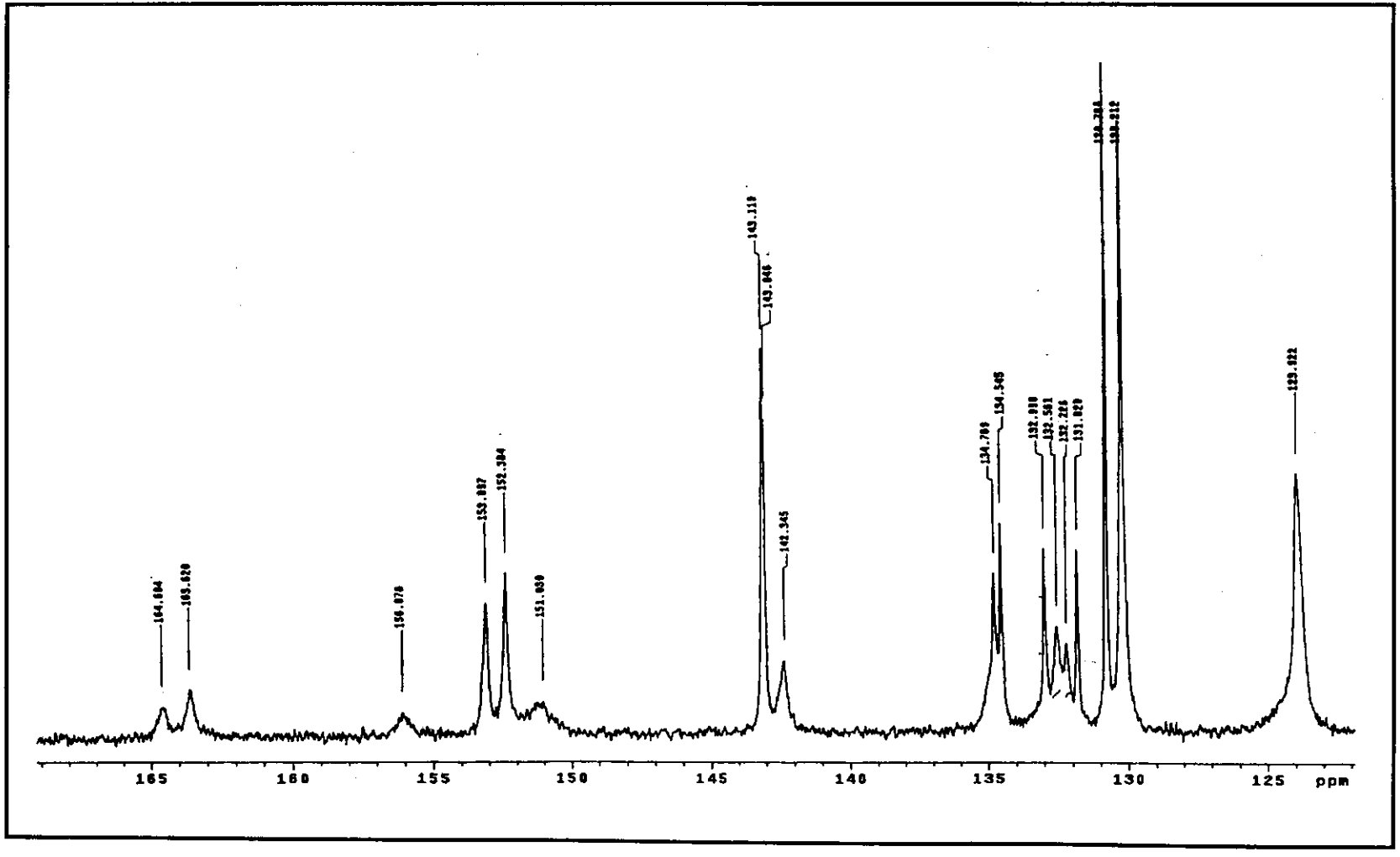

Figure 60 ^{13}C NMR spectrum of $[Ru(azpy)_3](PF_6)_2$ in acetone-d_6.

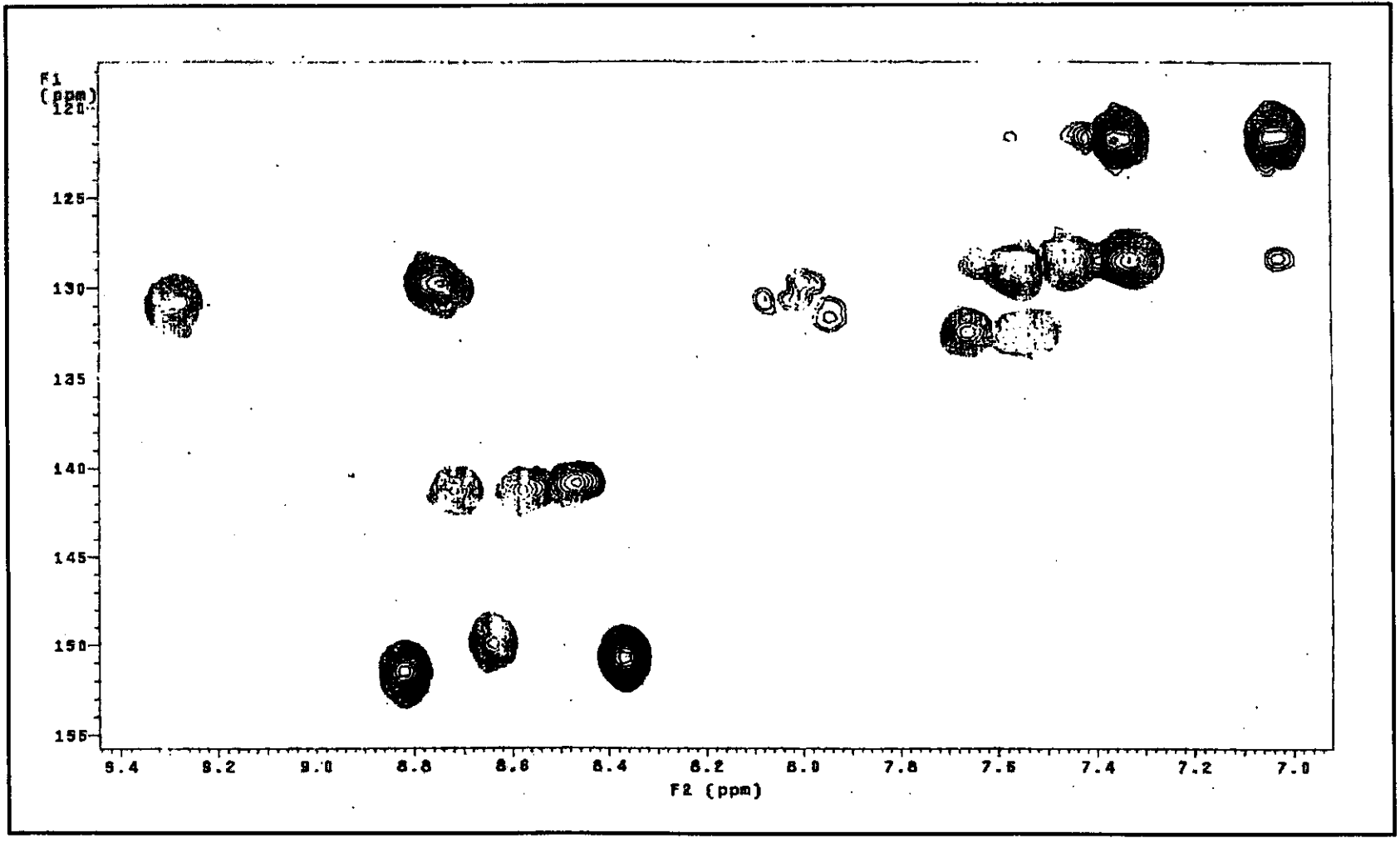

Figure 61 ^{1}H-^{13}C HMQC NMR spectrum of $[Ru(azpy)_3](PF_6)_2$ in acetone-d_6.

(b) $[Ru(azpy)_2azpym](PF_6)_2$ complex

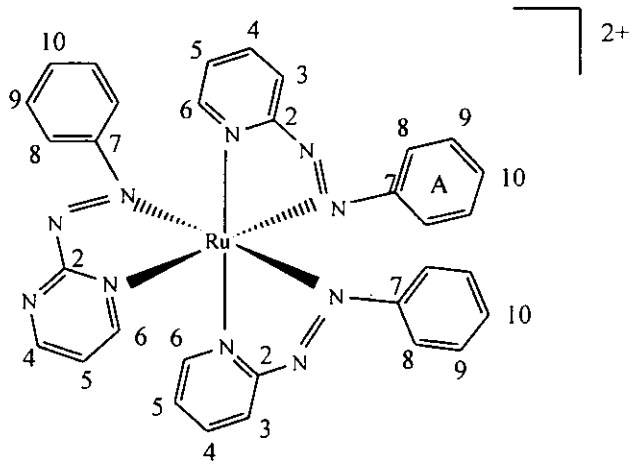

Since the $[Ru(azpy)_2azpym](PF_6)_2$ complex was unsymmetrically, therefore the ^1H NMR spectrum (Figure 62) showed 20 resonances, seven from each azpy ligand and six from azpym ligand in the region of 9.52-7.00 ppm. The protons on pyridine ring and pyrimidine ring appeared at downfield than phenyl ring. In addition, the first signal which exhibited at the lowest field was H4 of pyrimidine ring. Figure 63 showed ^1H-^1H COSY spectrum of this complex in the same solvent.

The ^{13}C NMR signal assignments (Figure 64) were based on the ^1H-^{13}C HMQC spectrum (Figure 65). The ^{13}C NMR spectrum showed twenty methine carbons, and six quaternary carbons. The chemical shifts were downfield of the free ligands positions. The chemical shift data and proton, carbon assignments of this complex are summarized in Table 23 .

Table 23 The NMR spectroscopic data of $[Ru(azpy)_2azpym](PF_6)_2$ in acetone-d_6

H-Position	^{1}H NMR			^{13}C NMR
	δ (ppm)	*J* (Hz)	Number of H	δ (ppm)
H4(azpym)	9.52 (m)		1	163.07
H3	9.31 (d)	7.5	1	130.09
H6	8.86 (d)	4.5	1	150.98
H3	8.78 (dd)	7.5, 1.0	1	129..97
H4	8.71 (d)	7.0	1	141.66
H6(azpym)	8.62 (d)	6.0	1	151.78
H4	8.58 (ddd)	8.0, 8.0	1	141.29
H6	8.40 (d)	4.5	1	150.52
H5	8.06 (ddd)	8.0, 5.5, 1.0	1	130.45
H5(azpym)	8.03 (d)	5.0	1	130.62
H5	8.01 (ddd)	8.0, 5.5, 1.0	1	130.38
H10	7.63 (m)		1	132.51
H10	7.56 (dd)	7.5, 1.5	1	132.57
H9	7.53 (dd)	7.5, 7.5	2	128.61
H10	7.52 (dd)	8.5, 1.5	1	132.61
H8	7.42 (d)	7.5	2	121.71
H9	7.35 (dd)	7.0, 7.0	2	128.78
H9	7.29 (dd)	7.0, 7.0	2	128.82
H8	7.02 (dd)	7.0, 7.0	2	121.49
H8	7.00 (dd)	7.5, 1.0	2	121.37

Table 23 (continued)

H-Position	^{1}H NMR			^{13}C NMR
	δ (ppm)	*J* (Hz)	Number of H	δ (ppm)
Quaternary Carbon	162.59, 150.13, 151.23, 141.62, 132.90, 131.22			

d = doublet, dd = doublet of doublet,

ddd = doublet of doublet of doublet and m = multiplet

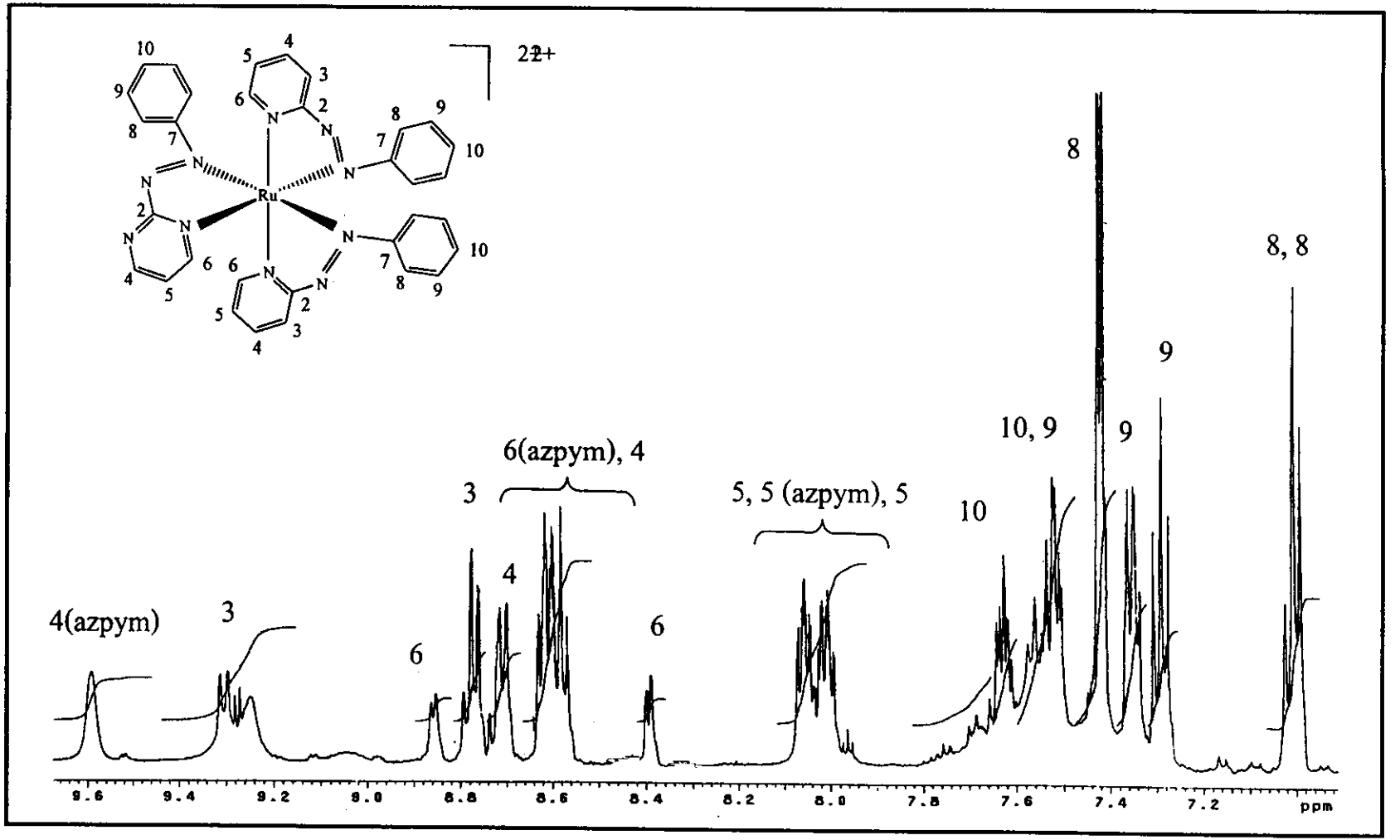

Figure 62 ^{1}H NMR spectrum of $[Ru(azpy)_2azpym](PF_6)_2$ in acetone-d_6

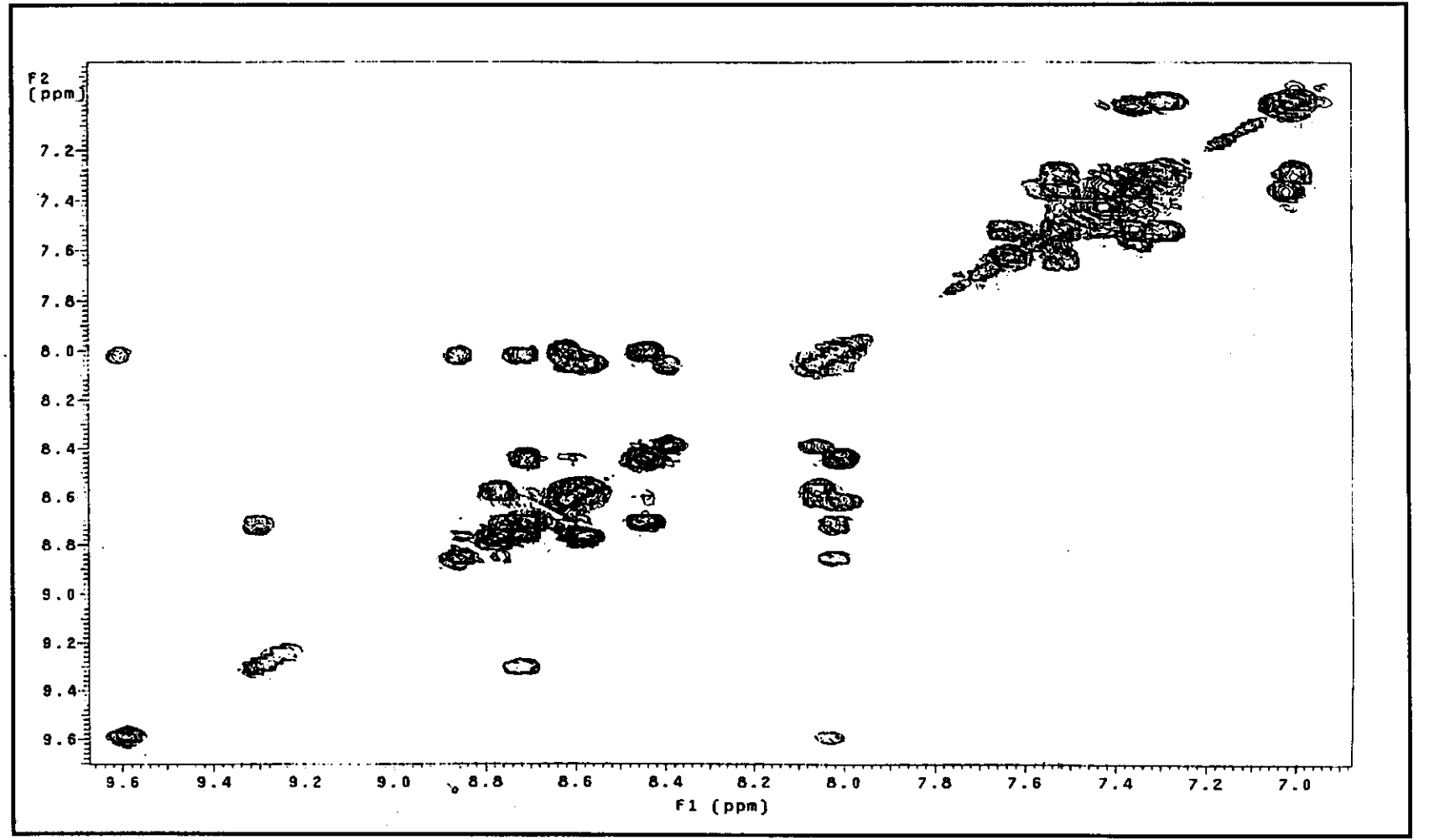

Figure 63 ^{1}H--^{1}H COSY NMR spectrum of $[Ru(azpy)_2azpym](PF_6)_2$ in acetone-d_6.

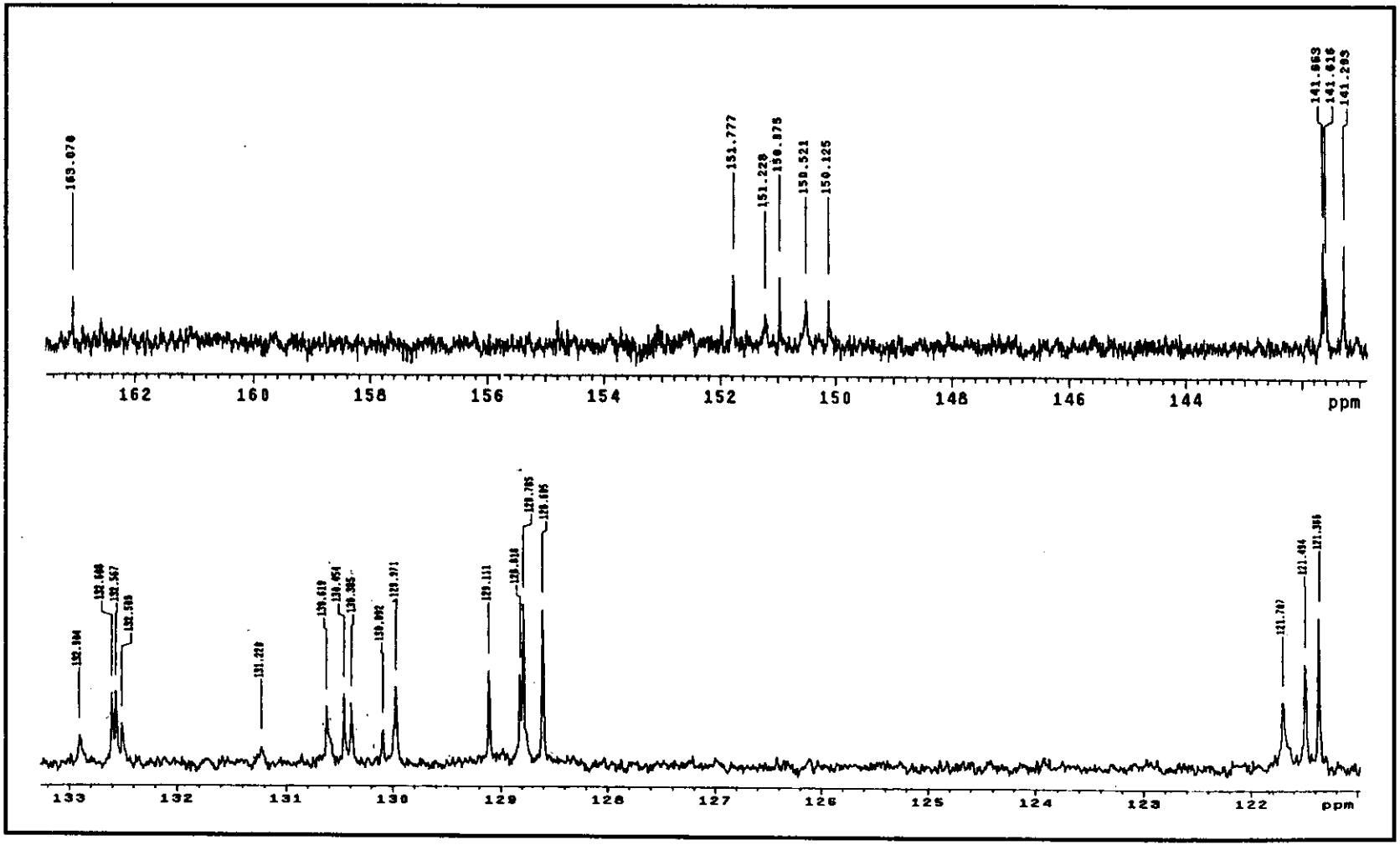

Figure 64 ^{13}C NMR spectrum of $[Ru(azpy)_2azpym](PF_6)_2$ in acetone-d_6.

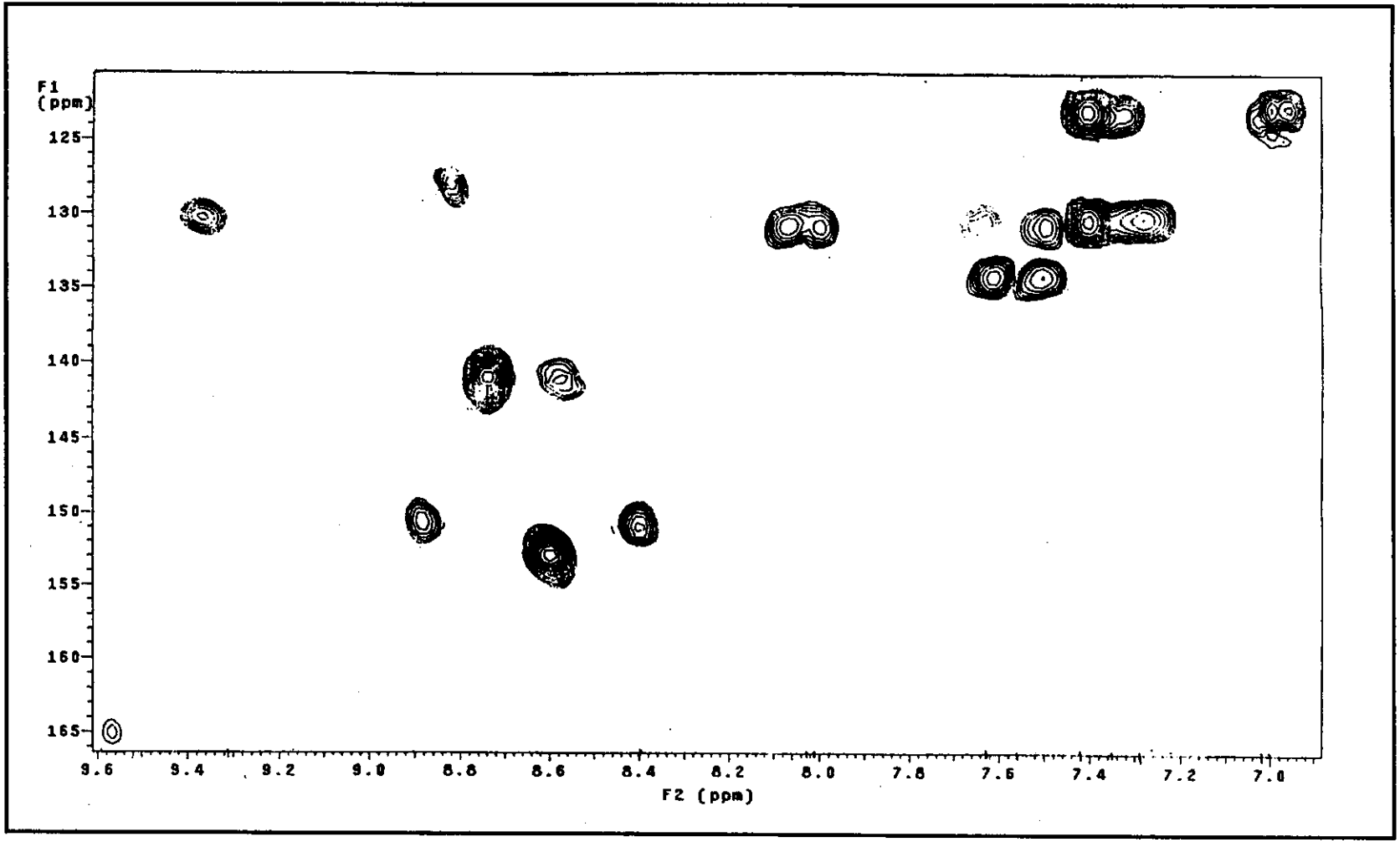

Figure 65 ^{1}H-^{13}C HMQC NMR spectrum of $[Ru(azpy)_2azpym](PF_6)_2$ in acetone-d_6.

(c) $[Ru(azpy)_2bpy](PF_6)_2$ complex

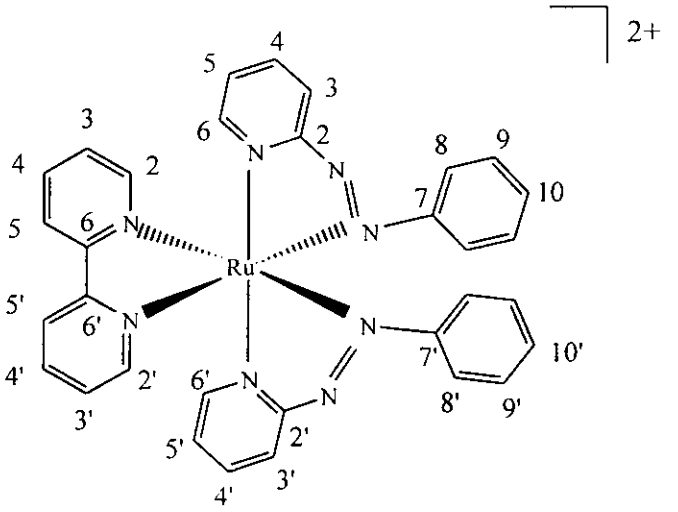

The ^1H NMR spectrum (Figure 66) of the $[Ru(azpy)_2bpy](PF_6)_2$ complex showed 11 resonances, seven from the azpy ligand and four from bpy ligand in the region of 8.99-7.33 ppm. The spectrum displayed distinct eleven peaks corresponding to only one set of ligand. It was due to the fact of the symmetry induced equivalent nature of each half of the molecule. The pyridine ring in azpy ligands exhibited at lower field than pyridine ring from the bpy ligand. The protons on pyridine ring appeared at downfield than phenyl ring. Figure 67 showed the ^1H-^1H COSY spectrum.

The ^{13}C NMR spectrum (Figure 68) showed eleven methine carbons, and three quaternary carbons (δ165.81, 156.01, 154.13 ppm). The signal in ^{13}C NMR spectrum of complex compared to the signal of the free ligands. The chemical shift data and proton, carbon assignments in this complex are summarized in Table 24 . The ^1H-^{13}C HMQC spectra is showed in Figure 69.

Table 24 The NMR spectroscopic data of $[Ru(azpy)_2bpy](PF_6)_2$ in acetone-d_6

H-Position	^{1}H NMR			^{13}C NMR
	δ (ppm)	*J* (Hz)	Number of H	δ (ppm)
5, 5′ (bpy)	8.99 (d)	8.0	2	126.45
3, 3′	8.79 (d)	7.5	2	130.93
4, 4′ (bpy)	8.43 (ddd)	8.0, 8.0, 1.5	2	141.96
4, 4′	8.42 (ddd)	8.0, 8.0, 1.5	2	141.55
2, 2′ (bpy)	8.41(d)	5.5	2	153.86
6, 6′	8.38 (d)	5.5	2	154.13
3, 3′ (bpy)	7.84 (m)	-	2	131.15
5, 5′	7.79 (ddd)	7.5, 5.0, 1.5	2	130.0
10,10	7.58 (m)	-	2	133.99
9, 9′	7.42 (dd)	8.0, 7.0	4	130.42
8, 8′	7.37 (m)	-	4	123.55
Quaternary Carbon		165.81, 154.13, 156.01		

d = doublet, dd = doublet of doublet,

ddd = doublet of doublet of doublet and m = multiplet

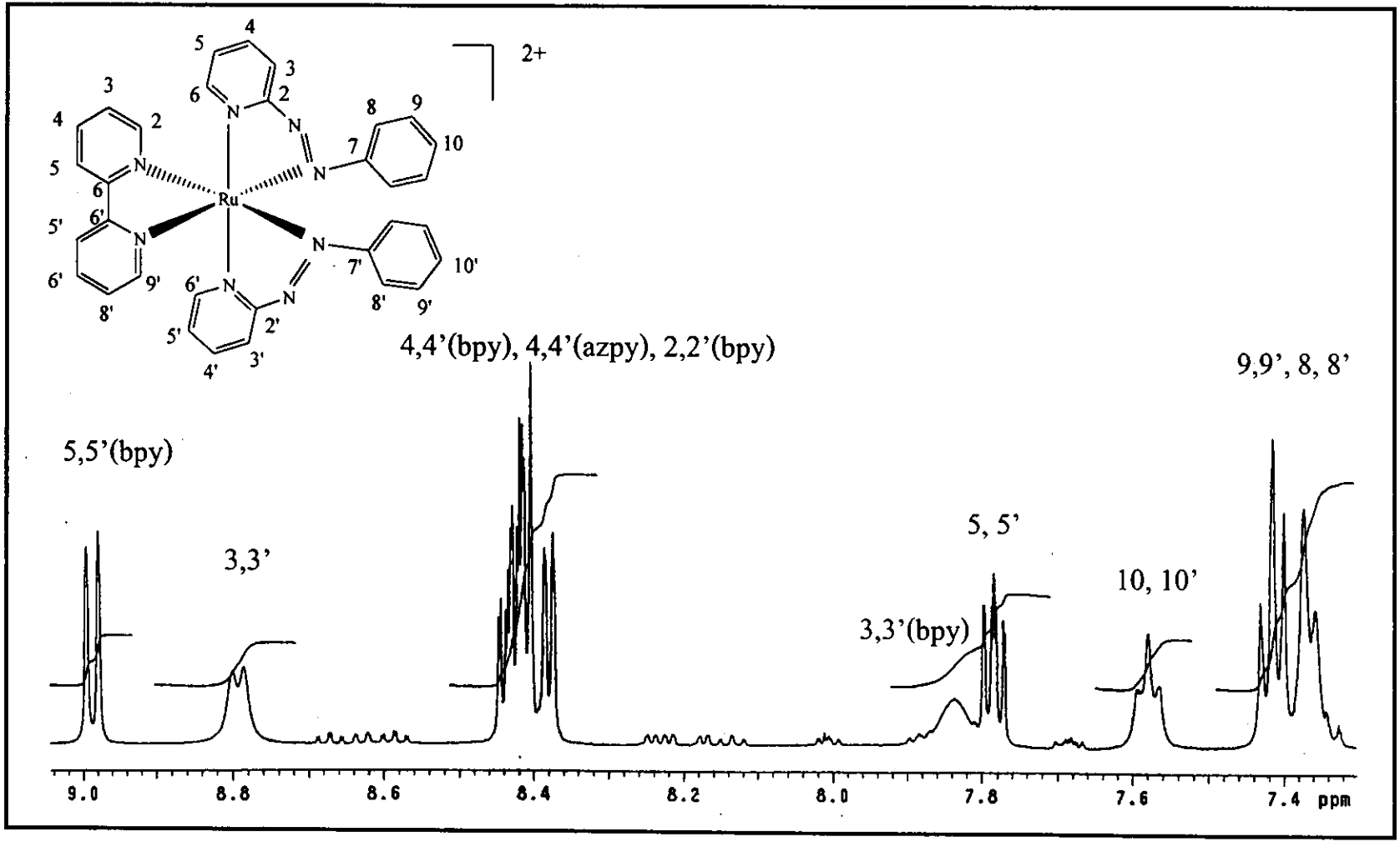

Figure 66 ^{1}H NMR spectrum of $[Ru(azpy)_2bpy](PF_6)_2$ in acetone-d_6.

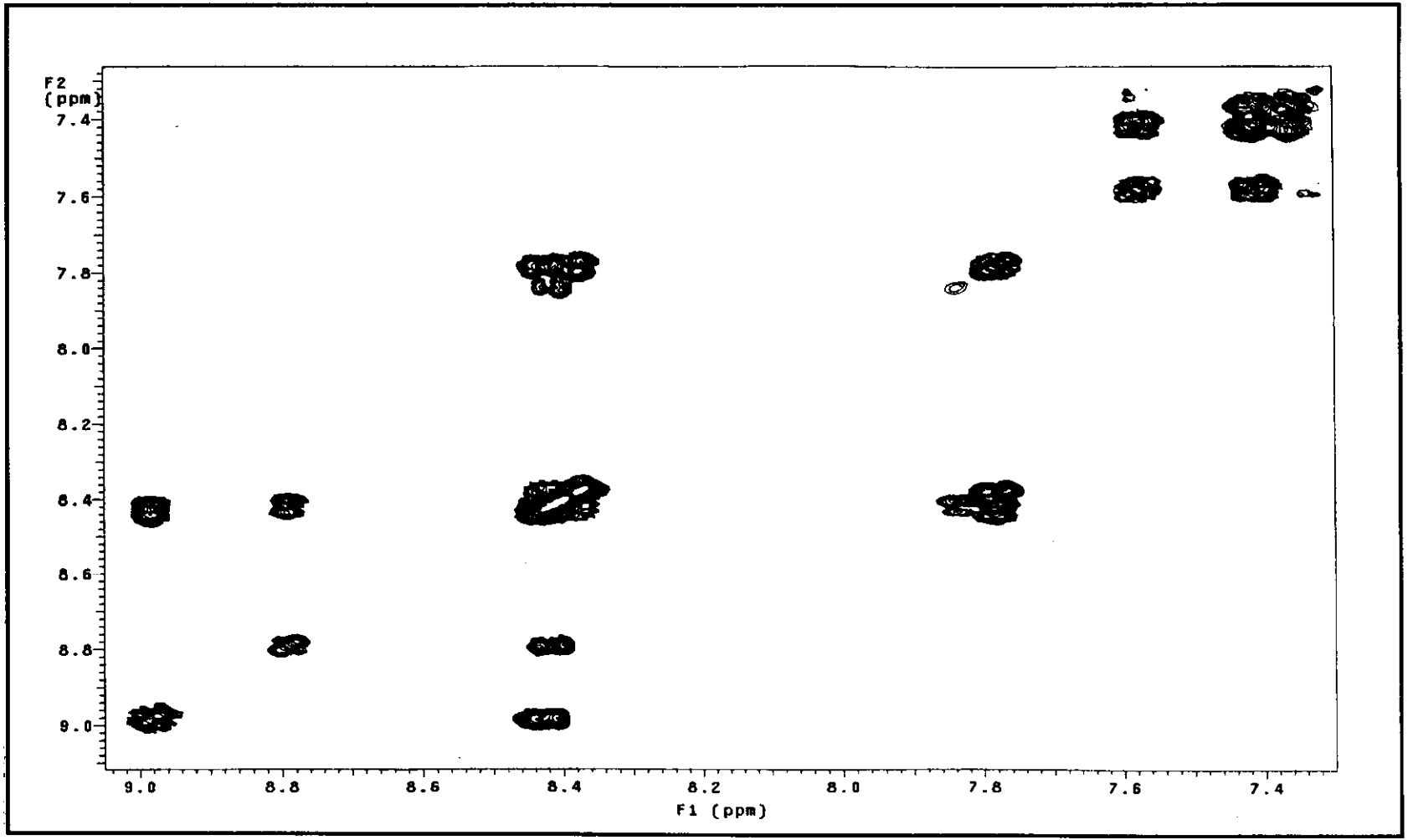

Figure 67 ^{1}H-^{1}H COSY NMR spectrum of $[Ru(azpy)_2bpy](PF_6)_2$ in acetone-d_6.

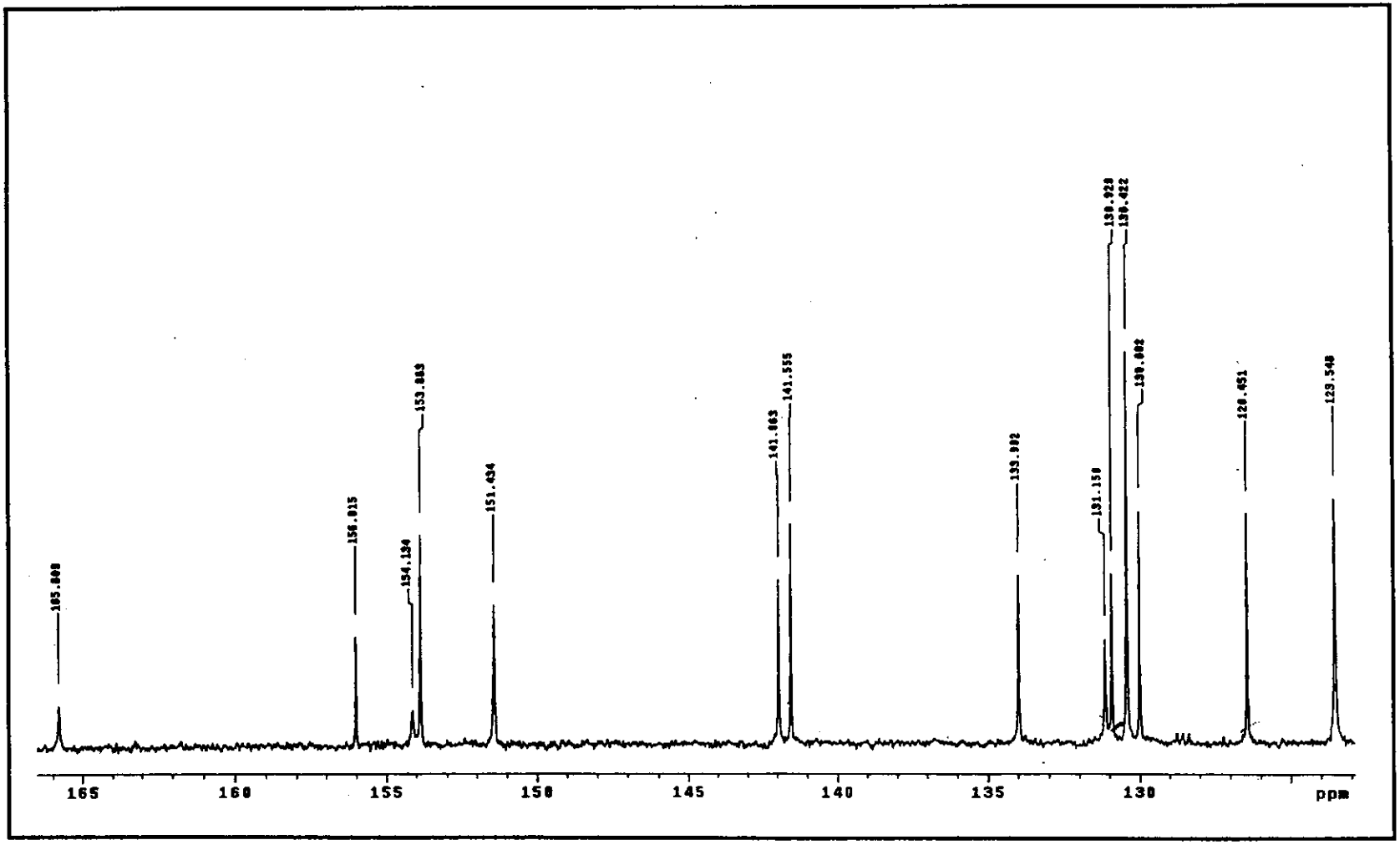

Figure 68 ^{13}C NMR spectrum of $[Ru(azpy)_2bpy](PF_6)_2$ in acetone-d_6.

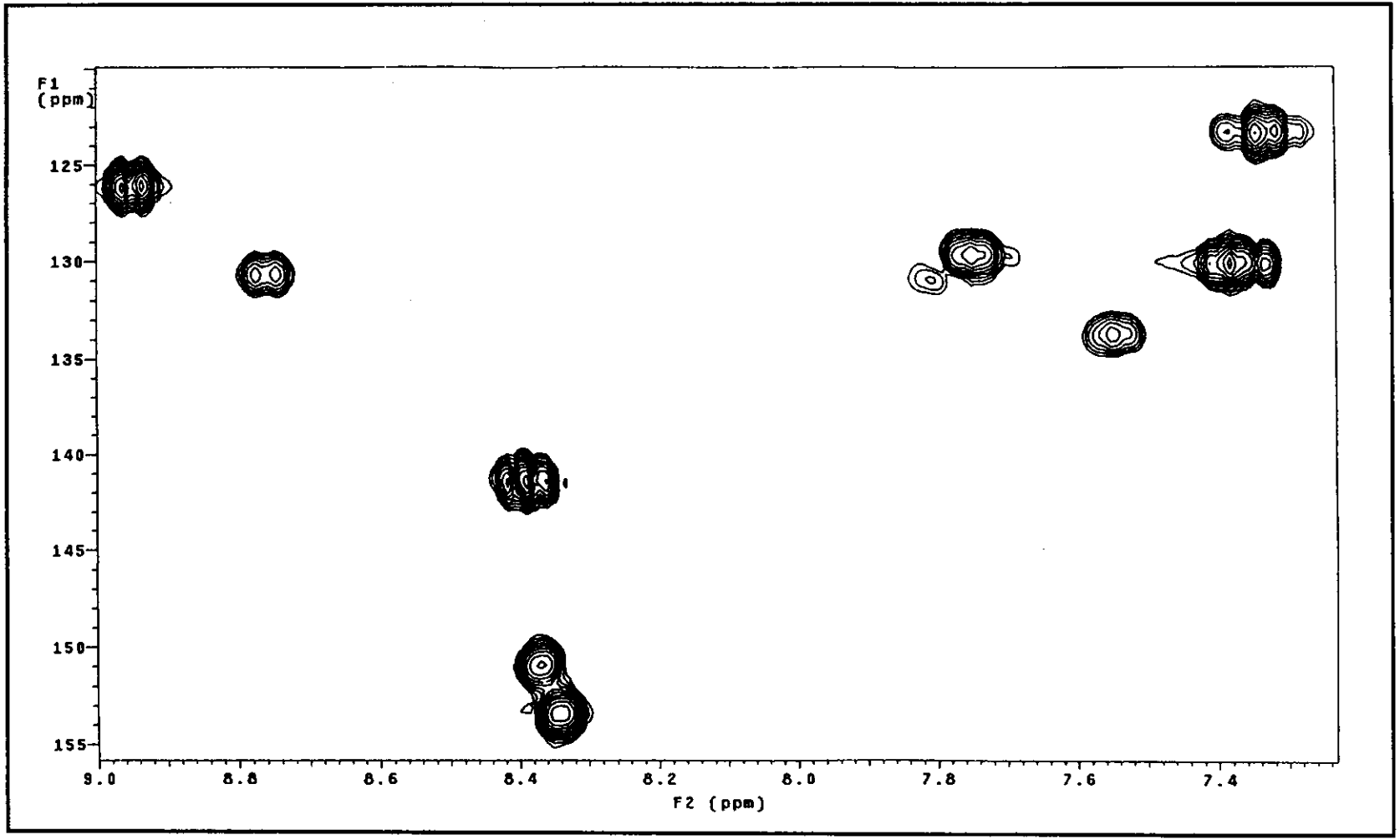

Figure 69 ^{1}H-^{13}C HMQC NMR spectrum of $[Ru(azpy)_2bpy](PF_6)_2$ in acetone-d_6

(d) $[Ru(azpy)_2phen](BF_4)_2$ complex

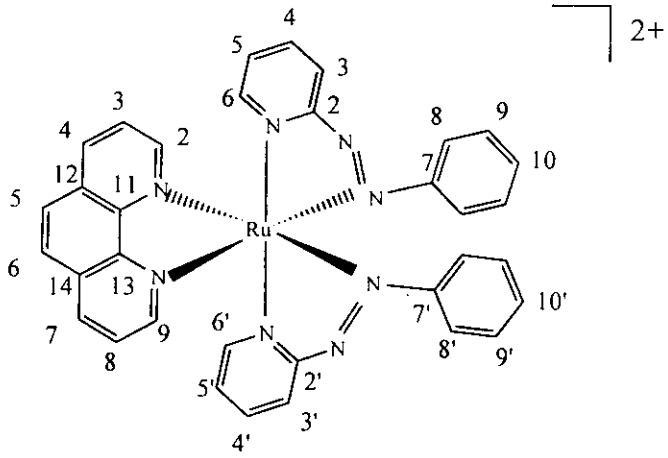

The ^1H NMR spectrum (Figure 70) and ^1H-^1H COSY spectrum (Figure 71) of the $[Ru(azpy)_2phen](BF_4)_2$ complex showed 11 resonances for 26 protons in the region of 9.05-7.43 ppm. The spectrum displayed distinct eleven peaks corresponding to only one set of ligand which was due to the fact of the symmetry of the molecule. The protons on pyridine ring appeared at downfield than phenyl ring. The proton H13 on phen ligand occurred at 9.05 ppm which was lower field than other proton and gave signal doublet of doublet.

The ^{13}C NMR spectrum (Figure 72) showed eleven methine carbons, and four quaternary carbons (δ 165.59, 154.37, 146.08, 130.77 ppm). The signals of ^{13}C NMR spectrum of complex were compared to the signals of the free ligands. The chemical shift data and proton, carbon assignments in this complex were summarized in Table 25 . Figure 73 showed ^1H-^{13}C HMQC spectrum.

Table 25 The NMR spectroscopic data of $[Ru(azpy)_2phen](BF_4)_2$ in acetone-d_6

H-Position	^{1}H NMR			^{13}C NMR
	δ (ppm)	*J* (Hz)	Number of H	δ (ppm)
4,7 (phen)	9.05 (dd)	8.5, 1.5	2	140.51
2,9 (phen)	8.86 (dd)	5.5, 1.5	2	154.47
3,3′	8.83 (m)		2	128.18
5,6 (phen)	8.52 (s)		2	130.86
4, 4′	8.36 (ddd)	8.0, 7.8, 1.5	2	141.70
6, 6′	8.16 (ddd)	6.0, 1.5, 1	2	151.37
3,8 (phen)	8.14 (dd)	8.5, 5.0	2	130.37
5, 5′	7.65 (t)	6.5, 6.5	2	129.34
10, 10′	7.60 (t)	7.0, 1.5	2	133.70
9, 9′	7.46	7.0, 7.0	4	132.39
8, 8′	7.43 (dd)	7.0, 2.0	4	123.43
Quaternary Carbon		165.59, 154.37, 146.08, 130.77		

d = doublet, dd = doublet of doublet,

ddd = doublet of doublet of doublet and m = multiplet

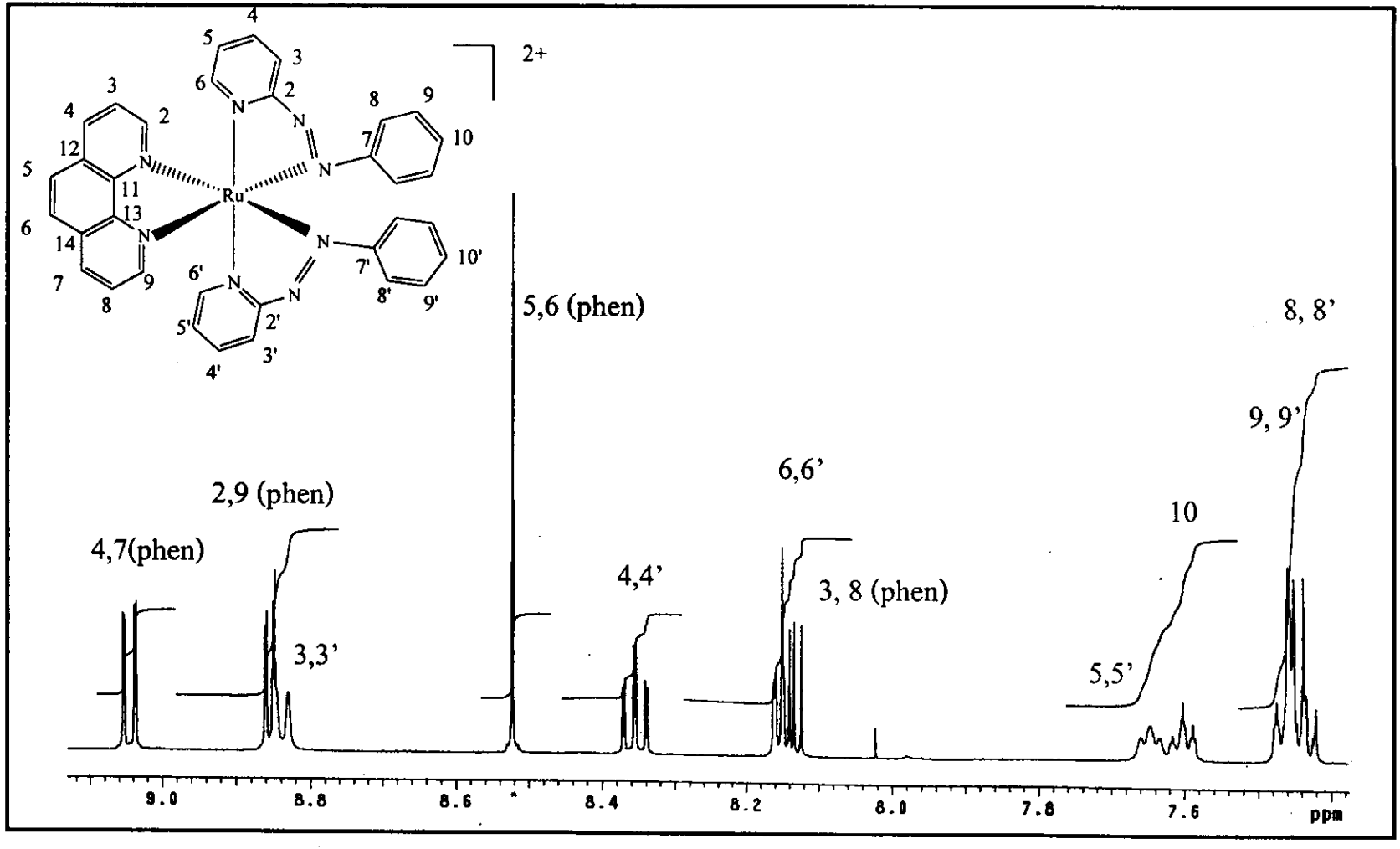

Figure 70 ^{1}H NMR spectrum of $[Ru(azpy)_2phen](BF_4)_2$ in acetone-d_6

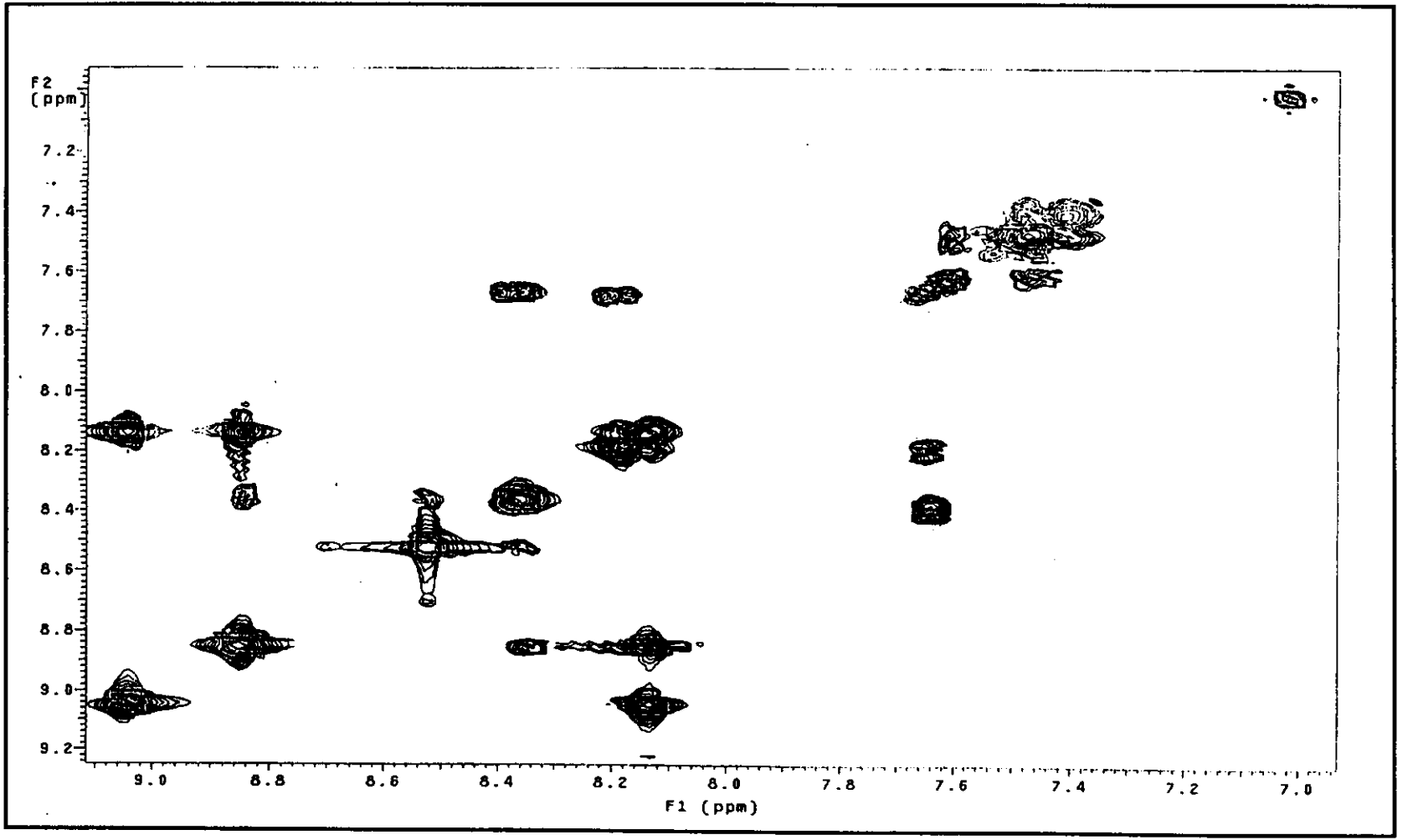

Figure 71 ^{1}H-^{1}H COSY NMR spectrum of $[Ru(azpy)_2phen](BF_4)_2$ in acetone-d_6

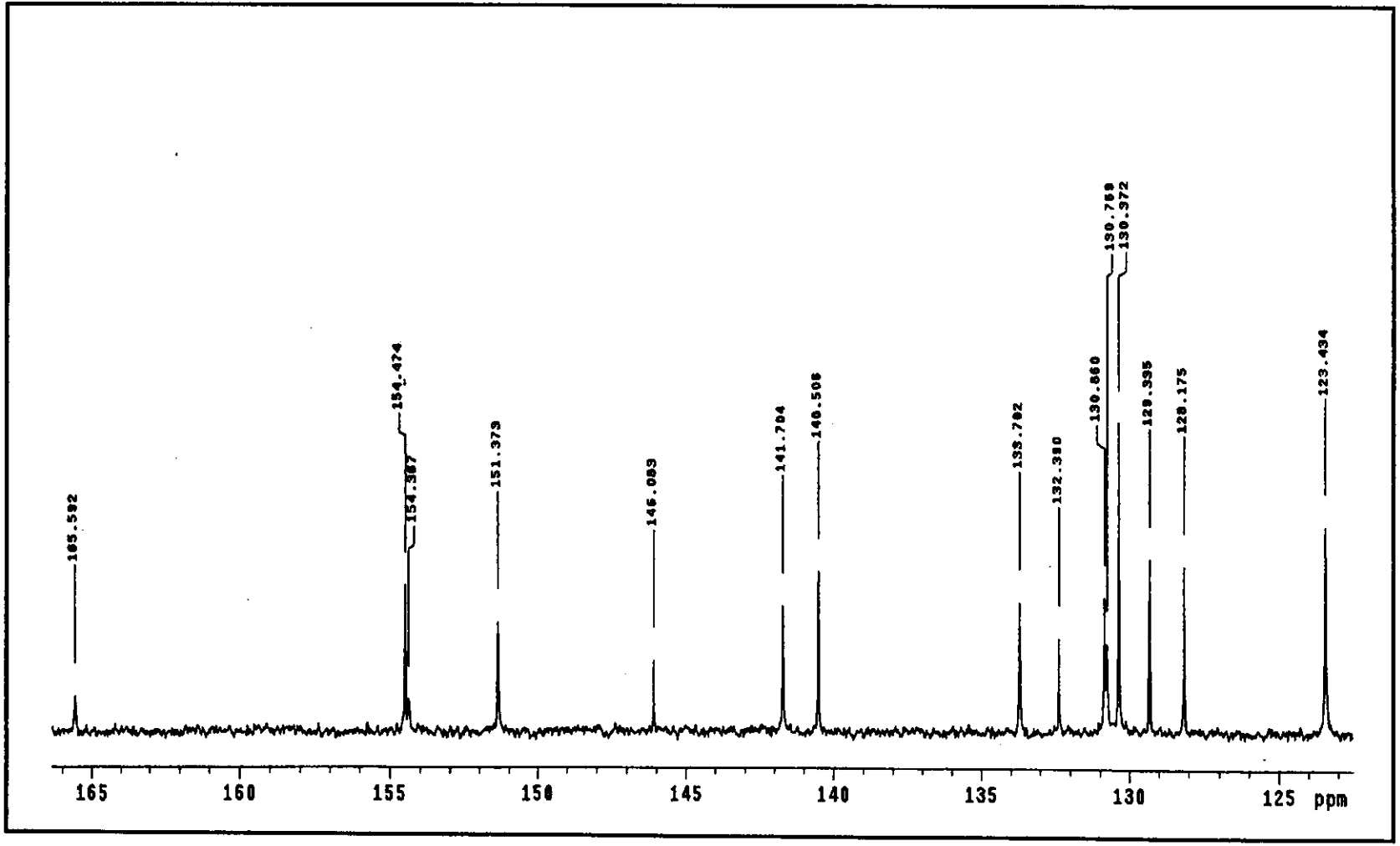

Figure 72 ^{13}C NMR spectrum of $[Ru(azpy)_2phen](BF_4)_2$ in acetone-d_6

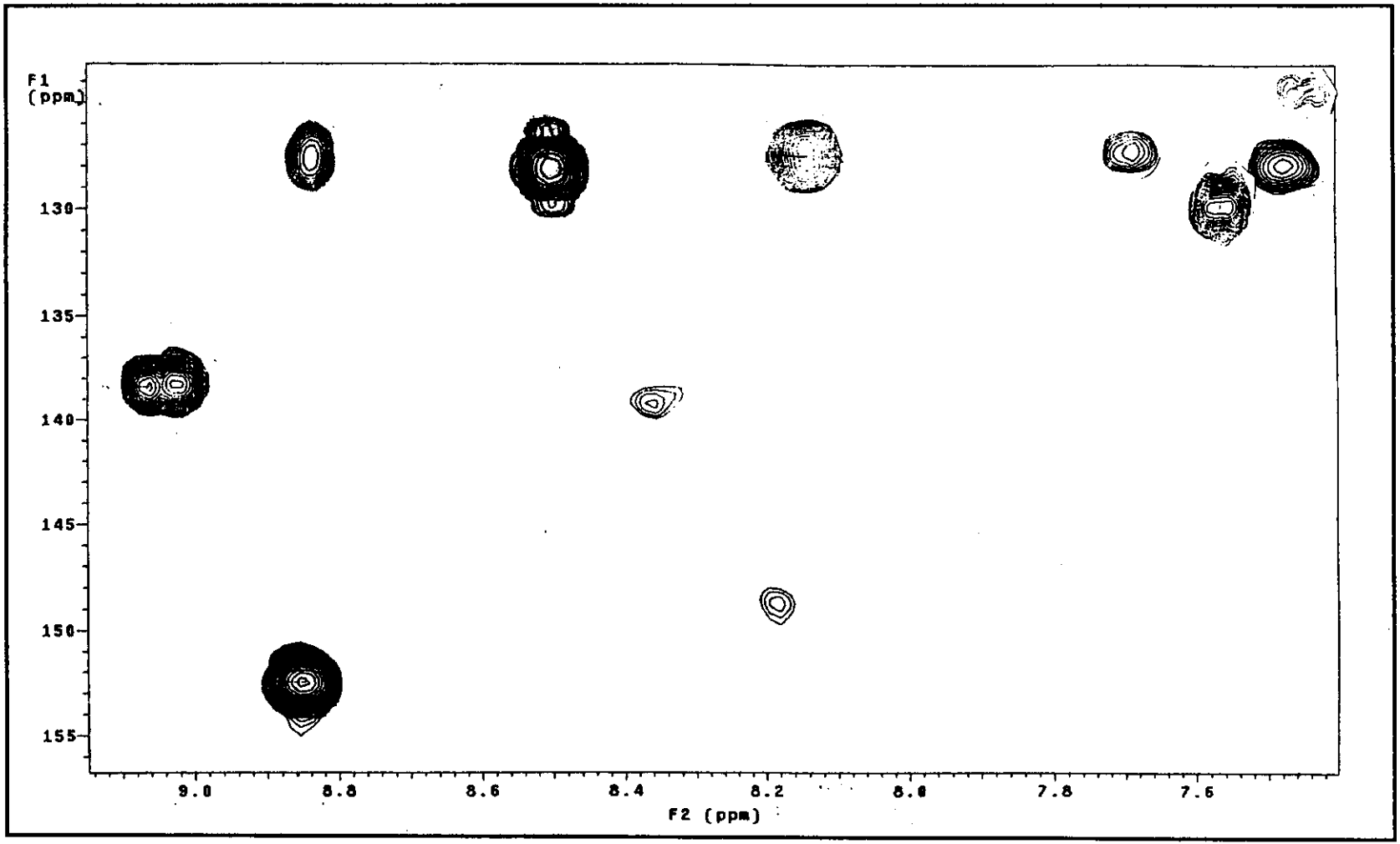

Figure 73 ^{1}H-^{13}C HMQC NMR spectrum of $[Ru(azpy)_2phen](BF_4)_2$ in acetone-d_6.

3.5.6 Cyclic voltammetry

Cyclic voltammetry was carried out in 0.1 M TBAH using acetonitrile as the solvent. The cyclic voltammetric data are presented in Table 26 and cyclic voltammograms of $[Ru(azpy)_2L]^{2+}$ (L = azpy, azpym, bpy and phen) are shown in Figure 74 to 77, respectively.

Table 26 Cyclic voltammetric data of $[Ru(azpy)_2L]^{2+}$ where L = azpy , azpym, bpy and phen in 0.1 M TBAH acetonitrile solution at scan rate 50 mV/s (ferrocene as an internal standard, ΔE_p = 65 mV)

$[Ru(azpy)_2L]^{2+}$ L =	$E_{1/2}$, V (ΔE_p, mV)					
	Oxidation range	Reduction range				
	Ru(II/III)	I	II	III	IV	V
azpy	n	-0.39 (85)	-0.70 (83)	-1.14 (140)	-1.78 (70)	-1.98 (110)
azpym	n	-0.29 (85)	-0.67 (85)	-1.14 (75)	-1.71 (85)	-1.96 (105)
bpy	n	-0.55 (105)	-1.03 (82)	-1.80 (100)	-2.17 (110)	-
phen	n	-0.51 (80)	-1.10 (70)	-1.79 (125)	-2.15 (100)	-

n = cannot be observe

Oxidation range

All complexes were studied in the range of 0.0-1.0 V. The couple of Ru(II/III) in this range were not observed, because the Ru(II/III) couple of azpy, azpym, bpy and phen complexes lied beyond the accessible potential range.

Reduction range

Reduction were observed in the potential range from 0 to –2.4 V. Five successive redox couples were observed in the azpy, azpym complexes but where in the bpy, phen complexes only four were detected experimentally. All the couple in this group of complexes were reversible couple.

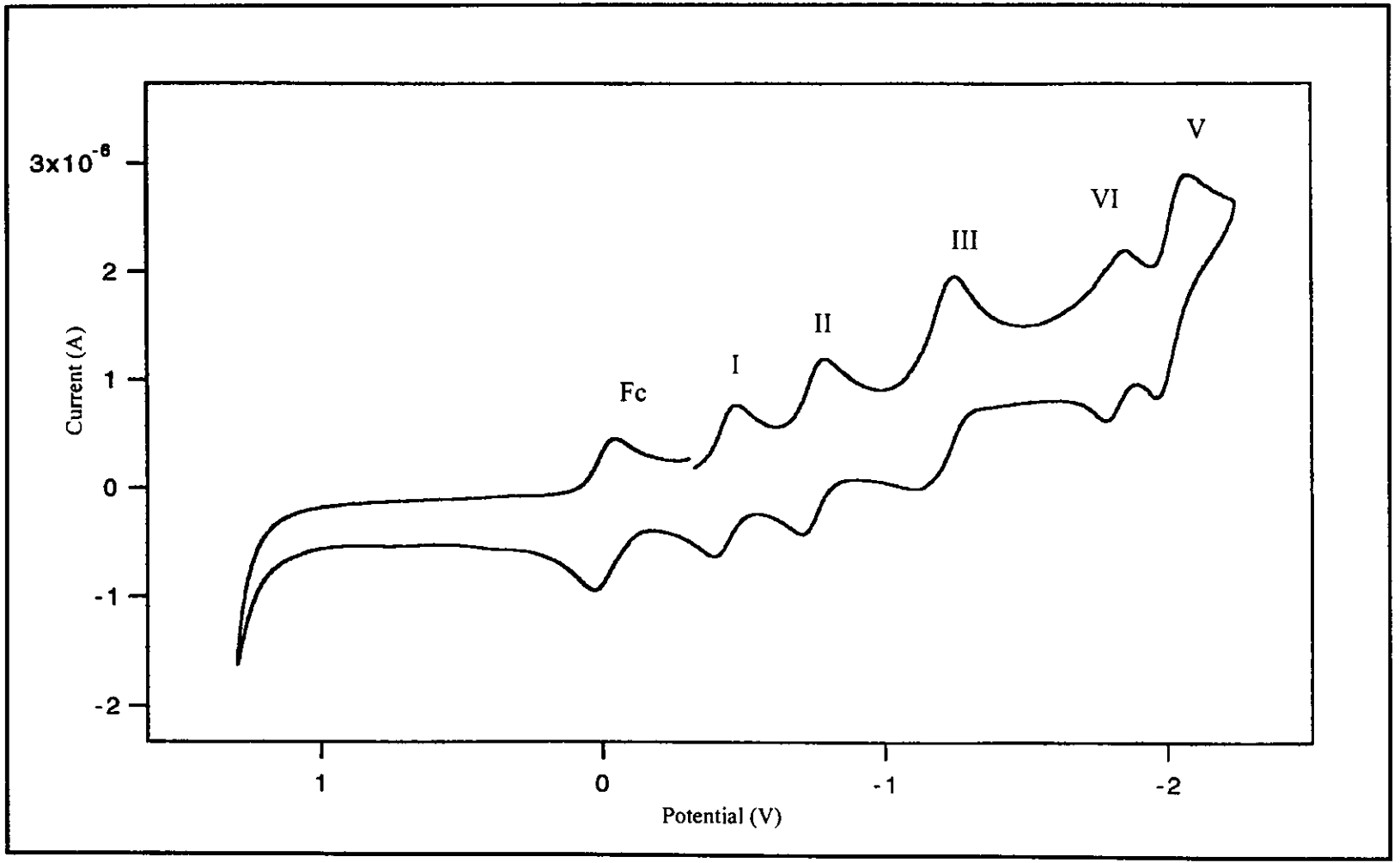

Figure 74 Cyclic voltammogram of $[Ru(azpy)_3](PF_6)_2$ in 0.1 M TBAH CH_3CN at scan rate 50 mV/s.

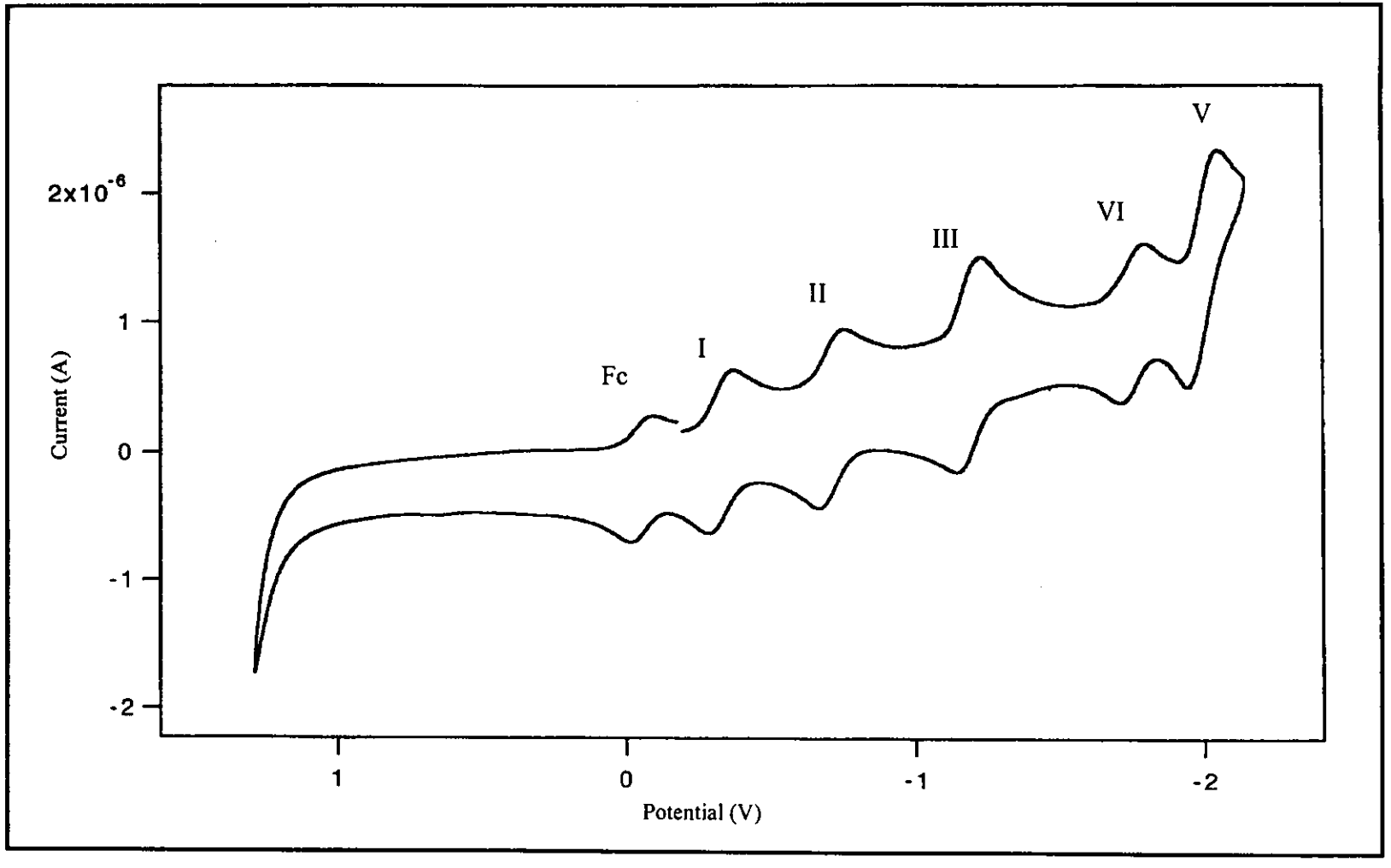

Figure 75 Cyclic voltammogram of $[Ru(azpy)_2azpym](PF_6)_2$ in 0.1 M TBAH CH_3CN at scan rate 50 mV/s.

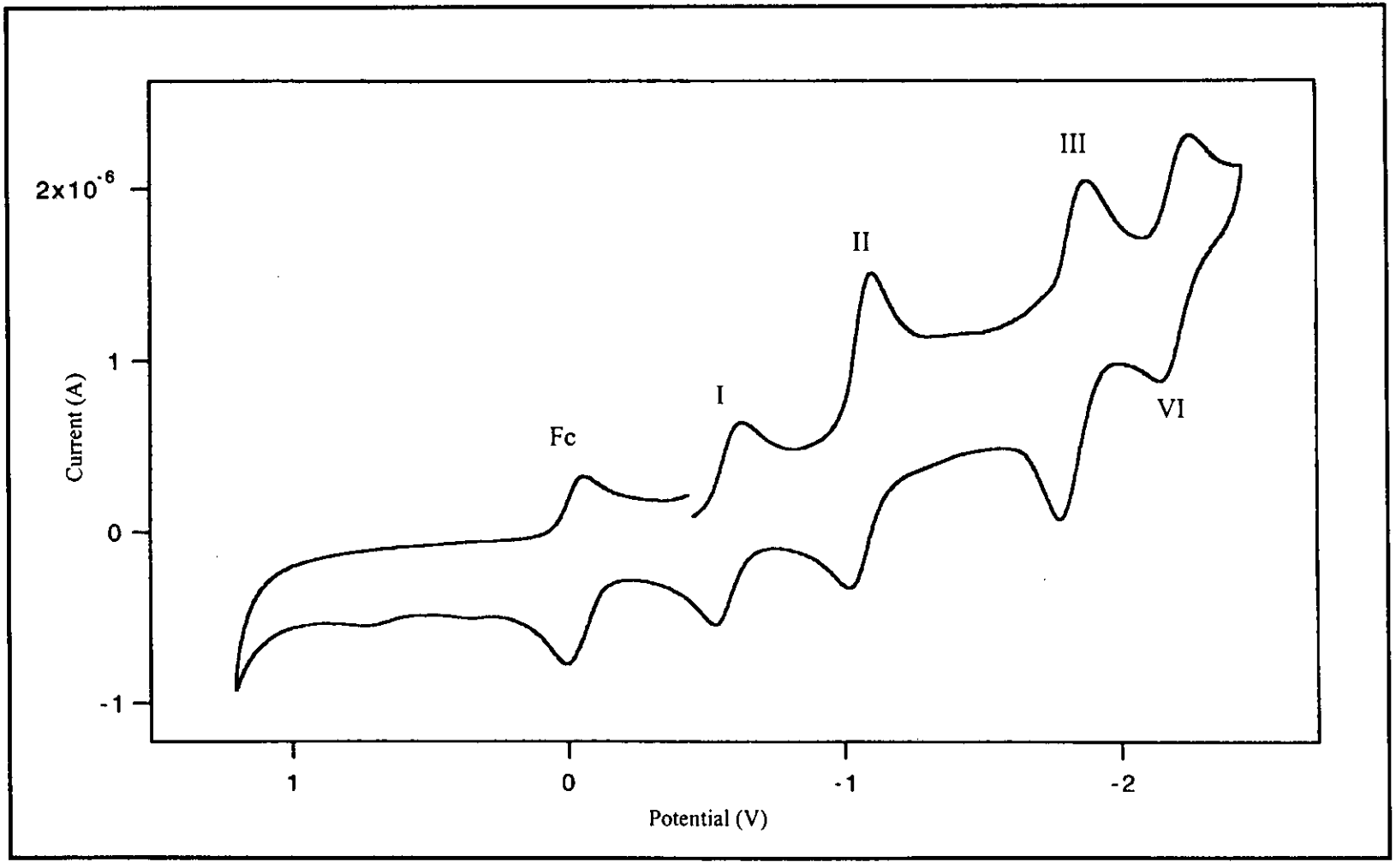

Figure 76 Cyclic voltammogram of $[Ru(azpy)_2bpy](PF_6)_2$ in 0.1 M TBAH CH_3CN at scan rate 50 mV/s.

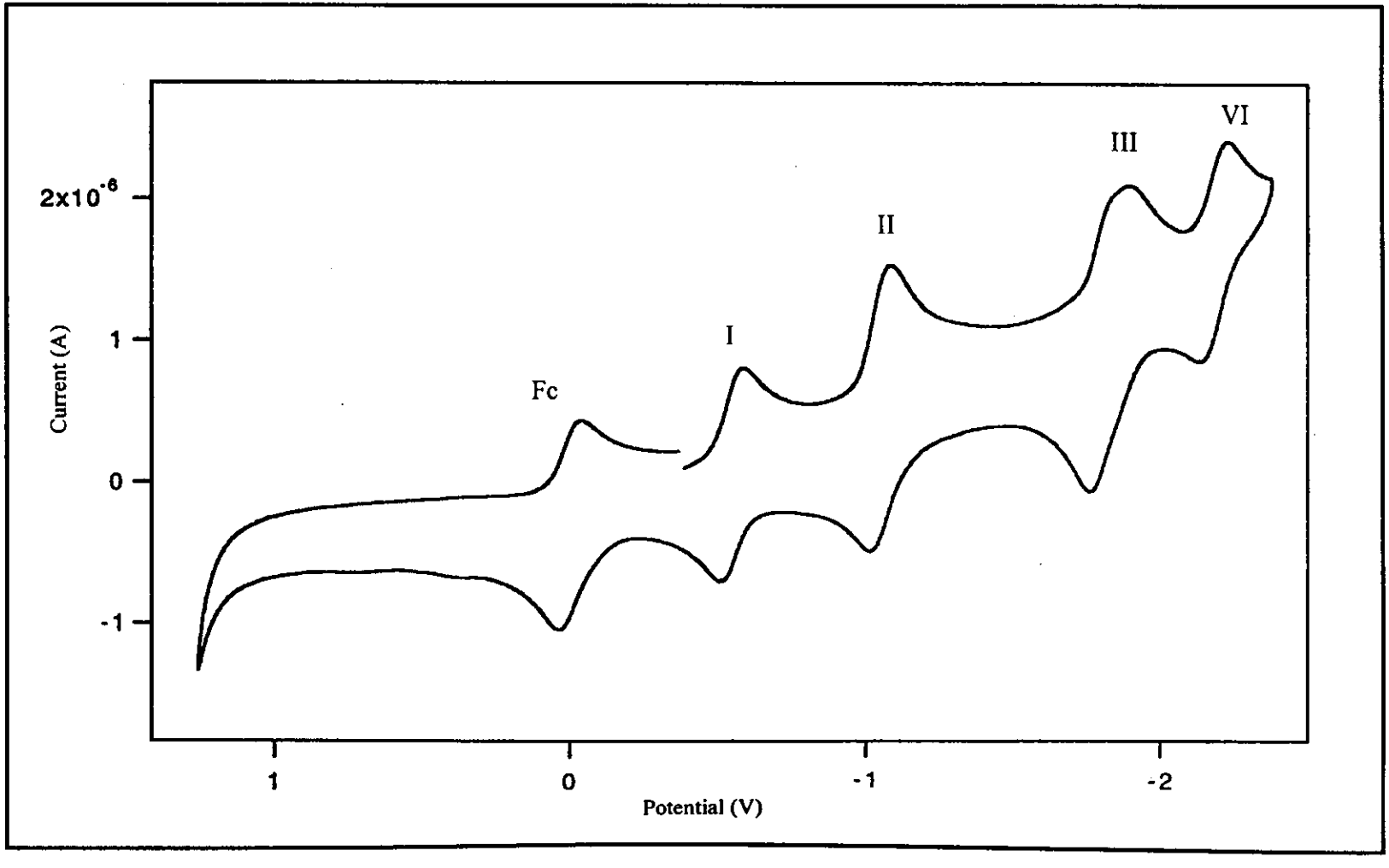

Figure 77 Cyclic voltammogram of $[Ru(azpy)_2phen](PF_6)_2$ in 0.1 M TBAH CH_3CN at scan rate 50 mV/s.

3.5.7 X-ray Crystallography

The X-ray Crystallography is a important technique to identify the geometry of the complexes. The structure of complexes showed six coordination around the ruthenium atom.

X-ray structure of $[Ru(azpy)_3](PF_6)_2$

X-ray quality crystals were obtained by evaporation methanol solvent slowly at room temperature. The crystal structure of the $[Ru(azpy)_3](PF_6)_2$ complex is shown in Figure 78. The bond lengths and angles within the coordination sphere of the ruthenium ion are listed in Table 27. The coordination sphere around ruthenium was approximately octahedral involving the three azpy ligands in meridional geometry.

Table 27 The selected bond distances (Å) and angles (°) and their estimated standard deviations for $[Ru(azpy)_3](PF_6)_2$

Distances			
Ru(1)-N(3)	2.111(8)	Ru(1)-N(7)	2.043(8)
Ru(1)-N(1)	2.068(8)	Ru(1)-N(4)	2.059(8)
Ru(1)-N(9)	2.050(8)	Ru(1)-N(6)	1.989(8)
N(3)-N(2)	1.24(1)N	(9)-N(8)	1.24(1)
N(6)-N(5)	1.29(1)Ru	(2)-N(17)	2.026(8)
Ru(2)-N(12)	2.038(8)	Ru(2)-N(18)	2.062(8)
Ru(2)-N(20)	2.050(9)	Ru(2)-N(15)	2.056(9)
Ru(2)-N(14)	2.051(8)	N(17)-N(16)	1.30(1)

N(20)-N(19)	1.31(1)	N(14)-N(13)	1.25(1)
		Angles	
N(3)-Ru(1)-N(1)	73.9(3)	N(7)-Ru(1)-N(9)	74.5(3)
N(4)-Ru(1)-N(6)	76.9(3)	N(3)-Ru(1)-N(6)	169.8(3)
N(7)-Ru(1)-N(1)	170.7(3)	N(4)-Ru(1)-N(9)	169.6(3)
N(17)-Ru(2)-N(15)	76.6(3)	N(17)-Ru(2)-N(14)	172.0(3)
N(12)-Ru(2)-N(20)	170.5(4)	N(12)-Ru(2)-N(14)	74.0(3)
N(18)-Ru(2)-N(20)	77.6(4)	N(18)-Ru(2)-N(15)	172.1(3)

Table 28 Crystallographic data of $[Ru(azpy)_3](PF_6)_2$

Empirical formula	$C_{33}H_{27}N_9P_2F_{12}Ru$
Formula weight	940.66
Crystal system	Triclinic
Space group	P1
Unit cell dimension	a = 9.4737(6), α = 86.4970(10)°
	b = 10.2718(6), β =88.7800(10) °
	c = 19.3025 , γ = 87.7360 (10) °
Volume	1873.1(2) $Å^3$
Z	2
Temperature	293(2) K
Wavelength	0.71073
Density	1.974 mg/m^3
Absorption coefficient	0.751 nm^{-1}
Goodness-of-fit on F^2	1.021
R indices (all data)	R = 0.0598, R_w = 0.0954

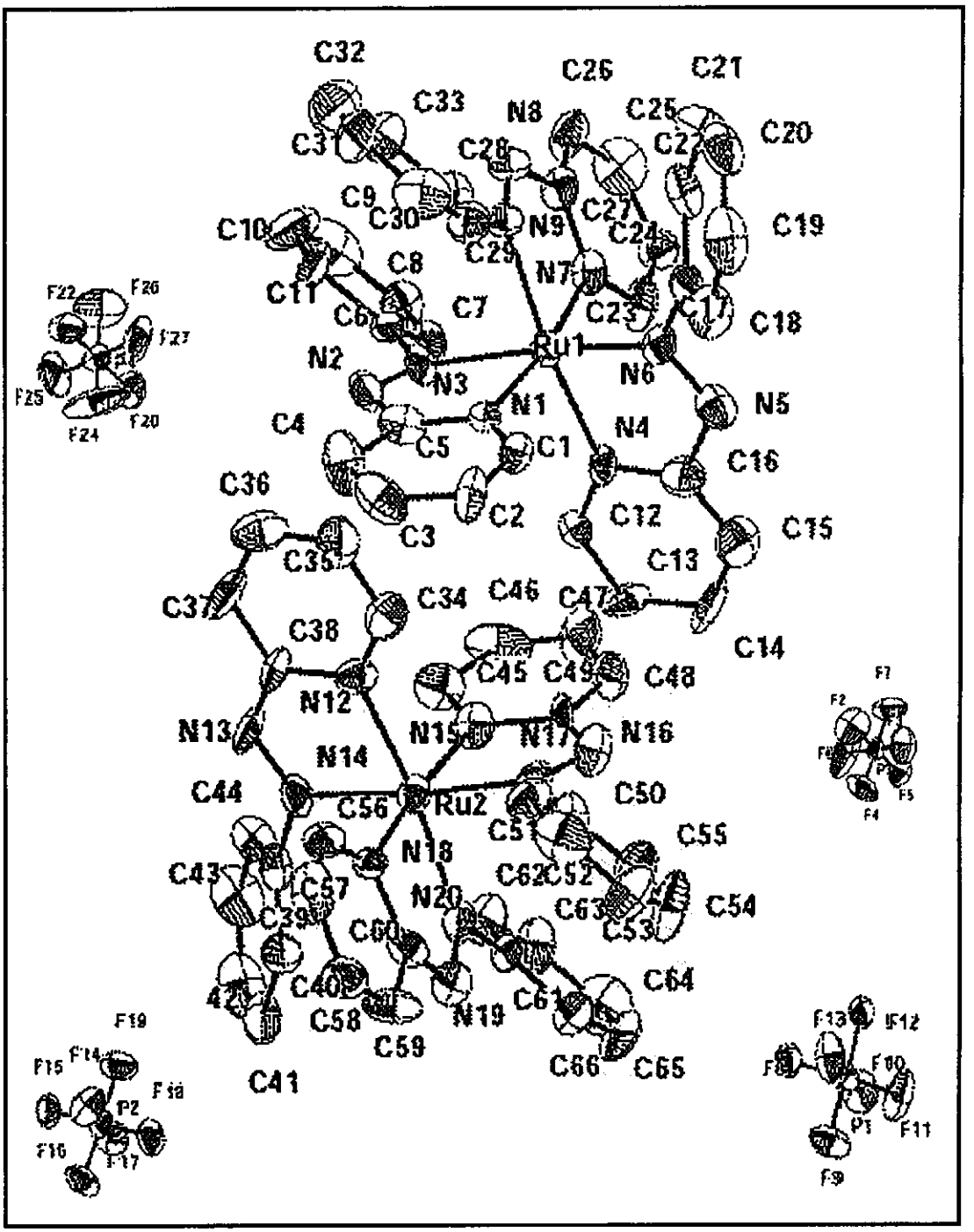

Figure 78 The structure of $[Ru(azpy)_3](PF_6)_2$ (H-atom omitted).

X-ray structure of $[Ru(azpy)_2bpy](PF_6)_2$

X-ray quality crystals were obtained by evaporation methanol solvent slowly at room temperature. The crystal structure of the $[Ru(azpy)_2bpy](PF_6)_2$ complex is shown in Figure 79. The bond lengths and angles within the coordination sphere of the ruthenium ion are listed in Table 28. In this case, the structure shows a distorted octahedral with hexa-coordination around Ru(II). The pyridine rings of both azpy ligands were trans position.

Table 29 The selected bond distances (Å) and angles (°) and their estimated standard deviations for $[Ru(azpy)_2bpy](PF_6)_2$

		Distances	
Ru(1)-N(8)	2.003(5)	Ru(1)-N(5)	2.036(5)
Ru(1)-N(6)	2.039(6)	Ru(1)-N(3)	2.047(5)
Ru(1)-N(2)	2.082(5)	Ru(1)-N(1)	2.090(5)
N(5)-N(4)	1.272(7)	N(8)-N(7)	1.269(8)
		Angles	
N(8)-Ru(1)-N(6)	76.1(2)	N(5)-Ru(1)-N3	75.9(2)
N(6)-Ru(1)-N(3)	171.3(2)	N(5)-Ru(1)-N(2)	175.9(2)
N(8)-Ru(1)-N(1)	172.7(2)	N(2)-Ru(1)-N(1)	77.9(2)

Table 30 Crystallographic data of $[Ru(azpy)_2bpy](PF_6)_2$

Empirical formula	$C_{32}H_{26}N_8P_2F_{12}Ru$
Formula weight	913.64
Crystal system	Orthorhombic
Space group	Pbca
Unit cell dimension	a = 19.4458(13), $\alpha = 90°$
	b = 16.3152(11), $\beta = 90°$
	c = 23.5827(6), $\gamma = 90°$
Volume	7.481.9(9) $Å^3$
Z	8
Temperature	293(2) K
Wavelength	0.71073 nm
Density	1.626 mg/m^3
Absorption coefficient	0.601 nm^{-1}
Goodness-of-fit on F^2	1.227
R indices (all data)	R = 0.1568, Rw = 0.1846

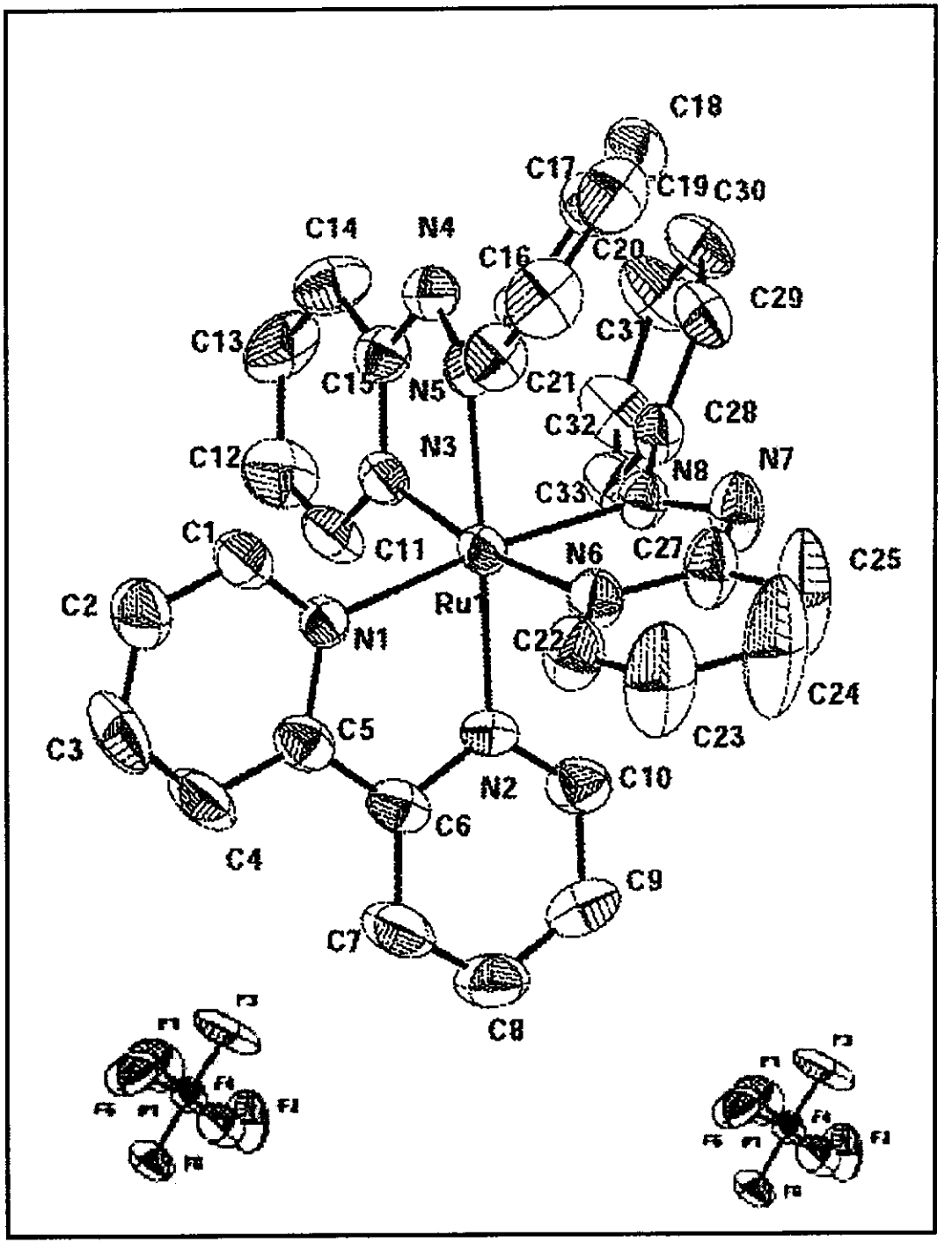

Figure 79 The structure of $[Ru(azpy)_2bpy](PF_6)_2$(H-atom omitted).

X-ray structure of $[Ru(azpy)_2phen](BF_4)_2$

X-ray quality crystals were obtained by evaporation methanol solvent slowly at room temperature. The crystal structure of the $[Ru(azpy)_2phen](BF_4)_2$ complex is shown in Figure 80. The bond lengths and angles within the coordination sphere of the ruthenium ion are listed in Table 31. The distorted RuN_6 octahedral was due to the coordination from two N-donor centres of a phen one and four N-donor centres of two azpy units.

Table 31 The selected bond distances (Å) and angles (°) and their estimated standard deviations for $[Ru(azpy)_2phen](BF_4)_2$

		Distances	
Ru(1)-N(5)	2.014(6)	Ru(1)-N(8)	2.021(5)
Ru(1)-N(3)	2.050(6)	Ru(1)-N(6)	2.054(6)
Ru(1)-N(2)	2.086(6)	Ru(1)-N(1)	2.085(6)
N(5)-N(4)	1.284(8)	N(8)-N(7)	1.279(8)
		Angles	
N(5)-Ru(1)-N(3)	76.3(2)	N(8)-Ru(1)-N(6)	76.1(2)
N(3)-Ru(1)-N(6)	174.3(2)	N(8)-Ru(1)-N(2)	174.4(2)
N(5)-Ru(1)-N(1)	174.1(2)	N(2)-Ru(1)-N(1)	78.7(2)

Table 32 Crystallographic data of $[Ru(azpy)_2phen](BF_4)_2$

Empirical formula	$C_{34}H_{26}N_8B_2F_8Ru$
Formula weight	821.07
Crystal system	Orthorhombic
Space group	Pbca
Unit cell dimension	$a = 17.7836(10)$, $\alpha = 90°$
	$b = 17.2139(10)$, $\beta = 90°$
	$c = 23.9126(13)$, $\gamma = 90°$
Volume	7320.2(7) $Å^3$
Z	8
Temperature	293(2) K
Wavelength	0.71073
Density	1.405 mg/m^3
Absorption coefficient	0.525 nm^{-1}
Goodness-of-fit on F^2	1.101
R indices (all data)	$R = 0.1316$, $R_w = 0.2730$

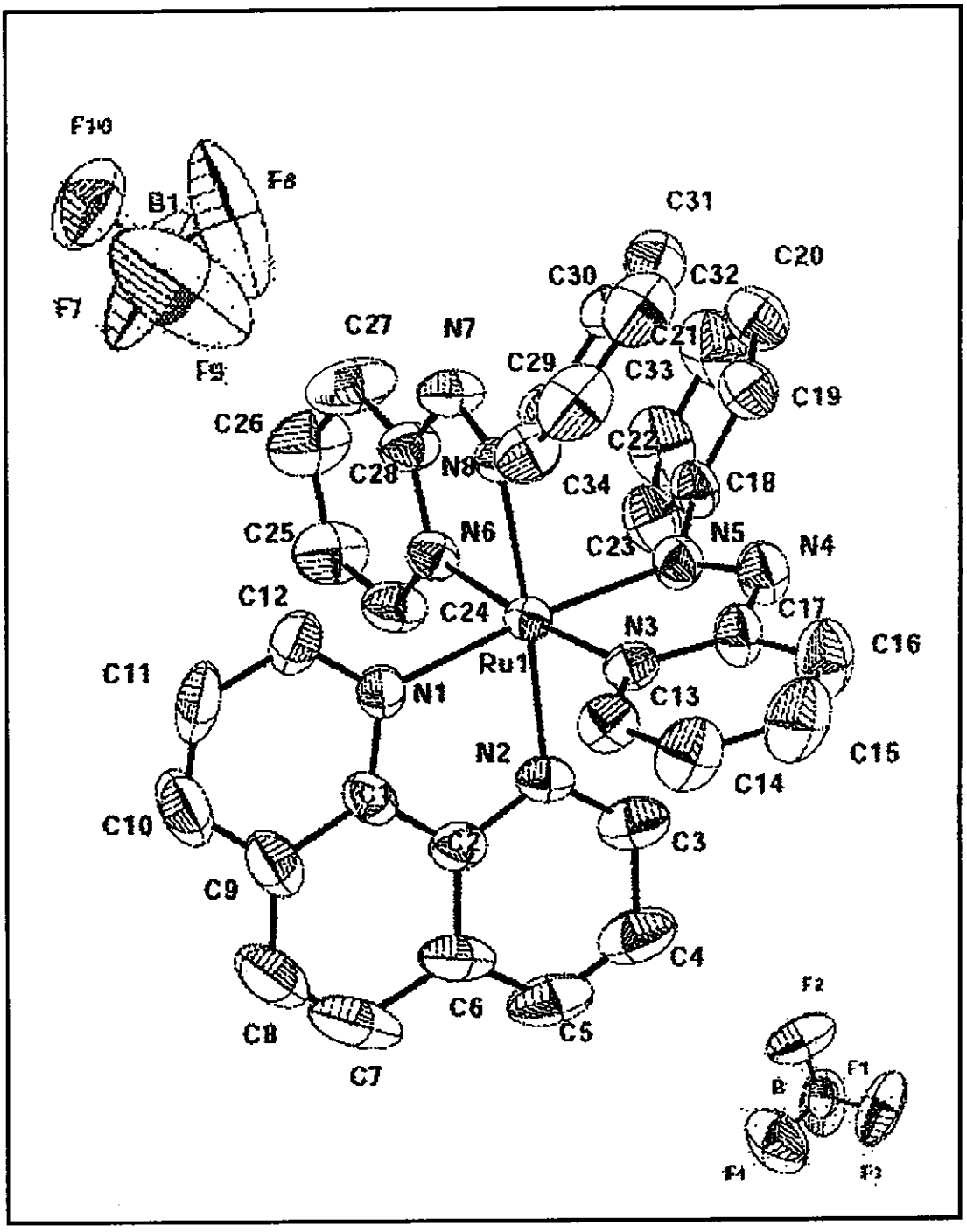

Figure 80 The structure of $[Ru(azpy)_2phen](BF_4)_2$ (H-atom omitted).